

APPLICATIONS OF DENSITY FUNCTIONAL THEORY:

RADIATION-INDUCED DNA DAMAGE

by

SUNGHWAN KIM

(Under the Direction of Henry F. Schaefer, III)

ABSTRACT

Exposure to high-energy radiation can cause mutations in living organisms by generating lethal lesions in DNA strands. Density functional theory has been employed to study microhydration effects on formation of the anions of three pyrimidine nucleic acid bases (NABs), thymine, uracil, and cytosine, which are thought to play an important role in the radiation-induced DNA damage process, by explicitly considering various structures of complexes of the three bases with up to five water molecules at the B3LYP/DZP++ level of theory. For all three bases, both the adiabatic electron affinities (AEAs) and vertical detachment energies (VDEs) are found to increase with the number of hydrating water molecules, implying that formation of the anions of the NABs are energetically favorable, although the anions of the NABs in the gas phase are not bound or weakly bound at most. For a given hydration number, uracil is predicted to have the largest electron affinities, while cytosine has the smallest. The methyl group of thymine is found to lower the AEA by 0.04 eV, compared to the AEA of uracil. These results are qualitatively consistent with available experimental results from photodetachment-photoelectron spectroscopy studies of Schiedt et al. [Chem. Phys. **239**, 511 (1998)].

The hydrogen-abstracted radicals from the adenine-uracil base pair have also been studied at the B3LYP/DZP++ level of theory. The radical arising from removal of an amino hydrogen of the adenine moiety which forms a hydrogen bond with the uracil O4 atom resulted in a significant decrease in the base pair dissociation energy ($5.9 \text{ kcal mol}^{-1}$). This radical is more likely to dissociate into the two isolated bases than to recover the hydrogen bond with the O4 atom through the N6-H bond rotation along the C6-N6 bond. On the contrary, removal of the uracil N3 hydrogen atom does not affect the base pair dissociation energy of the resulting radical, due to electron density transfer from the adenine N1 atom to the uracil N3 atom.

INDEX WORDS: Density functional theory, Radiation-induced DNA damage, nucleic acid base, uracil, cytosine, thymine, electron affinity, microhydration, hydrogen-atom abstraction, adenine-uracil base pair

APPLICATIONS OF DENSITY FUNCTIONAL THEORY:
RADIATION-INDUCED DNA DAMAGE

by

SUNGHWAN KIM

B.S., Hanyang University, 1999, Republic of Korea

M.S., Hanyang University, 2001, Republic of Korea

A Dissertation Submitted to the Graduate Faculty of The University of Georgia in Partial

Fulfillment of the Requirements for the Degree

DOCTOR OF PHILOSOPHY

ATHENS, GEORGIA

2007

© 2007

Sunghwan Kim

All Rights Reserved

APPLICATIONS OF DENSITY FUNCTIONAL THEORY:
RADIATION-INDUCED DNA DAMAGE

by

SUNGHWAN KIM

Major Professor: Henry F. Schaefer, III

Committee: Nigel G. Adams
Geoffrey D. Smith

Electronic Version Approved:

Maureen Grasso
Dean of the Graduate School
The University of Georgia
May 2007

DEDICATION

For all people who have supported me

ACKNOWLEDGEMENTS

I would like to acknowledge those without whom the completion of this work and this degree would have been impossible. First of all, I must express my gratitude to Professor Schaefer for allowing me the great opportunity to be a member of the CC(Q)C. His advising style allowed for freedom to explore any area of quantum chemistry that is of personal interest. Professor Allen and Drs. Yamaguchi and Xie also deserve a great deal of appreciation for their patience to teach and willingness to help me understand key concepts. Next, the administrative staff of the CC(Q)C must be greatly appreciated: Mrs. Linda Rowe, Mrs. Amy Peterson, and Mrs. Karen Branch. Their continuous effort to shield all of us from the bureaucracies of the University is greatly treasured.

I would like to express my appreciation to Dr. Steven Wheeler for helping me a lot as a mentor since I joined the group. I'm grateful to Dr. Justin Turney and Richard Remington for all prompt help with any computer problems. I appreciate the kindness of my (ex-) officemates, Maria Lind, David Zhang, Nicholas Marshall, Zachary Owens, Justin Ingels, and Franklin Leech as well as Drs. Veronika Kasalova and Suyun Wang. I thank Partha Bera, Andy Simmonett, and Francesco Evangelista for helpful discussion on my research projects. I also thank other former graduate students, Drs. Kurt Sattlemeyer, Lubos Horny, Nathan De Yonker, Michael, Schuurman, Joe Larkin, Ankan Paul, and Brian Papas. Without their help, my life in the US could have been miserable from the beginning. Of course, our first-year graduate students must be appreciated: Heather Jeager, Jeremiah Wilke, Frank Pickard, Lucas Speakman, and Nathan

Stibrich. It has been an enjoyable four years with these people and I hope to remain in contact with each of you for years to come.

There are of course people I would like to thank that are not associated with the group. I to thank to Korean people in the Chemistry Department at the University: Jae-Min Lim, Jihye Shim, Jay Y. Kim, and Dr. Youn-Geun Kim. I also thank to Monica Choi, Evita Sprawl, Sunil Kim, Wonjong Oh, and Mi Yeon Shim, who helped me settle down in Athens. I must not forget to express my special gratitude to Sunil's aunt and uncle in Atlanta. Lastly, I must thank to my wife, Sun Ae, and my family in Korea, who has believed in me.

TABLE OF CONTENTS

	Page
ACKNOWLEDGEMENTS	v
LIST OF TABLES	ix
LIST OF FIGURES	xi
CHAPTER	
1 INTRODUCTION AND BACKGROUND MATERIAL	1
1.1 DENSITY FUNCTIONAL THEORY	2
1.2 RADIATION-INDUCED DNA DAMAGE	4
1.3 REFERENCES	6
2 MICROHYDRATION OF THYMINE AND ITS RADICAL ANION	12
2.1 ABSTRACT	13
2.2 INTRODUCTION	13
2.3 COMPUTATIONAL METHODS	17
2.4 RESULTS	19
2.5 CONCLUSIONS	27
2.6 ACKNOWLEDGEMENTS	29
2.7 REFERENCES	30
3 MICROHYDRATION OF URACIL AND ITS RADICAL ANION	46
3.1 ABSTRACT	47
3.2 INTRODUCTION	47

3.3	COMPUTATIONAL METHODS	51
3.4	RESULTS.....	53
3.5	CONCLUSIONS	61
3.6	ACKNOWLEDGEMENTS	62
3.7	REFERENCES.....	63
4	MICROHYDRATION OF CYTOSINE AND ITS RADICAL ANION	80
4.1	ABSTRACT	81
4.2	INTRODUCTION.....	81
4.3	COMPUTATIONAL METHODS	85
4.4	RESULTS.....	86
4.5	CONCLUSIONS	97
4.6	ACKNOWLEDGEMENTS	98
4.7	REFERENCES.....	99
5	HYDROGEN ATOM ABSTRACTION FROM THE ADENINE-URACIL BASE PAIR.....	117
5.1	ABSTRACT	118
5.2	INTRODUCTION.....	119
5.3	COMPUTATIONAL METHODS	120
5.4	RESULTS.....	122
5.5	DISCUSSION	129
5.6	ACKNOWLEDGEMENTS	131
5.7	REFERENCES.....	132
6	CONCLUDING REMARKS.....	150

LIST OF TABLES

	Page
Table 2.1: Relative energies (E_{rel}) and hydration energies (E_{hyd}) in kcal mol ⁻¹ of thymine hydrates and their anions (ZPVE-corrected values in parentheses).....	34
Table 2.2: Vertical detachment energies (VDEs) and adiabatic electron affinities (AEAs) in eV for thymine and its hydrates (ZPVE-corrected values in parentheses).....	35
Table 2.3: Absolute adiabatic electron affinities (AEA_{abs}) in eV of thymine and its hydrates (ZPVE-corrected values in parentheses).....	36
Table 3.1: Relative energies (E_{rel}) and hydration energies (E_{hyd}) in kcal mol ⁻¹ of uracil hydrates and their anions (ZPVE-corrected values in parentheses).....	67
Table 3.2: Vertical detachment energies (VDEs) and adiabatic electron affinities (AEAs) in eV for uracil and its hydrates (ZPVE-corrected values in parentheses).....	68
Table 3.3: Absolute adiabatic electron affinities (AEA_{abs}) in eV of uracil and its hydrates (ZPVE-corrected values in parentheses).....	69
Table 4.1: Relative energies (E_{rel}) and microhydration energies (E_{hyd}) in kcal mol ⁻¹ for the cytosine hydrates and their anions (ZPVE-corrected values in parentheses).....	104
Table 4.2: Vertical detachment energies (VDEs) and adiabatic electron affinities (AEAs) in eV for cytosine and its hydrates (ZPVE-corrected values in parentheses).....	105
Table 4.3: Absolute adiabatic electron affinities (AEA_{abs}) in eV of cytosine and its hydrates (ZPVE-corrected values in parentheses).....	106

Table 5.1: Relative energies (E_{rel}), dissociation energies (DE), and relaxation energies (RE) (kcal mol^{-1}) of the AU-H radicals generated by hydrogen atom abstraction from the adenine-uracil pair (ZPVE-corrected values in parentheses).....	138
Table 5.2: Selected interatomic distances (\AA) for the A-U base pair and its hydrogen abstracted radicals.....	139
Table 5.3: Relative energies (E_{rel}) in kcal mol^{-1} of the isolated A-H and U-H radicals.....	140
Table 5.4: X-H bond dissociation energies (BDE) in eV for adenine, uracil, and A-U base pair. Each entry is labeled by the name of the particular radical resulting from hydrogen atom removal.....	141

LIST OF FIGURES

	Page
Figure 2.1: Numbering scheme for the canonical structure of thymine.	37
Figure 2.2: Molecular structures for thymine monohydrates (left column) and their respective anions (right column) displaying selected geometrical parameters, optimized at the B3LYP/DZP++ level of theory.	38
Figure 2.3: Singly-occupied molecular orbital (SOMO) for the thymine monohydrate radical anion 1B⁻	39
Figure 2.4: Selected structures for neutral (upper row) and anionic (lower row) dihydrates of thymine, optimized at the B3LYP/DZP++ level of theory.	40
Figure 2.5: The three most stable structures for the neutral tri-, tetra-, and pentahydrates of thymine, optimized at the B3LYP/DZP++ level of theory.	41
Figure 2.6: The three most stable structures for the anionic tri-, tetra-, and pentahydrates, optimized at the B3LYP/DZP++ level of theory.	42
Figure 2.7: The second stable structure 4H⁻ for anionic thymine tetrahydrate, optimized at the B3LYP/DZP++ level of theory.	43
Figure 2.8: Electron affinities (in eV) for thymine hydrates with up to five water molecules: VDEs for most stable anionic hydrates (◆); ZPVE-corrected AEAs for the lowest-lying anionic (■) and neutral (●) hydrates; and ZPVE-corrected absolute AEAs (▲).	44
Figure 2.9: Four water-binding sites in thymine, populated in the order: A > B > C > D.	45

Figure 3.1: Atom numbering scheme for the canonical structure of uracil.	70
Figure 3.2: Molecular structures for uracil monohydrates (left column) and their respective anions (right column) with selected geometrical parameters, optimized at the B3LYP/DZP++ level of theory.	71
Figure 3.3: The singly occupied molecular orbitals (SOMOs) for the anions of the uracil monohydrates.	72
Figure 3.4: Prospective water-binding sites of uracil, populated in the order: A > B > C > D for the neutral monohydrate.	73
Figure 3.5: Selected structures for neutral uracil dihydrates (left column) and their respective anions (right column), optimized at the B3LYP/DZP++ level of theory.	74
Figure 3.6: The most stable structures for the neutral tri-, tetra-, and pentahydrates of uracil, optimized at the B3LYP/DZP++ level of theory.	75
Figure 3.7: The most stable structures for the anionic tri-, tetra-, and pentahydrates of uracil, optimized at the B3LYP/DZP++ level of theory.	76
Figure 3.8: The second stable structure for the uracil tetrahydrate anion, optimized at the B3LYP/DZP++ level of theory.	77
Figure 3.9: Electron affinities in eV for uracil hydrates with up to five water molecules: VDEs for the most stable anionic hydrates(◆); ZPVE-corrected AEAs for the lowest-lying anionic (■) and neutral (●) hydrates; and ZPVE-corrected absolute AEAs (▲).....	78
Figure 3.10: Comparison of the VDE and AEA between the uracil hydrates and the thymine hydrates.	79
Figure 4.1: The canonical structure of cytosine with atom numbering scheme.	107

Figure 4.2: Molecular structures for cytosine monohydrates (left column) and their respective anions (right column), optimized at the B3LYP/DZP++ level of theory.....	108
Figure 4.3: Singly occupied molecular orbitals (SOMOs) for the anions of cytosine and its monohydrates: (a) the cytosine anion, (b) $1A^-$, (c) $1B^-$, and (d) $1C^-$	109
Figure 4.4: The three lowest-energy structures for the cytosine dihydrate and their respective anions.....	110
Figure 4.5: The molecular structures of the anion $2D$ and its anion conformers, $2D_a^-$ and $2D_b^-$. Electron attachment to $2D$ results in $2D_a^-$, while electron detachment from either $2D_a^-$ or $2D_b^-$ results in $2D$	111
Figure 4.6: The most stable structures for the neutral tri-, tetra-, and pentahydrates of cytosine.....	112
Figure 4.7: Selected theoretical structures for the anionic tri-, tetra-, pentahydrates of cytosine.....	113
Figure 4.8: Electron affinities in eV for cytosine hydrates with up to five water molecules: VDEs for the most stable anionic hydrates (\blacklozenge), ZPVE-corrected AEAs for the most stable anionic (\blacksquare) and neutral (\bullet) hydrates, and ZPVE-corrected absolute AEAs (\blacktriangle).....	114
Figure 4.9: Comparison of the VDE and AEA among the uracil, thymine, and cytosine hydrates.	115
Figure 4.10: Prospective water-binding sites of cytosine. While site B is preferred by the neutral cytosine, site B' is preferred by the cytosine anion.	116
Figure 5.1: Optimized molecular geometry of the adenine-uracil (AU) base pair with atom numbering scheme.....	142

Figure 5.2: Optimized molecular structures of the radicals generated by hydrogen atom abstraction from the adenine unit of the AU base pair.....	143
Figure 5.3: Optimized molecular structures of the radicals generated by hydrogen atom abstraction from the uracil unit of the AU base pair.	144
Figure 5.4: Spin density plots for the radicals generated by hydrogen abstraction from the AU base pair.....	145
Figure 5.5: The schematic energy diagram for the dissociation of base pair radicals A(N6a)-U and A(N6b)-U and the rotational barrier connecting them (ZPVE-corrected values in parentheses).....	146
Figure 5.6: Transition structure between radicals A(N6a)-U and A(N6b)-U	147
Figure 5.7: Two possible orientation of the unpaired electron in the A-U(N3) radical.....	148
Figure 5.8: Two possible pathways to generating the hydrogen abstracted radicals from the isolated adenine and uracil bases.....	149

CHAPTER 1

INTRODUCTION AND BACKGROUND MATERIAL

1.1 DENSITY FUNCTIONAL THEORY

The electron density, $\rho(\mathbf{r})$, can provide all information necessary for construction of the Hamiltonian operator, which depends only on the positions and atomic numbers of the nuclei and the total number of electrons of a system.¹ Integrating the electron density over all space gives the total number of electrons.

$$N = \int \rho(\mathbf{r}) d\mathbf{r}$$

If the exact electron density is known, the positions of the nuclei correspond to local maxima in the electron density and the nuclear atomic charges can be determined because for a nucleus A located at an electron density maximum \mathbf{r}_A ,

$$\left. \frac{\partial \bar{\rho}(r_A)}{\partial r_A} \right|_{r_A=0} = -2Z_A \rho(\mathbf{r}_A)$$

where Z_A is the atomic number of A, r_A is the radial distance from A, and $\bar{\rho}$ is the spherically averaged density. Therefore, once the exact electron density of a system is given, the Hamiltonian operator of the Schrödinger equation is known completely, and hence, the wave function and energy of the system are also known. In addition, there is a very important advantage of working with the electron density in determining the energy (and other properties), compared to working with the wave function.^{1,2} Because the wave function depends on three spatial coordinates (and one spin coordinate) for every electron, it contains $3N$ spatial

coordinates for an N-electron system, implying that the complexity of a wave function increases with the number of electrons. On the other hand, the electron density depends only on three spatial coordinates, independently of the size of a system.

The Hohenberg-Kohn existence theorem³ tells us that there exists a one-to-one correspondence between the non-degenerate ground-state electron density and energy. However, the exact form of the functional connecting the electron density and energy is not yet known, although many different density functionals have been proposed. The simplest functional is the local density approximation (LDA),⁴⁻⁶ where the electron density is treated locally as a uniform electron gas. Although the LDA tends to overestimate the bond strengths, it often provides a similar accuracy to that of the Hartree-Fock (HF) method. Improvements over the LDA approach can be achieved by employing the generalized gradient approximation (GGA),⁷⁻¹⁰ where the exchange and correlation energies depend derivatives of the density as well as the density. The hybrid method, where the exact HF exchange is included in the density functional, is another way of designing a density functional.^{11,12}

In general, the DFT method is more accurate than the HF method because some electron correlation can be included in the functionals.^{1,2} In addition, the DFT method scales as N^3 , while the HF method scales as N^4 (where N is the number of basis functions). The formal scaling behavior of the high-level electron correlation methods is even worse (e.g., the CCSD(T) method

scales as N^7). Therefore, the DFT approach is considered as a relatively inexpensive yet reliable theoretical method. It has been successful in predicting many chemical properties of larger molecular systems which cannot be handled by current high-level ab initio methods.

1.2 RADIATION-INDUCED DNA DAMAGE

High-energy ionizing radiation can cause mutations in living organisms by generating lethal DNA lesions, such as modified bases, abasic sites, interstrand cross-links, and single- and double-strand breaks (SSBs and DSBs). In the initial stage of radiation-induced DNA damage, ionizing radiation may generate positive holes in the DNA strands through the one-electron oxidation process.¹³⁻¹⁶ Due to guanine having the lowest ionization potential among the nucleic acid bases (NABs),¹⁷⁻²⁹ these positive holes migrate to guanine sites through the DNA strands.³⁰⁻
³⁷ In particular, the 5'-terminus of polyguanine (G_n) sequences in DNA is a very efficient trap for the positive holes. Subsequent reactions of the cationic guanine radicals with reactive oxygen species, generated by radiolysis of water, give rise to 8-oxo-7,8-dihydroguanine and other oxidation products.^{31,33,38-40} Another pathway leading to DNA damage involves the formation and transport of negative charges within the DNA strands. Low-energy electrons (with energies lower than 30 eV), generated upon radiolysis of water, can be trapped on the pyrimidine NABs such as thymine and cytosine. Sanche and coworkers⁴¹ showed that such

electrons can also cause SSBs and DSBs even if their energies are lower than the ionization thresholded (7.5 eV) of DNA. Recent theoretical and experimental studies suggested that electrons with energies even at or near 0 eV can result in DNA strand breaks.⁴²⁻⁴⁵ In addition, as shown in the experimental studies of Bowen and coworkers⁴⁶⁻⁴⁸ using anion photoelectron spectroscopy, electron attachment to the NABs can produce non-canonical tautomers through barrier-free proton transfer.

Many experimental and theoretical studies have been reported on gas-phase electron affinities of NABs. It is generally believed that conventional (valence-bound) anions are not bound or weakly bound at most with AEAs less than 0.2 eV.⁴⁹⁻⁵¹ However, the electron affinities of NABs in aqueous solution may be quite different from those in the gas phase. In the photodetachment-photoelectron spectroscopy study of Schiedt *et al.*⁵⁰ the electron affinities of thymine, uracil, and cytosine increased linearly with the number of hydrating water molecules. Thus, quantifying the effects of solvation on the electron affinities of NABs is crucial to understanding the mechanism of radiation-induced DNA damage in aqueous solution and living organisms. In Chapter 2 through 4, microhydration effects on the electron affinities of the three pyrimidine DNA/RNA bases are investigated by explicitly considering various structures of the NAB complexes with up to five water molecules.⁵²⁻⁵⁴

During the radiation-induced DNA damage process, a variety of neutral radicals can be generated along with the positively and negatively charged species. For example, hydrogen-abstracted NAB radicals may be generated either by the homolytic cleavage of a C-H or N-H bond or by deprotonation of the oxidized (cationic) NABs.⁵⁵⁻⁶⁵ These radicals are considered as important intermediates leading to lethal lesions in DNA, because hydrogen abstraction from the NABs may cause a significant change in the hydrogen bonding pattern of a base pair in the DNA duplex, leading to critical modifications in DNA. Indeed, the radical arising from abstraction of one hydrogen atom from the methyl group of thymine is known to be readily oxidized to give rise to modified NABs such as 5-(hydroxymethyl)uracil or 5-formyluracil. In addition, this radical has been found to generate an interstrand cross-link in double-stranded DNA.⁶⁶⁻⁶⁹ In Chapter 5, effects of hydrogen-atom abstraction from the adenine-uracil (AU) base pair are studied. Although uracil is predominantly found in RNA, the AU base pair is also of great importance because of its structural similarity to the adenine-thymine base pair in DNA duplexes.

1.3 REFERENCES

- ¹ C. J. Cramer, *Essentials of Computational Chemistry: Theories and Models*. (John Wiley & Sons Ltd, West Sussex, England, 2002).

- ² F. Jensen, *Introduction to Computational Chemistry*. (John Wiley & Sons Ltd, West Sussex, England, 1999).
- ³ P. Hohenberg and W. Kohn, *Phys. Rev.* **136**, B864 (1964).
- ⁴ J. C. Slater, *Phys. Rev.* **81**, 385 (1951).
- ⁵ D. M. Ceperley and B. J. Alder, *Phys. Rev. Lett.* **45**, 566 (1980).
- ⁶ S. H. Vosko, L. Wilk, and M. Nusair, *Can. J. Phys.* **58**, 1200 (1980).
- ⁷ J. P. Perdew and W. Yue, *Physical Review B* **33**, 8800 (1986).
- ⁸ J. P. Perdew and W. Yue, *Physical Review B* **40**, 3399 (1989).
- ⁹ A. D. Becke, *Phys. Rev. A* **38**, 3098 (1988).
- ¹⁰ C. Lee, W. Yang, and R. G. Parr, *Phys. Rev. B* **37**, 785 (1988).
- ¹¹ J. Harris, *Phys. Rev. A* **29**, 1648 (1984).
- ¹² A. D. Becke, *J. Chem. Phys.* **98**, 5648 (1993).
- ¹³ S. K. Kim, W. Lee, and D. R. Herschbach, *J. Phys. Chem.* **100**, 7933 (1996).
- ¹⁴ H.-W. Jochims, M. Schwell, H. Baumgaertel, and S. Leach, *Chem. Phys.* **314**, 263 (2005).
- ¹⁵ S. Steenken, *Chem. Rev.* **89**, 503 (1989).
- ¹⁶ M. Ratner, *Nature* **397**, 480 (1999).
- ¹⁷ X. Li, Z. Cai, and M. D. Sevilla, *J. Phys. Chem. A* **106**, 9345 (2002).

- ¹⁸ C. E. Crespo-Hernandez, R. Arce, Y. Ishikawa, L. Gorb, J. Leszczynski, and D. M. Close, J. Phys. Chem. A **108**, 6373 (2004).
- ¹⁹ A. O. Colson, B. Besler, D. M. Close, and M. D. Sevilla, J. Phys. Chem. **96**, 661 (1992).
- ²⁰ M. Hutter and T. Clark, J. Am. Chem. Soc. **118**, 7574 (1996).
- ²¹ J. Sponer, J. Leszczynski, and P. Hobza, J. Phys. Chem. **100**, 5590 (1996).
- ²² F. Prat, K. N. Houk, and C. S. Foote, J. Am. Chem. Soc. **120**, 845 (1998).
- ²³ N. S. Hush and A. S. Cheung, Chem. Phys. Lett. **34**, 11 (1975).
- ²⁴ V. M. Orlov, A. N. Smirnov, and Y. M. Varshavsky, Tetrahedron Lett. **48**, 4377 (1976).
- ²⁵ A. O. Colson, B. Besler, and M. D. Sevilla, J. Phys. Chem. **97**, 13852 (1993).
- ²⁶ M. D. Sevilla, B. Besler, and A.-O. Colson, J. Phys. Chem. **99**, 1060 (1995).
- ²⁷ N. Russo, M. Toscano, and A. Grand, J. Comput. Chem. **21**, 1243 (2000).
- ²⁸ S. D. Wetmore, R. J. Boyd, and L. A. Eriksson, Chem. Phys. Lett. **322**, 129 (2000).
- ²⁹ S. P. Walch, Chem. Phys. Lett. **374**, 496 (2003).
- ³⁰ P. Swiderek, Angew. Chem., Int. Ed. **45**, 4056 (2006).
- ³¹ I. Saito, T. Nakamura, K. Nakatani, Y. Yoshioka, K. Yamaguchi, and H. Sugiyama, J. Am. Chem. Soc. **120**, 12686 (1998).
- ³² S. Kanvah and G. B. Schuster, J. Am. Chem. Soc. **124**, 11286 (2002).
- ³³ G. Pratviel and B. Meunier, Chem. Eur. J. **12**, 6018 (2006).

- ³⁴ U. Diederichsen, *Angew. Chem., Int. Ed. Engl.* **36**, 2317 (1997).
- ³⁵ E. Nir, K. Kleinermanns, and M. S. de Vries, *Nature* **408**, 949 (2000).
- ³⁶ J. Bertran, A. Oliva, L. Rodriguez-Santiago, and M. Sodupe, *J. Am. Chem. Soc.* **120**, 8159 (1998).
- ³⁷ V. Guallar, A. Douhal, M. Moreno, and J. M. Lluch, *J. Phys. Chem. A* **103**, 6251 (1999).
- ³⁸ G. B. Schuster, *Acc. Chem. Res.* **33**, 253 (2000).
- ³⁹ F. D. Lewis, R. L. Letsinger, and M. R. Wasielewski, *Acc. Chem. Res.* **34**, 159 (2001).
- ⁴⁰ C. J. Burrows and J. G. Muller, *Chem. Rev.* **98**, 1109 (1998).
- ⁴¹ B. Boudaiffa, P. Cloutier, D. Hunting, M. A. Huels, and L. Sanche, *Science* **287**, 1658 (2000).
- ⁴² X. Li, M. D. Sevilla, and L. Sanche, *J. Am. Chem. Soc.* **125**, 13668 (2003).
- ⁴³ X. Bao, J. Wang, J. Gu, and J. Leszczynski, *Proc. Natl. Acad. Sci. U. S. A.* **103**, 5658 (2006).
- ⁴⁴ J. Simons, *Acc. Chem. Res.* **39**, 772 (2006).
- ⁴⁵ I. Bald, J. Kopyra, and E. Illenberger, *Angew. Chem., Int. Ed.* **45**, 4851 (2006).
- ⁴⁶ I. Dabkowska, J. Rak, M. Gutowski, J. M. Nilles, S. T. Stokes, and K. H. Bowen, *J. Chem. Phys.* **120**, 6064 (2004).
- ⁴⁷ M. Haranczyk, I. Dabkowska, J. Rak, M. Gutowski, J. M. Nilles, S. Stokes, D. Radisic, and K. H. Bowen, *J. Phys. Chem. B* **108**, 6919 (2004).

- ⁴⁸ D. Radisic, K. H. Bowen, I. Dabkowska, P. Storoniak, J. Rak, and M. Gutowski, *J. Am. Chem. Soc.* **127**, 6443 (2005).
- ⁴⁹ S. S. Wesolowski, M. L. Leininger, P. N. Pentchev, and H. F. Schaefer, *J. Am. Chem. Soc.* **123**, 4023 (2001).
- ⁵⁰ J. Schiedt, R. Weinkauff, D. M. Neumark, and E. W. Schlag, *Chem. Phys.* **239**, 511 (1998).
- ⁵¹ C. Desfrancois, H. Abdoul-Carime, and J. P. Schermann, *J. Chem. Phys.* **104**, 7792 (1996).
- ⁵² S. Kim, S. E. Wheeler, and H. F. Schaefer, *J. Chem. Phys.* **124**, 204310 (2006).
- ⁵³ S. Kim and H. F. Schaefer, *J. Chem. Phys.* **125**, 144305 (2006).
- ⁵⁴ S. Kim and H. F. Schaefer, *J. Chem. Phys.* **126**, 064301 (2007).
- ⁵⁵ Y. Chen and D. Close, *J. Mol. Struct.* **549**, 55 (2001).
- ⁵⁶ D. M. Close, L. A. Eriksson, E. O. Hole, E. Sagstuen, and W. H. Nelson, *J. Phys. Chem. B* **104**, 9343 (2000).
- ⁵⁷ S. D. Wetmore, R. J. Boyd, and L. A. Eriksson, *J. Phys. Chem. B* **102**, 5369 (1998).
- ⁵⁸ E. O. Hole, E. Sagstuen, W. H. Nelson, and D. M. Close, *J. Phys. Chem.* **95**, 1494 (1991).
- ⁵⁹ S. D. Wetmore, R. J. Boyd, and L. A. Eriksson, *J. Phys. Chem. B* **102**, 10602 (1998).
- ⁶⁰ E. Sagstuen, E. O. Hole, W. H. Nelson, and D. M. Close, *J. Phys. Chem.* **96**, 1121 (1992).
- ⁶¹ E. Malinen and E. Sagstuen, *Radiat. Res.* **160**, 186 (2003).
- ⁶² D. M. Close, *Radiat. Res.* **135**, 1 (1993).

- ⁶³ W. A. Bernhard, *Adv. Radiat. Biol.* **9**, 199 (1981).
- ⁶⁴ D. Becker and M. D. Sevilla, *Adv. Radiat. Biol.* **17**, 121 (1993).
- ⁶⁵ W. A. Bernhard, J. Barnes, K. R. Mercer, and N. Mroczka, *Radiat. Res.* **140**, 199 (1994).
- ⁶⁶ I. S. Hong and M. M. Greenberg, *J. Am. Chem. Soc.* **127**, 3692 (2005).
- ⁶⁷ I. S. Hong and M. M. Greenberg, *J. Am. Chem. Soc.* **127**, 10510 (2005).
- ⁶⁸ I. S. Hong, H. Ding, and M. M. Greenberg, *J. Am. Chem. Soc.* **128**, 485 (2006).
- ⁶⁹ I. S. Hong, H. Ding, and M. M. Greenberg, *J. Am. Chem. Soc.* **128**, 2230 (2006).

CHAPTER 2

MICROHYDRATION OF THYMINE AND ITS RADICAL ANION[†]

[†] Reproduced with permission from Sunghwan Kim, Steven E. Wheeler, and Henry F. Schaefer, *J. Chem. Phys.* **124**(20), 204310/1-8 (2006). Copyright 2006, American Institute of Physics.

2.1 ABSTRACT

The effects of solvation on the stability of thymine and its negative ion have been investigated by explicitly considering the structures of complexes of thymine with up to five water molecules and the respective anions at the B3LYP/DZP++ level of theory. The vertical detachment energy of thymine was predicted to increase gradually with the hydration number, consistent with experimental observations from a photodetachment-photoelectron spectroscopy study [Schiedt, Weinkauff, Neumark, and Schlag, *Chem. Phys.* **239**, 511 (1998)]. The adiabatic electron affinity of thymine was also found to increase with the hydration number, which implies that while the conventional valence anion of thymine is only marginally bound in the gas phase, it may form a stable anion in aqueous solution.

2.2 INTRODUCTION

High-energy radiation-induced damage to DNA can be classified into two categories according to the initial pathway leading to lethal DNA lesions: one is “direct” and the other is “indirect.”¹⁻³ While the former is caused by one-electron oxidation due to the direct interaction with high-energy ionizing radiation, the latter arises from reactions initialized by secondary species generated by the ionizing radiation. Typical examples of these secondary species are reactive oxygen species such as OH, O₂⁻, and H₂O₂, generated upon radiolysis of water; their

roles in DNA damage have been studied extensively.¹⁻⁵ The radiolysis of water also gives rise to low-energy electrons with energies 1–20 eV, which are the most abundant of the secondary species.⁶⁻⁹ By irradiating plasmid DNA with a very low energy electron source under ultravacuum conditions, Huels and coworkers³ showed that low-energy electrons can cause lethal DNA lesions such as single- and double-strand breaks (SSBs and DSBs), even if their energies are below the ionization threshold of DNA (~7.5 eV). Thus, the damage due to these electrons is also of great importance, in addition to indirect damage caused by other secondary species. Walch¹⁰ concluded in a theoretical study on DNA models using density functional theory (DFT) that attachment of an excess electron is most favorable on a nucleic acid base (NAB) among DNA components, while removal of an electron is most favorable from the PO₄⁻ group. Because the electron affinity of a molecule is a measure of its ability to capture an additional electron, electron affinities of NABs are key to understanding the destiny of an excess electron, and thus, the mechanism of radiation-induced DNA damage.

Electron affinities of the NABs have been extensively studied, both experimentally and theoretically. Chen and coworkers¹¹ empirically estimated the gas-phase adiabatic electron affinities (AEAs) of five DNA and RNA bases, adenine, cytosine, guanine, thymine, and uracil, from the AEAs of pyrimidine and purine using substitution and replacement rules. They predicted the AEAs of all five NABs to be 0.6 eV or larger, which implied that the anions of

NABs were strongly bound. The AEAs estimated from the scaled reversible reduction potentials in aprotic solvent^{12,13} were similar to those from the substitution and replacement rules, and a theoretical study using the AM1 semiempirical method also supported this result.¹⁴ On the contrary, the AEA values of NABs from other studies are smaller than those of Chen and coworkers. By using negative ion photoelectron spectroscopy, Bowen and coworkers¹⁵ found the AEAs of uracil and thymine to be much smaller and less than 0.10 eV (0.093 ± 0.007 for uracil and 0.069 ± 0.007 eV for thymine). Desfrancois *et al.*¹⁶ determined, using Rydberg electron transfer spectroscopy, the AEAs of uracil, thymine, and adenine to be 0.054 ± 0.035 eV, 0.068 ± 0.020 eV, and 0.012 ± 0.005 eV, respectively. These small AEAs were believed to arise from dipole-bound anion states, the existence of which was predicted theoretically by Adamowicz and coworkers.^{17,18}

On the other hand, experimental and theoretical studies of the conventional valence anion of NABs have also been reported. Desfrancois *et al.*¹⁶ detected what appear to be the conventional valence anions for uracil and thymine, but not for adenine, although the absolute values for the corresponding AEAs could not be determined. This observation was consistent with the theoretical prediction of Sevilla *et al.*¹⁹ In a photodetachment-photoelectron (PD-PE) spectroscopy study, Schiedt *et al.*²⁰ estimated the gas-phase AEAs of uracil, thymine, and cytosine arising from the valence anion states by extrapolating the electron affinities of NABs

and their complexes with up to five water molecules. The determined AEAs were 0.150 ± 0.120 , 0.120 ± 0.120 , and 0.130 ± 0.120 eV for uracil, thymine, and cytosine, respectively. As Wesolowski *et al.*²¹ concluded in their DFT study on gas-phase AEAs of NABs, it is generally believed that the conventional (valence-bound) anions of the NABs are not bound or are, at most, weakly bound ($EA \leq 0.2$ eV).

The electron affinities of NABs in aqueous solution may be quite different from those in the gas phase. Indeed, another important observation in the PD-PE spectroscopy study of Schiedt *et al.*²⁰ was that the electron affinities of thymine, uracil, and cytosine increased linearly with the number of hydrating water molecules. Thus, quantifying the effects of solvation on the electron affinities of NABs is crucial to understand the mechanism of radiation-induced DNA damage in aqueous solution and in living organisms. In this study, we have probed the effects of microsolvation on the electron affinity of thymine. Although some theoretical studies on the electron affinities of thymine have been reported previously,^{10,19,21-25} most have dealt with a gas-phase AEA. Li *et al.*²² have investigated the AEAs of thymine using the polarized continuum model (PCM), but this approach cannot account for key effects like intermolecular hydrogen bonding between solvent and solute. We have investigated the effect of solvation explicitly by considering structures of thymine complexed with up to five water molecules.

2.3 COMPUTATIONAL METHODS

All geometry optimizations and harmonic vibrational frequency analyses have been performed using the Gaussian 94 package of programs.²⁶ To construct the thymine-water clusters, we began with the canonical structure of thymine (Figure 2.1) among its various tautomeric forms, assuming that all water molecules in the microsolvation shell bind directly to thymine through at least one hydrogen bond. While the two oxygen atoms in thymine could potentially form hydrogen bonds with water molecules above or below the plane of the thymine ring, such an arrangement would not be favorable, due to the resulting disruption of resonance between the nitrogen lone pairs and the carbonyl groups. As such, only structures with the water molecules placed roughly in the plane of thymine were considered.

The equilibrium structures of thymine and its complexes with up to five water molecules have been fully optimized using the B3LYP density functional, which is Becke's three-parameter functional (B3)²⁷ with the correlation functional of Lee, Yang, and Parr (LYP).²⁸ We employed a double- ζ quality basis set with polarization and diffuse functions (DZP++), constructed by adding one set of *p*-type polarization functions for each H atom and one set of five *d*-type polarization functions for each C, N, and O atom [where $\alpha_p(\text{H})=0.75$, $\alpha_d(\text{C})=0.75$, $\alpha_d(\text{N})=0.80$, and $\alpha_d(\text{O})=0.85$] to the Huzinaga-Dunning *sp* contractions.^{29,30} This set was further augmented with one even tempered *s*-diffuse function for each H atom and even tempered *s*- and *p*-diffuse

functions for each heavy atom to complete the DZP++ basis set. The even tempered orbital exponents were determined according to the prescription of Lee and Schaefer³¹ [$\alpha_s(\text{H})=0.04415$, $\alpha_s(\text{C})=0.04302$, $\alpha_p(\text{C})=0.03629$, $\alpha_s(\text{N})=0.06029$, $\alpha_p(\text{N})=0.05148$, $\alpha_s(\text{O})=0.08227$, and $\alpha_p(\text{O})=0.06508$]. The final DZP++ basis set contains six functions per H atom and 19 functions per C, N, or O atom.

We also fully optimized the respective anions of thymine and its hydrates using the B3LYP functional with the DZP++ basis set. In this study, we considered the vertical detachment energy (VDE), adiabatic electron affinity (AEA), and absolute AEA (AEA_{abs}), which were given by the following definitions:

$$\text{VDE} = E(\text{neutral at optimized anion geometry}) - E(\text{optimized anion})$$

$$\text{AEA} = E(\text{optimized neutral}) - E(\text{optimized anion})$$

$$\text{AEA}_{\text{abs}} = E(\text{global minimum optimized neutral}) - E(\text{global minimum optimized anion}).$$

All stationary points presented were confirmed to be minima by the absence of imaginary frequencies in the harmonic vibrational frequency analyses. Extensive calibrative studies have shown the DZP++ B3LYP method to be particularly well suited to the prediction of electron affinities.³²

2.4 RESULTS

Geometries of the thymine complexes with up to five water molecules and their respective anions have been optimized at the B3LYP/DZP++ level of theory. Structures of all optimized local minima are included as supplementary material³³ and their relative energies (E_{rel}) and hydration energies (E_{hyd}) are listed in Table 2.1. For convenience, we denote the neutral hydrated thymine clusters with a number followed by a letter. The number indicates the number of the hydrating water molecules for a given neutral structure and the letter represents its relative stability among the structures with the same hydration number, based on their zero-point vibrational energy (ZPVE)-corrected energies. For example, **2C** refers to the third stable structure among neutral dihydrates. The corresponding anion for a given neutral hydrate is indicated with a negative-sign superscript, (*e.g.*, **2C**⁻). Note that the letter in the notation for anionic species refers to the relative stability of the corresponding neutral species, not of the anionic species. This allows for direct structural comparisons, *e.g.*, **2C** vs. **2C**⁻.

2.4.1 THYMINE MONOHYDRATES AND THEIR ANIONS

Four structures for thymine monohydrate have been found and displayed in Figure 2.2 along with the geometries of the respective anions. In the most stable structure, **1A**, the water molecule forms a cyclic hydrogen bond (*i.e.*, involving two hydrogen bonds) with thymine via

the H₁ and O₂ atoms (See Figure 2.1 for numbering). The N₁-H₁⋯O_w and O_w-H_w⋯O₂ hydrogen bond lengths are 1.923 and 1.894 Å, respectively (where O_w and H_w indicate the water oxygen and hydrogen). The formation of this cyclic hydrogen bond system in **1A** contributes to a hydration energy (E_{hyd}) of 8.4 kcal mol⁻¹. This dissociation energy (T·H₂O → T + H₂O) is much greater than the standard hydrogen bond energy (~5 kcal mol⁻¹) for the water dimer, supporting the conclusion that the thymine monohydrate incorporates two hydrogen bonds. Cyclic hydrogen bond formation is also found in structures **1B** and **1C**, which are higher in energy than **1A** by 1.6 and 1.9 kcal mol⁻¹, respectively. Although all the three monohydrates have O_w-H_w⋯N and N-H⋯O_w hydrogen bonds in common, monohydrate **1A** shows the greater stability over **1B** and **1C**, due to its dipole moment of 3.69 Debye, which is smaller than those of the other two (4.79 and 5.01 Debye for **1B** and **1C**, respectively). On the other hand, the least stable structure, **1D**, does not involve a cyclic hydrogen bond, and lies 3.8 kcal mol⁻¹ above **1A**. Clearly, the two hydrogen bonds involved in the formation of a cyclic hydrogen bond are an important factor in the stabilization of thymine monohydrates.

The energy ordering for the anionic thymine monohydrates is different from that for the neutrals: while structure **1B** lies 1.6 kcal mol⁻¹ above **1A**, the former's corresponding anion, **1B**⁻, which is the most stable among the anionic monohydrates, lies 1.8 kcal mol⁻¹ below **1A**⁻. The most pronounced geometrical changes in **1B** upon electron attachment (to form **1B**⁻) are a

shortening of the $O_w-H_w\cdots O_4$ hydrogen bond by 0.251 Å (to a rather short 1.635 Å) and an increase in the $N_3-H_3\cdots O_w$ hydrogen bond distance by 0.567 Å (to a very long 2.530 Å). The increase in the $O_w-H_w\cdots O_4$ angle also reflects the changes in the strength of the intermolecular hydrogen bonds. These changes are due to the presence of the negative charge, which is localized on the thymine moiety in anion $1B^-$. Figure 2.3 shows the singly occupied molecular orbital (SOMO) of $1B^-$. Because an electron now occupies the π^* orbital of thymine, as shown in Figure 2.3, the excess charge is localized mainly on the thymine moiety. If the thymine moiety forms a hydrogen bond with a water molecule as a hydrogen-bond acceptor (as depicted in the $O_w-H_w\cdots O_4$ bond), the result is a strengthening of the hydrogen bond. On the contrary, a hydrogen bond where the thymine moiety acts as a hydrogen-bond donor (as in the $N_3-H_3\cdots O_w$ bond) is unfavorable because electron density is transferred from water to thymine, resulting in more localization of negative charge on the thymine moiety.

The same offsetting effects can be found in the other two cyclic hydrogen-bonded structures, $1A^-$ and $1C^-$. The stability of the second stable anionic monohydrate, $1D^-$, is also related to this effect: in this case there is only one hydrogen bond ($O_w-H_w\cdots O_4$), in which thymine acts as a hydrogen bond acceptor and electron density is transferred from thymine to water without the offsetting transfer from water back to thymine, as in the other three structures. As such,

structure **1D**⁻ lies only 0.3 kcal mol⁻¹ above **1B**⁻, even though the corresponding neutral **1D** was the highest-lying neutral minimum structure.

2.4.2 THYMINE DIHYDRATES AND THEIR ANIONS

Selected structures for the neutral and anionic dihydrates are displayed in Figure 2.4. In the most stable dihydrate, **2A**, two water molecules form a cyclic hydrogen bond via H₁ and O₂. The stabilization due to the hydration from **1A** to **2A**, which is estimated from the difference in E_{hyd} between **1A** (8.4 kcal mol⁻¹) and **2A** (18.5 kcal mol⁻¹), is 10.1 kcal mol⁻¹. Because the predicted dimerization energy of water is 5.6 kcal⁻¹ at the B3LYP/DZP++ level, structure **2A** can be considered to show an additional stability of 4.5 (= 10.1 - 5.6) kcal mol⁻¹, due to the increase in the intermolecular hydrogen bond strength between thymine and the water molecules. Note that the O_w-H_w...O₂ and N₁-H₁...O_w hydrogen bond lengths in **2A** are both shorter than those of **1A** by 0.147 Å. In general, the strength of X-H...O hydrogen bonds (X=N, O) is maximized when the X-H...O hydrogen bond angle is linear. However, in **1A**, where only one water molecule is involved in a cyclic hydrogen bond, the N₁-H₁...O_w and O_w-H_w...O₂ bond angles (143.6° and 145.7°, respectively) deviate from linearity, and the resulting hydrogen bonds in **1A** are relatively weak. In **2A**, on the other hand, hydration with two water molecules allows for

nearly linear $N_1-H_1\cdots O_w$ and $O_w-H_w\cdots O_2$ bond angles (176.8° and 168.6° , respectively) and the intermolecular hydrogen bonds between thymine and water molecules become stronger.

The formation of one cyclic hydrogen bond involving two water molecules is energetically more favorable than the formation of two cyclic hydrogen bonds involving one water molecule. For example, structure **2C**, in which one water molecule is hydrogen bonded to thymine via H_1 and O_2 atoms and the other water via the H_3 and O_4 , lies $3.0 \text{ kcal mol}^{-1}$ above **2A**. Structure **2C** lies even higher in energy than dihydrate **2B** (by $0.4 \text{ kcal mol}^{-1}$), in which two water molecules are associated with thymine via the H_3 and O_4 atoms. The stabilization energy of **2C** can be considered to be additive: E_{hyd} of $15.5 \text{ kcal mol}^{-1}$ for **2C** is almost the same as the sum of E_{hyd} for **1A** and **1B** ($15.2 \text{ kcal mol}^{-1} = 8.4 \text{ kcal mol}^{-1} + 6.8 \text{ kcal mol}^{-1}$).

As mentioned in the previous section, because electron attachment to the neutral monohydrates strengthens the $O_w-H_w\cdots O$ hydrogen bonds and weakens the $N-H\cdots O_w$ hydrogen bonds, the resulting hydrogen bond angles of the anionic monohydrates are almost linear. Thus, in the anionic dihydrates, the formation of a cyclic hydrogen bond involving two water molecules cannot result in the additional stabilization found in the neutral dihydrates. Indeed, the most stable anionic dihydrate, **2H⁻**, does not have such a cyclic hydrogen bond. It can be considered as a combined structure of the two lowest anionic monohydrates, **1B⁻** and **1D⁻**, in which both of the water molecules form hydrogen bonds to thymine via the O_3 atom. Another

notable structure among the anionic dihydrates is complex **2B⁻**, which lies 1.4 kcal mol⁻¹ above **2H⁻**. In the corresponding neutral, **2B**, the two water molecules form a cyclic hydrogen bond via the H₃ and O₄ atoms. In **2B⁻**, however, electron attachment results in the shift of a water molecule by breaking of the N₃-H₃···O_w hydrogen bond and formation of the O_w-H_w···O₂ hydrogen bond (See Figure 2.4). As a result, **2B⁻** can be stabilized more effectively, because both water molecules act as a hydrogen bond donor, which can delocalize the negative charge on the thymine moiety.

2.4.3 THYMINE TRI-, TETRA-, AND PENTAHYDRATES AND THEIR ANIONS

Figure 2.5 shows the most stable structures for neutral tri-, tetra-, and pentahydrates of thymine. Because four local minima were found for the monohydrate, we can consider that thymine has four water-binding sites. Considering the relative energies of the monohydrates, the most favorable is the space between the H₁ and O₂ atoms (as in **1A**). After this site is occupied with up to two water molecules (as in **2A**), further hydration is expected at the next favorable site, that is, between the H₃ and O₄ (as in **1B**). Indeed, as one can see in Figure 2.5, the most stable tri- and tetrahydrates, **3A** and **4A**, correspond to structures in which one and two water molecules bind to the dihydrate **2A** through the O_w-H_w···O₄ and N₃-H₃···O_w hydrogen bonds, respectively. Further hydration with one more water molecule results in pentahydrate

5A, in which all five water molecules participate in cyclic hydrogen bonding with thymine and at least one other water molecule.

The most stable structures for the anionic tri-, tetra-, and pentahydrates are presented in Figure 2.6. The most stable anionic tri- and tetrahydrates, **3H⁻** and **4D⁻**, correspond to structures in which one and two water molecules are added to the most stable dihydrate, **2H⁻**, through O_w-H_w⋯O₂ and N₁-H₁⋯O_w hydrogen bond, respectively. Although anion **4D⁻** has the lowest ZPVE-corrected energy among the anionic tetrahydrates, the energy without the ZPVE-correction is higher by 0.5 kcal mol⁻¹ than that of the second stable structure, **4H⁻** (Figure 2.7). The difference in ZPVE-corrected energies between them is only 0.3 kcal mol⁻¹. Indeed, as one can see from Figures 2.6 and 2.7, the most stable pentahydrate, **5D⁻**, can be considered to arise from further hydration of **4H⁻**, not **4D⁻**.

2.4.4 ELECTRON AFFINITIES OF THYMINE AND ITS HYDRATES

Tables 2.2 and 2.3 list the computed electron affinities of thymine and its hydrates with up to five water molecules, and Figure 2.8 displays the VDE for the most stable anionic hydrates, AEA for the most stable anionic and neutral hydrates, and AEA_{abs}, as a function of the number of hydrating water molecules. Schiedt *et al.*²⁰ have found that the VDE for thymine increases with the hydration number. As shown in Figure 2.8, the presently predicted VDEs for the most

stable anionic hydrates increase gradually with the number of hydration. Note that we used the VDE and AEA of $4\mathbf{H}^-$ instead of the values of $4\mathbf{D}^-$. The VDE for the lowest ZPVE-corrected structure, $4\mathbf{D}^-$, is 1.37 eV, and lower than that of $3\mathbf{H}^-$ (1.46 eV). As mentioned before, the ZPVE-corrected energy of $4\mathbf{D}^-$ differs only by 0.3 kcal mol⁻¹ from that of the second stable structure, $4\mathbf{H}^-$, and the most stable anionic pentahydrate, $5\mathbf{D}^-$, arises from further hydration of $4\mathbf{H}^-$, not $4\mathbf{D}^-$. In addition, the experimental photoelectron spectra usually arise from a Boltzmann distribution of energetically accessible structures, not from the global minimum structure. Thus, if we use the VDE of $4\mathbf{H}^-$ instead of that of $4\mathbf{D}^-$, the resulting plot increases almost linearly with the hydration number, consistent with experiment.²⁰ The AEA of the thymine anion also increases gradually with the hydration number if we use the AEA of $4\mathbf{H}^-$ (0.86 eV). The computed AEAs for the most stable neutrals and absolute AEAs (AEA_{abs}) become larger upon hydration in general. The increase in the AEA of thymine indicates that thymine can form a thermodynamically stable anion in aqueous solution (relative to the neutral thymine molecule). However, it should be noted that the increased AEA does not indicate kinetic stability of the thymine anion, since it is readily protonated in aqueous solution at the O₄ atom and as well as competitively at the C₆ position.³⁴⁻³⁶ Thus, the thymine anion should be considered as an intermediate during cascades of reactions leading to radiation-induced DNA damage.

It seems likely that hydration effect increases the AEA of adenine-thymine (AT) base pair as well. Richardson *et al.* predicted the gas-phase AEA of the AT base pair to be 0.36 eV at the B3LYP/DZP++ level of theory.³⁷ This value is smaller than the AEA of the monohydrate thymine **1B** (0.45 eV). On the other hand, in a DFT study of Kumar *et al.*,³⁸ the AT base pair hydrated with 5 and 13 water molecules was found to have an AEA of 0.97 and 0.92 eV at the B3LYP/6-31+G** level of theory, respectively. Although the basis sets used in these two studies were not the same, this difference is not expected to change the qualitative results.

2.5 CONCLUSIONS

We have optimized the geometries of neutral and anionic thymine hydrates with up to five water molecules, along with predicted vertical detachment energies and adiabatic electron affinities. In general, the lowest-energy structures for neutral and anionic thymine-water clusters follow an *aufbau* principle, with each successive solvating water molecule being added to the previous lowest energy structure. An exception is the hydration from **4D⁻** to **5D⁻**, where reorganization of water molecules is necessary. Instead, it is more likely that the global minimum **5D⁻** results from a low-lying anionic tetrahydrate, **4H⁻**, because further hydration of **4H⁻** can give **5D⁻** without substantial reorganization. Indeed, without ZPVE correction, **4H⁻** is lower in energy than **4D⁻**. Accounting for ZPVE effects, **4H⁻** is just 0.3 kcal mol⁻¹ higher lying

than the global minimum tetrahydrate $4\mathbf{D}^-$, which is within the expected error bounds of the theoretical methods.

Examining the present results for *neutral* mono- through pentahydrated thymine, clear rules emerge regarding energetically favorable arrangements of water molecules in the first solvation shell:

- (1) For the neutral monohydrates, cyclic arrangements of hydrogen bonds are favored over structures in which water participates in only one hydrogen bond.
- (2) For the higher hydrates, cyclic arrangements incorporating two water molecules and thymine are favored over those in which each water molecule forms a cyclic hydrogen bond individually.
- (3) Water-binding sites in thymine (Figure 2.9) are populated in the order: $A > B > C > D$.

While these rules will not be strictly followed in the case of other NABs, they provide general guiding principles for the exploration of low-lying structures of microsolvated uracil, cytosine, guanine, and adenine. On the other hand, this paradigm is altered somewhat upon electron attachment to form the corresponding anion species, primarily due to the strengthening of the $\text{O}_w\text{-H}_w\cdots\text{O}$ hydrogen bonds and the weakening of the $\text{N-H}\cdots\text{O}_w$ hydrogen bonds. These changes in the hydrogen bonding result in delocalization of excess negative charge on thymine by donating electron density from thymine to water. As a result, anionic structures maximizing the

number of hydrogen bonds in which thymine accepts a proton are favored energetically.

Predicted electron affinities are in good qualitative agreement with results from the PD-PE spectroscopic study of Schiedt, Weinkauff, Neumark, and Schlag²⁰ in which the electron affinity of thymine was shown to increase monotonically with hydration number. In the present work, the VDE and AEA of the pentahydrate are predicted to be 1.60 and 0.91 eV, respectively. Although these estimates are significantly lower than the PCM results of Li *et al.*²² (2.06 eV for the AEA), a direct comparison is not appropriate since our approach considered only microsolvation effect, while the PCM study consider macrosolvation effects. Regardless, it is clear that while the valence bound thymine anion is marginally bound in the gas phase, hydration by just a few water molecules results in a strongly bound anionic system.

2.6 ACKNOWLEDGEMENTS

This research was performed in part using the computational resources of the Research Computing Center (RCC) at the University of Georgia, which is administered by Enterprise Information Technology Services (EITS) and the Office of Research Services (ORS). This work was supported by the U.S. National Science Foundation, Grant CHE-0451445.

2.7 REFERENCES

- ¹ J. Cadet, T. Douki, D. Gasparutto, and J.-L. Ravanat, *Radiat. Phys. Chem.* **72**, 293 (2005).
- ² G. Slupphaug, B. Kavli, and H. E. Krokan, *Mutat. Res.* **531**, 231 (2003).
- ³ B. Boudaiffa, P. Cloutier, D. Hunting, M. A. Huels, and L. Sanche, *Science* **287**, 1658 (2000).
- ⁴ J.-L. Ravanat, T. Douki, and J. Cadet, *J. Photochem. Photobiol., B* **63**, 88 (2001).
- ⁵ J. Cadet, T. Delatour, T. Douki, D. Gasparutto, J.-P. Pouget, J.-L. Ravanat, and S. Sauvaigo, *Mutat. Res.* **424**, 9 (1999).
- ⁶ V. Cobut, Y. Frongillo, J. P. Patau, T. Goulet, M.-J. Fraser, and J.-P. Jay-Gerin, *Radiat. Phys. Chem.* **51**, 229 (1998).
- ⁷ S. M. Pimblott and J. A. LaVerne, in *Radiation Damage in DNA: Structure/Function Relationships at Early Times*, edited by A. F. Fuciarelli and J. D. Zimbrick (Battelle, Columbus, OH, 1995), pp. 3.
- ⁸ D. Srdoc, M. Inokuti, and I. Krajcar-Bronic, in *IAEA CRP Atomic and Molecular Data for Radiotherapy and Radiation Research*, edited by M. Inokuti (IAEA Press, Vienna, 1995), pp. 547.
- ⁹ *ICRU Report 31, Average Energy Required to Produce an Ion Pair*. (International Commission of Radiation Units and Measurements, Washington, DC, 1979).
- ¹⁰ S. P. Walch, *Chem. Phys. Lett.* **374**, 496 (2003).

- ¹¹ E. C. M. Chen, E. S. D. Chen, and W. E. Wentworth, *Biochem. Biophys. Res. Commun.* **171**, 97 (1990).
- ¹² J. R. Wiley, J. M. Robinson, S. Ehdaie, E. C. M. Chen, E. S. D. Chen, and W. E. Wentworth, *Biochem. Biophys. Res. Commun.* **180**, 841 (1991).
- ¹³ E. S. D. Chen, E. C. M. Chen, N. Sane, and S. Shulze, *Bioelectrochemistry and Bioenergetics* **48**, 69 (1999).
- ¹⁴ Q. Zhang and E. C. M. Chen, *Biochem. Biophys. Res. Commun.* **217**, 755 (1995).
- ¹⁵ J. H. Hendricks, S. A. Lyapustina, H. L. de Clercq, J. T. Snodgrass, and K. H. Bowen, *J. Chem. Phys.* **104**, 7788 (1996).
- ¹⁶ C. Desfrancois, H. Abdoul-Carime, and J. P. Schermann, *J. Chem. Phys.* **104**, 7792 (1996).
- ¹⁷ G. H. Roehrig, N. A. Oyler, and L. Adamowicz, *J. Phys. Chem.* **99**, 14285 (1995).
- ¹⁸ N. A. Oyler and L. Adamowicz, *J. Phys. Chem.* **97**, 11122 (1993).
- ¹⁹ M. D. Sevilla, B. Besler, and A.-O. Colson, *J. Phys. Chem.* **99**, 1060 (1995).
- ²⁰ J. Schiedt, R. Weinkauff, D. M. Neumark, and E. W. Schlag, *Chem. Phys.* **239**, 511 (1998).
- ²¹ S. S. Wesolowski, M. L. Leininger, P. N. Pentchev, and H. F. Schaefer, *J. Am. Chem. Soc.* **123**, 4023 (2001).
- ²² X. Li, Z. Cai, and M. D. Sevilla, *J. Phys. Chem. A* **106**, 1596 (2002).
- ²³ S. D. Wetmore, R. J. Boyd, and L. A. Eriksson, *Chem. Phys. Lett.* **322**, 129 (2000).

- ²⁴ N. Russo, M. Toscano, and A. Grand, *J. Comput. Chem.* **21**, 1243 (2000).
- ²⁵ A. A. Voityuk, M. E. Michel-Beyerle, and N. Rosch, *Chem. Phys. Lett.* **342**, 231 (2001).
- ²⁶ M. J. Frisch, G. W. Trucks, H. B. Schlegel, P. M. W. Gill, B. G. Johnson, M. A. Robb, J. R. Cheeseman, T. Keith, G. A. Petersson, J. A. Montgomery, K. Raghavachari, M. A. Al-Laham, V. G. Zakrzewski, J. V. Ortiz, J. B. Foresman, J. Cioslowski, B. B. Stefanov, A. Nanayakkara, M. Challacombe, C. Y. Peng, P. Y. Ayala, W. Chen, M. W. Wong, J. L. Andres, E. S. Replogle, R. Gomperts, R. L. Martin, D. J. Fox, J. S. Binkley, D. J. Defrees, J. Baker, J. P. Stewart, M. Head-Gordon, C. Gonzalez, and J. A. Pople, *Gaussian 94* (Gaussian, Inc., Pittsburgh PA, 1995).
- ²⁷ A. D. Becke, *J. Chem. Phys.* **98**, 5648 (1993).
- ²⁸ C. Lee, W. Yang, and R. G. Parr, *Phys. Rev. B: Condens. Matter Mater. Phys.* **37**, 785 (1988).
- ²⁹ S. Huzinaga, *J. Chem. Phys.* **42**, 1293 (1965).
- ³⁰ T. H. Dunning, *J. Chem. Phys.* **53**, 2823 (1970).
- ³¹ T. J. Lee and H. F. Schaefer, *J. Chem. Phys.* **83**, 1784 (1985).
- ³² J. C. Rienstra-Kiracofe, G. S. Tschumper, H. F. Schaefer, S. Nandi, and G. B. Ellison, *Chem. Rev.* **102**, 231 (2002).
- ³³ See EPAPS Document No. E-JCPSA6-124-301618 for optimized geometries of all structures considered. This document can be reached via a direct link in the online article's HTML reference section or via the EPAPS homepage (<http://www.aip.org/pubservs/epaps.html>).

³⁴ C. von Sonntag, *The Chemical Basis of Radiation Biology*. (Taylor & Francis, Philadelphia, 1987).

³⁵ H. M. Novais and S. Steenken, *J. Am. Chem. Soc.* **108**, 1 (1986).

³⁶ P. C. Shragge and J. W. Hunt, *Radiat. Res.* **60**, 233 (1974).

³⁷ N. A. Richardson, S. S. Wesolowski, and H. F. Schaefer, *J. Phys. Chem. B* **107**, 848 (2003).

³⁸ A. Kumar, P. C. Mishra, and S. Suhai, *J. Phys. Chem. A* **109**, 3971 (2005).

Table 2.1. Relative energies (E_{rel}) and hydration energies (E_{hyd}) in kcal mol⁻¹ of thymine hydrates and their anions (ZPVE-corrected values in parentheses). See Figures for numbering of the different structures.

Structure	E_{rel}^a	E_{hyd}^b	Structure	E_{rel}^a	E_{hyd}^c
1A	0.0 (0.0)	10.7 (8.4)	1A⁻	1.6 (1.8)	13.0 (10.9)
1B	1.7 (1.6)	9.0 (6.8)	1B⁻	0.0 (0.0)	14.7 (12.7)
1C	2.1 (1.9)	8.6 (6.5)	1C⁻	2.7 (2.6)	11.9 (10.1)
1D	4.2 (3.8)	6.4 (4.6)	1D⁻	0.5 (0.3)	14.2 (12.4)
2A	0.0 (0.0)	23.3 (18.5)	2A⁻	3.2 (3.9)	24.4 (19.8)
2B	2.8 (2.6)	20.5 (15.9)	2B⁻	0.5 (1.4)	27.1 (22.3)
2C	3.5 (3.0)	19.8 (15.5)	2C⁻	0.1 (0.5)	27.4 (23.2)
2D	3.8 (3.4)	19.5 (15.1)	2D^{-d}	0.5 (1.4)	27.1 (22.3)
2E	4.5 (4.0)	18.8 (14.5)	2E⁻	3.8 (4.1)	23.8 (19.6)
2F	6.2 (5.4)	17.1 (13.1)	2F⁻	0.8 (1.0)	26.8 (22.8)
2G	8.1 (7.1)	15.2 (11.4)	2G⁻	2.0 (1.9)	25.5 (21.8)
2H	8.5 (7.6)	14.8 (10.9)	2H⁻	0.0 (0.0)	27.5 (23.7)
3A	0.0 (0.0)	32.6 (25.6)	3A⁻	1.2 (1.6)	38.9 (32.3)
3B	1.2 (1.1)	31.4 (24.5)	3B⁻	2.0 (2.1)	38.1 (31.7)
3C	1.4 (1.3)	31.2 (24.3)	3C⁻	5.3 (5.5)	34.8 (28.3)
3D	1.9 (1.9)	30.8 (23.7)	3D⁻	0.2 (1.4)	39.8 (32.5)
3E	2.8 (2.4)	29.8 (23.2)	3E⁻	1.9 (2.1)	38.2 (31.7)
3F	3.0 (2.7)	29.6 (22.9)	3F⁻	4.0 (4.4)	36.0 (29.5)
3G	6.5 (6.0)	26.1 (19.7)	3G⁻	0.6 (1.0)	39.5 (32.8)
3H	7.0 (6.1)	25.7 (19.6)	3H⁻	0.0 (0.0)	40.0 (33.9)
3I	7.2 (6.2)	25.5 (19.4)	3I⁻	3.1 (2.8)	37.0 (31.0)
4A	0.0 (0.0)	44.2 (34.8)	4A⁻	1.9 (2.0)	49.6 (40.9)
4B	2.5 (2.3)	41.7 (32.5)	4B⁻	4.2 (4.9)	47.4 (38.0)
4C	3.0 (2.8)	41.2 (31.9)	4C⁻	0.0 (0.9)	51.6 (42.1)
4D	5.7 (5.0)	38.5 (29.8)	4D⁻	0.0 (0.0)	51.5 (42.9)
4E	6.3 (5.5)	37.9 (29.2)	4E⁻	3.4 (3.2)	48.1 (39.8)
4F	7.2 (6.5)	37.0 (28.3)	4F⁻	1.3 (1.1)	50.2 (41.8)
4G	7.9 (6.9)	36.3 (27.9)	4G⁻	2.9 (3.2)	48.7 (39.8)
4H	7.9 (7.2)	36.4 (27.5)	4H⁻	-0.5 (0.3)	52.0 (42.7)
5A	0.0 (0.0)	53.7 (41.8)	5A⁻	1.0 (1.3)	62.6 (50.8)
5B	3.8 (3.2)	49.9 (38.5)	5B⁻	1.8 (1.0)	61.8 (51.1)
5C	5.1 (4.3)	48.5 (37.5)	5C⁻	3.7 (3.5)	59.9 (48.6)
5D	6.8 (6.0)	46.8 (35.7)	5D⁻	0.0 (0.0)	63.6 (52.1)

^a Relative to the most stable structure among anionic or neutral structures with a given hydration number.

^b Enthalpy (0 K) of the reaction: $\text{T} \cdot (\text{H}_2\text{O})_n \rightarrow \text{T} + n\text{H}_2\text{O}$.

^c Enthalpy (0 K) of the reaction: $[\text{T} \cdot (\text{H}_2\text{O})_n]^- \rightarrow \text{T}^- + n\text{H}_2\text{O}$.

^d Structure **2D⁻** is the same as **2B⁻**.

Table 2.2. Vertical detachment energies (VDEs) and adiabatic electron affinities (AEAs) in eV for thymine and its hydrates (ZPVE-corrected values in parentheses). See Figures for the numbering of the different structures.

Structure	VDE	AEA
Thymine	0.68	0.07 (0.20)
1A/1A⁻	0.88	0.17 (0.31)
1B/1B⁻	1.05	0.31 (0.45)
1C/1C⁻	1.00	0.21 (0.36)
1D/1D⁻	1.08	0.40 (0.54)
2A/2A⁻	0.80	0.11 (0.26)
2B/2B⁻	1.31	0.35 (0.48)
2C/2C⁻	1.20	0.40 (0.54)
2D/2D⁻	1.31	0.39 (0.51)
2E/2E⁻	1.16	0.28 (0.42)
2F/2F⁻	1.25	0.48 (0.62)
2G/2G⁻	1.36	0.51 (0.65)
2H/2H⁻	1.34	0.62 (0.75)
3A/3B⁻	1.12	0.34 (0.49)
3B/3B⁻	1.22	0.35 (0.51)
3C/3C⁻	1.01	0.22 (0.37)
3D/3D⁻	1.30	0.46 (0.58)
3E/3E⁻	1.17	0.43 (0.57)
3F/3F⁻	1.34	0.34 (0.48)
3G/3G⁻	1.63	0.65 (0.77)
3H/3H⁻	1.46	0.69 (0.82)
3I/3I⁻	1.49	0.56 (0.70)
4A/4A⁻	1.14	0.30 (0.47)
4B/4B⁻	1.31	0.31 (0.44)
4C/4C⁻	1.39	0.51 (0.64)
4D/4D⁻	1.37	0.63 (0.77)
4E/4E⁻	1.36	0.51 (0.66)
4F/4F⁻	1.40	0.64 (0.78)
4G/4G⁻	1.66	0.60 (0.72)
4H/4H⁻	1.51	0.74 (0.86)
5A/5A⁻	1.28	0.45 (0.59)
5B/5B⁻	1.31	0.58 (0.74)
5C/5C⁻	1.57	0.56 (0.68)
5D/5D⁻	1.60	0.79 (0.91)

Table 2.3. Absolute adiabatic electron affinities (AEA_{abs}) in eV of thymine and its hydrates (ZPVE-corrected values in parentheses).

Hydration number	Structure	AEA_{abs}	
0		0.07	(0.20)
1	1A/1B⁻	0.24	(0.38)
2	2A/2H⁻	0.25	(0.43)
3	3A/3H⁻	0.39	(0.56)
4	4A/4D⁻	0.38	(0.55)
	4A/4H^{-a}	0.40	(0.54)
5	5A/5D⁻	0.50	(0.65)

^a While **4D⁻** has the lowest ZPVE-corrected energy, **4H⁻** is lower lying without ZPVE correction.

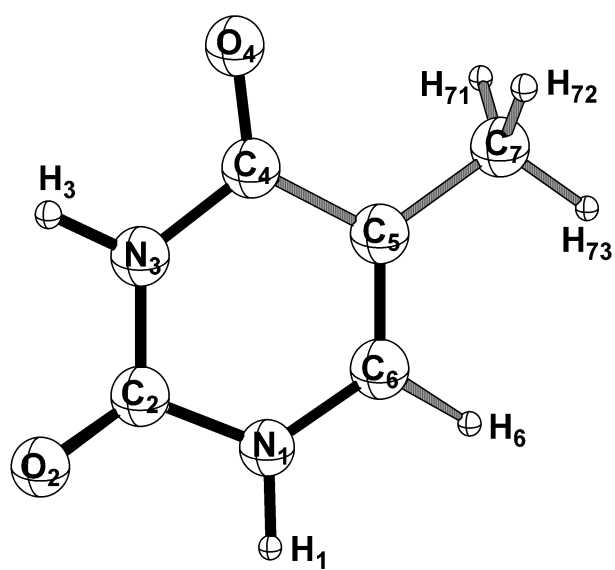
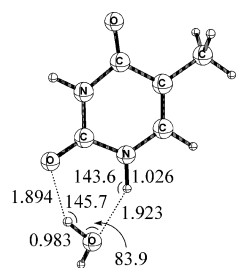
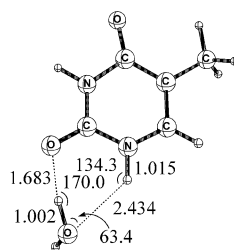


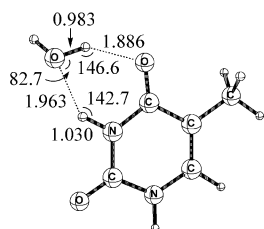
Figure 2.1. Numbering scheme for the canonical structure of thymine.



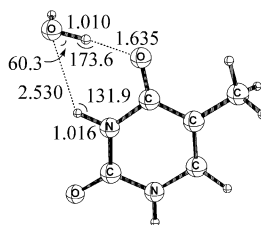
1A



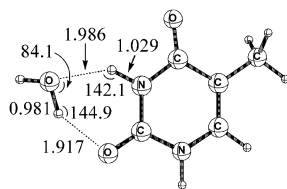
1A⁻



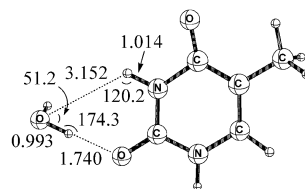
1B



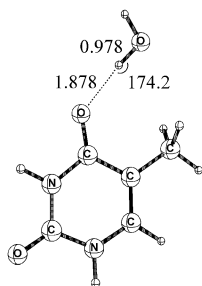
1B⁻



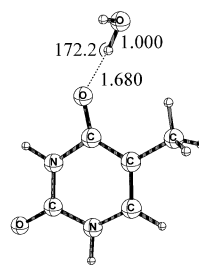
1C



1C⁻



1D



1D⁻

Figure 2.2. Molecular structures for thymine monohydrates (left column) and their respective anions (right column) displaying selected geometrical parameters, optimized at the B3LYP/DZP++ level of theory. Note that all structural parameters were rigorously optimized.

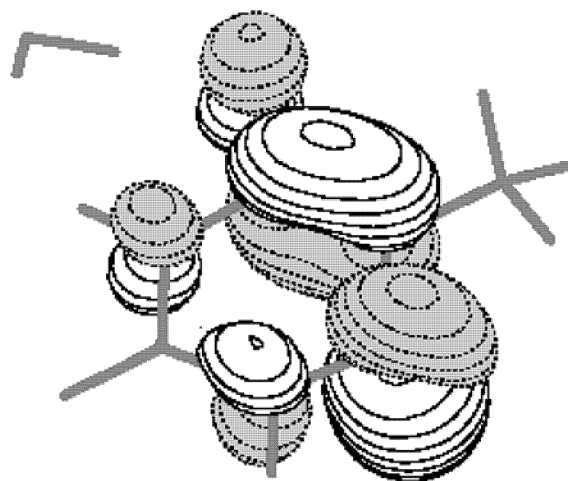


Figure 2.3. Singly-occupied molecular orbital (SOMO) for the thymine monohydrate radical anion $1B^-$.

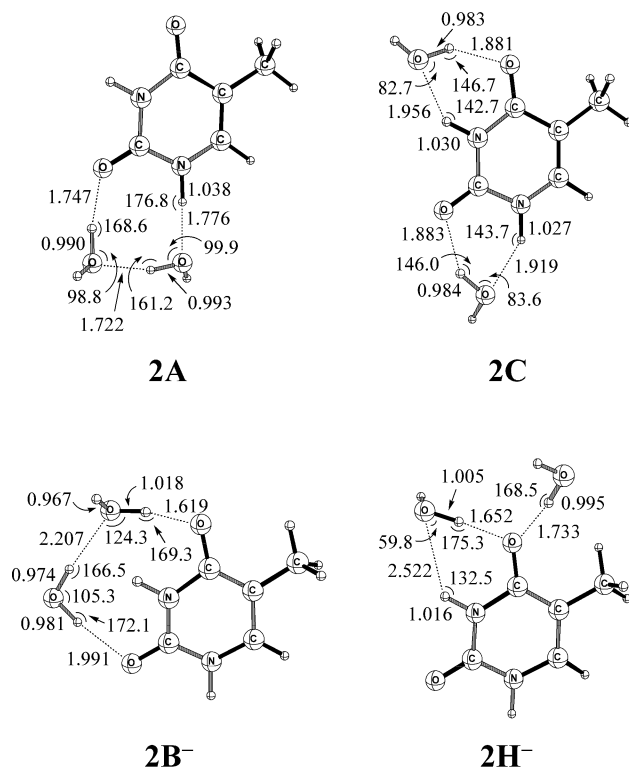
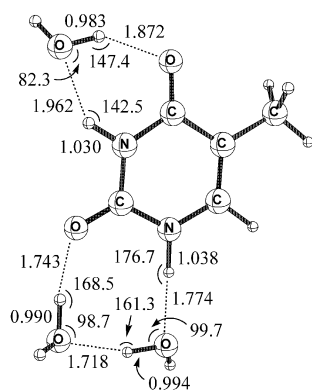
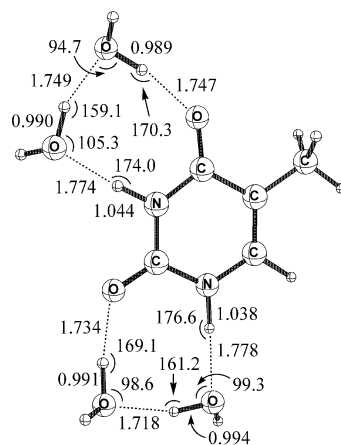


Figure 2.4. Selected structures for neutral (upper row) and anionic (lower row) dihydrates of thymine, optimized at the B3LYP/DZP++ level of theory.

3A



4A



5A

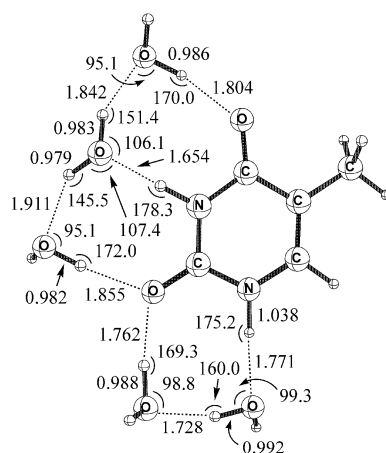


Figure 2.5. The three most stable structures for the neutral tri-, tetra-, and pentahydrates of thymine, optimized at the B3LYP/DZP++ level of theory.

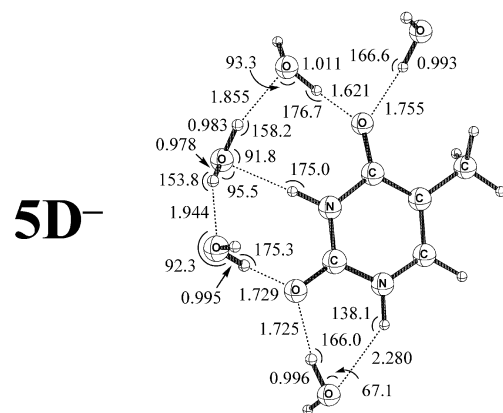
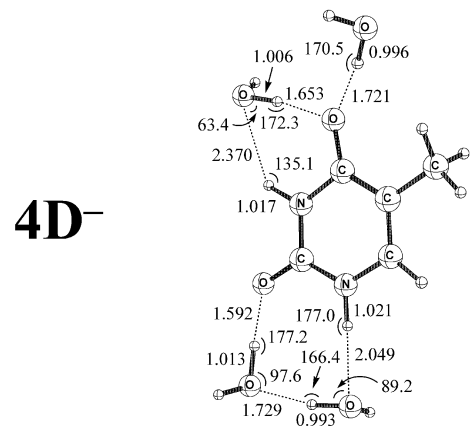
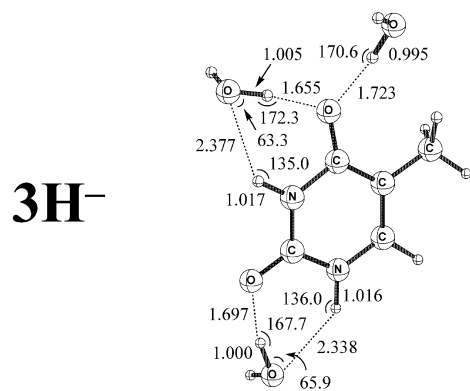


Figure 2.6. The three most stable structures for the anionic tri-, tetra-, and pentahydrates, optimized at the B3LYP/DZP++ level of theory.

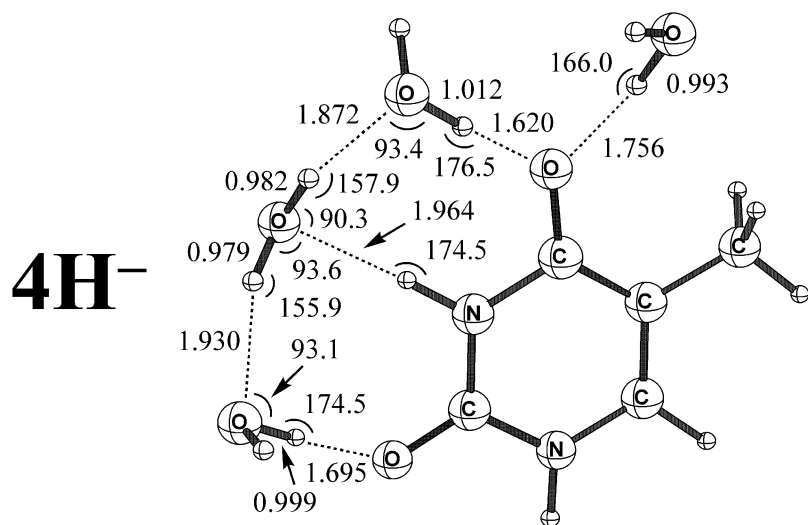


Figure 2.7. The second stable structure **4H⁻** for anionic thymine tetrahydrate, optimized at the B3LYP/DZP++ level of theory. Without ZPVE correction, this structure lies 0.46 kcal mol⁻¹ lower than **4D⁻**.

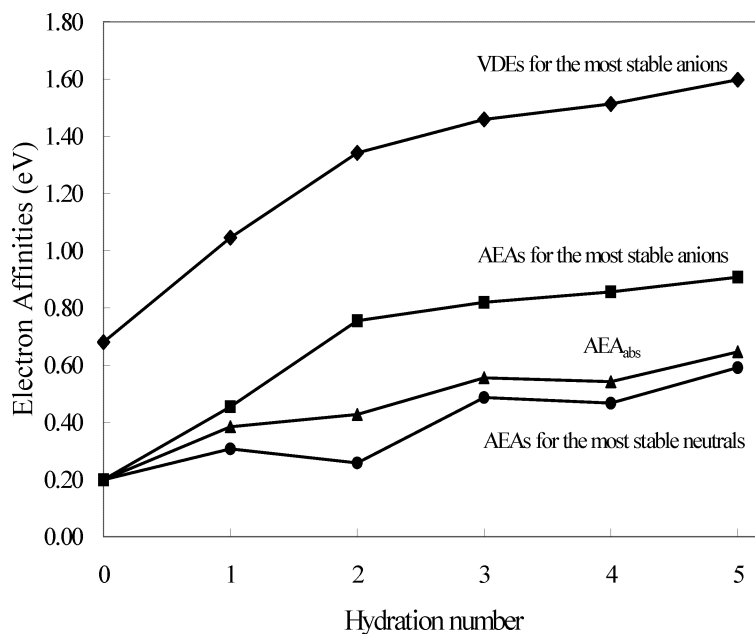


Figure 2.8. Electron affinities (in eV) for thymine hydrates with up to five water molecules: VDEs for most stable anionic hydrates (\blacklozenge); ZPVE-corrected AEAs for the lowest-lying anionic (\blacksquare) and neutral (\bullet) hydrates; and ZPVE-corrected absolute AEAs (\blacktriangle). Note that the VDE and AEA of the second lowest-lying anionic tetrahydrate, $4\mathbf{H}^-$, are placed among the most stable anions. The ZPVE-corrected energy difference between $4\mathbf{H}^-$ and $4\mathbf{D}^-$ is only $0.28 \text{ kcal mol}^{-1}$.

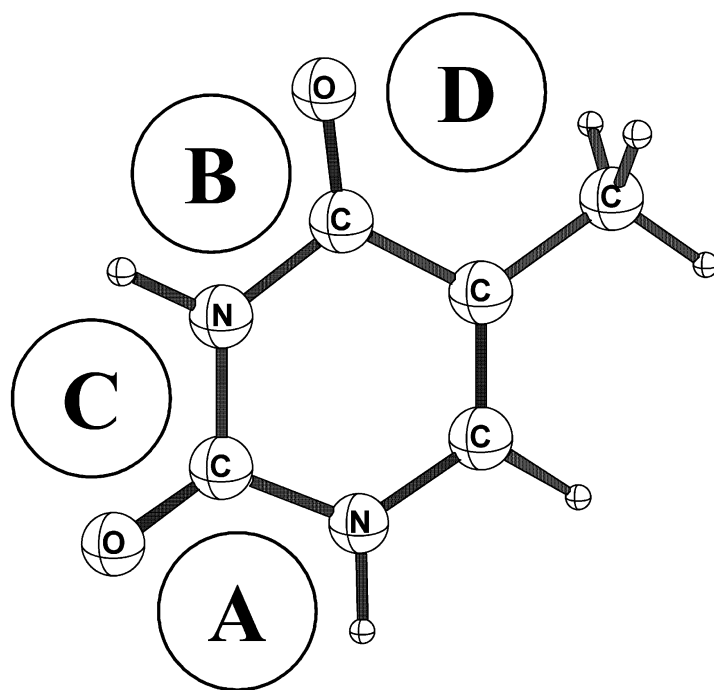


Figure 2.9. Four water-binding sites in thymine, populated in the order: $A > B > C > D$.

CHAPTER 3

MICROHYDRATION OF URACIL AND ITS RADICAL ANION[†]

[†] Reproduced with permission from Sunghwan Kim and Henry F. Schaefer, *J. Chem. Phys.* **125**(14), 144305/1-9 (2006). Copyright 2006, American Institute of Physics.

3.1 ABSTRACT

Microsolvation effects on the stabilities of uracil and its anion have been investigated by explicitly considering the structures of complexes of uracil with up to five water molecules at the B3LYP/DZP++ level of theory. For all five systems, the global minimum of the neutral cluster has a different equilibrium geometry from that of the radical anion. Both the vertical detachment energy (VDE) and adiabatic electron affinity (AEA) of uracil are predicted to increase gradually with the number of hydrating molecules, qualitatively consistent with experimental results from a photodetachment-photoelectron (PD-PE) spectroscopy study [Chem. Phys. **239**, 511 (1998)]. The trend in the AEAs implies that while the conventional valence radical anion of uracil is only marginally bound in the gas phase, it will form a stable anion in aqueous solution. The gas-phase AEA of uracil (0.24 eV) was higher than that of thymine by 0.04 eV and this gap was not significantly affected by microsolvation. The largest AEA is that predicted for uracil·(H₂O)₅, namely 0.96 eV. The VDEs range from 0.76 eV to 1.78 eV.

3.2 INTRODUCTION

DNA damage arising from exposure to high-energy radiation may cause mutations of living organisms.¹⁻⁴ A key step in this radiation-induced DNA damage is thought to involve electron trapping on nucleic acid bases (NABs).⁴⁻⁸ Because the electron affinity of a molecule is a thermodynamic parameter reflecting its electron capturing ability, the electron affinities of NABs and larger DNA and RNA subunits are central to understanding the mechanism of radiation-induced DNA damage.

The first empirical estimates for the gas-phase adiabatic electron affinities (AEAs) of five DNA and RNA bases, adenine, cytosine, guanine, thymine, and uracil were derived by Chen *et al.*,⁹ from the AEAs of pyrimidine and purine using substitution and replacement rules. The AEAs for all five NABs were incorrectly thought to be 0.6 eV or larger, which were similar to those obtained from the scaled reversible reduction potentials^{10,11} and also comparable with the theoretical results using the Austin Model 1 (AM1) semiempirical method.^{11,12} These results suggested that anions of the NABs were strongly bound.

Adamowicz and coworkers¹³⁻¹⁵ theoretically predicted the existence of the stable anions of NABs, and their AEAs were much smaller than the estimates of Chen and coworkers (0.086, 0.088, and 0.122 eV for uracil,¹³ thymine,¹⁴ and adenine,¹⁵ respectively). These so-called “dipole-bound” anions of Adamowicz are distinct from the conventional (valence-bound) anions in that an excess electron is trapped in a dipole field of the neutral molecule, rather than occupying the valence antibonding orbitals. Subsequently, the existence of the dipole-bound anions of NABs was proved experimentally as well.

Using Rydberg electron transfer (RET) spectroscopy, Schermann and coworkers¹⁶ detected the dipole-bound anions of uracil, thymine, and adenine with the AEAs of 0.054 ± 0.035 , 0.068 ± 0.020 , 0.012 ± 0.005 eV, respectively. In a negative ion photoelectron spectroscopy (PE) study, Bowen and coworkers¹⁷ determined the AEAs of uracil and thymine to be 0.093 ± 0.007 and

0.069 ± 0.007 eV, respectively. On the other hand, there have also been studies reported on the valence-bound anions of NABs.

Sevilla *et al.*¹⁸ in their 1995 *ab initio* study predicted valence-bound anions to exist for uracil, thymine, and cytosine with AEAs of 0.4, 0.3, and 0.2 eV, respectively. The AEAs for adenine and guanine were negative, implying that their covalent anions are unstable compared to the corresponding neutrals. In the RET spectroscopy study of Schermann and coworkers,¹⁶ what appear to be the conventional valence anions were detected for uracil and thymine, although the absolute values for the corresponding AEAs could not be determined.

Schiedt, Weinkauff, Neumark, and Schlag,¹⁹ employed photodetachment-photoelectron (PD-PE) spectroscopy for the determination of the gas-phase AEAs of uracil, thymine, and cytosine, arising from valence-bound anionic states. Extrapolating from the AEAs of their water clusters, they estimated the AEAs to be 0.150 ± 0.120 , 0.120 ± 0.120 , and 0.130 ± 0.120 eV for uracil, thymine, and cytosine, respectively. In the density functional theory (DFT) study of Wesolowski *et al.* the AEA of uracil was predicted to be the largest among the five NABs, but only ~ 0.2 eV.²⁰ Thus, they concluded that the conventional (valence-bound) anions of NABs are unbound or only marginally bound, in agreement with Schiedt.¹⁹

Although dipole-bound anions may act as intermediates for electron attachment in the gas phase, it is generally agreed that a dipole bound anion should not exist in a biological system

because such diffuse states are strongly destabilized in the condensed (or aqueous) phase.^{21,22} However, the conventional valence anions of NABs are thought to be relevant to the biological system. Thus, when the bare anion experiences solvation effects in a biologically relevant environment, a transformation from dipole-bound to valence anions may be expected. From photoelectron spectra of uracil anions complexed with noble-gas atoms (Ar, Kr, and Xe), Bowen and coworkers²³ observed that the gradual conversion from dipole-bound to covalent anions was observed when the noble-gas atom changed from Ar to Kr to Xe. They also found that only one water molecule was required for complete transformation to valence anions, consistent with the RET spectroscopy study of Periquet *et al.*²⁴

In their PD-PE spectroscopy study of thymine, uracil, and cytosine, Schiedt *et al.*¹⁹ observed that electron affinities which arise from valence anionic states increase linearly with the number of hydrating water molecules. Thus, investigating the effects of microsolvation on the electron affinities of NABs is central to understanding the mechanism of radiation-induced DNA damage in aqueous solution and in living organisms. There have been theoretical studies reported of solvation effects on the electron affinities of uracil,²⁵⁻³¹ as well as studies of its gas-phase electron affinities.³²⁻³⁵ However, most of these investigations considered only one solvating water molecule²⁵⁻²⁷ or focused on the dipole-bound states, which are not relevant to biological systems.^{28,29}

Some researchers³⁰ employed the polarized continuum model (PCM), which cannot account for explicit microsolvation effects such as hydrogen bonding between solute and solvent molecules. In the present study, we have investigated the effect of microsolvation by explicitly considering various structures of uracil hydrated with up to five water molecules. In addition, we discuss the effect of methylation of uracil, by comparing the results from this study with those recently reported for thymine hydrates.³⁶

3.3 COMPUTATIONAL METHODS

Geometry optimizations have been performed using the B3LYP method, which is Becke's three-parameter functional (B3)³⁷ with the correlation functional of Lee, Yang, and Parr (LYP).³⁸ All stationary points were confirmed to be minima by harmonic vibrational frequency analyses. We employed a double- ζ quality basis set with polarization and diffuse functions (DZP++), constructed by adding one set of *p*-type polarization functions for each H atom and one set of five *d*-type polarization functions for each C, N, and O atom [where $\alpha_p(\text{H})=0.75$, $\alpha_d(\text{C})=0.75$, $\alpha_d(\text{N})=0.80$, and $\alpha_d(\text{O})=0.85$] to the Huzinaga-Dunning (9s5p) contractions.^{39,40} This set was further augmented with one even-tempered *s*-diffuse function for each H atom and even-tempered *s*- and *p*-diffuse functions for each heavy atom to complete the DZP++ basis set. The even-tempered orbital exponents were determined according to the prescription of Lee and

Schaefer⁴¹ [$\alpha_s(\text{H})=0.04415$, $\alpha_s(\text{C})=0.04302$, $\alpha_p(\text{C})=0.03629$, $\alpha_s(\text{N})=0.06029$, $\alpha_p(\text{N})=0.05148$, $\alpha_s(\text{O})=0.08227$, and $\alpha_p(\text{O})=0.06508$]. The final DZP++ basis set contains six functions per H atom and 19 functions per C, N, or O atom.

We constructed the initial structures of uracil-water clusters starting from the canonical structure of uracil (Figure 3.1) among its various tautomeric forms, assuming that all water molecules in the microsolvation shell bind directly to uracil through at least one hydrogen bond. Because the hydrogen bond donors and acceptors of uracil (N-H hydrogen atoms and carbonyl oxygen lone pairs) are located in the molecular plane of uracil, water molecules are also roughly located in the molecular plane. The equilibrium structures of uracil and its complexes (with up to five water molecules) optimized at the B3LYP/DZP++ level of theory were used as initial geometries for subsequent optimizations of the analogous anions. In this study, we considered the vertical detachment energy (VDE), adiabatic electron affinity (AEA), and absolute AEA (AEA_{abs}), which are given by the following definitions:

$$\text{VDE} = E(\text{neutral at optimized anion geometry}) - E(\text{optimized anion})$$

$$\text{AEA} = E(\text{optimized neutral}) - E(\text{optimized anion})$$

$$\text{AEA}_{\text{abs}} = E(\text{global minimum optimized neutral}) - E(\text{global minimum optimized anion}).$$

Extensive calibrative studies have shown the B3LYP/DZP++ method to be particularly well suited to the prediction of electron affinities.⁴² All geometry optimizations and harmonic

vibrational frequency analyses have been carried out using the Gaussian 94 package of programs.⁴³

3.4 RESULTS

Table 3.1 lists the relative energies (E_{rel}) and hydration energies (E_{hyd}) of uracil and its hydrates and their respective anions optimized at the B3LYP/DZP++ level of theory. All optimized structures are included as supplementary material.⁴⁴ For convenience, we denote the neutral hydrated uracil with a number followed by a letter. The number indicates the number of the hydrating water molecules for a give neutral structure, and the letter represents its relative stability among the neutral structures with the same hydration number, based on their zero-point vibration energy (ZPVE)-corrected energies. The corresponding anion for a given neutral hydrate is indicated with a superscript negative-sign. Of course, we cannot be certain that the procedures used here will generate all the global minimum structures. The requirement that all waters be adjacent to the uracil rules out some structures which are better represented as a uracil molecule hydrogen bonded to a self-contained water polymer. However, our procedure does guarantee that the structures found here do begin to simulate the uracil molecule in aqueous solution.

3.4.1 URACIL MONOHYDRATES AND THEIR ANIONS

Figure 3.2 depicts four local minima for the uracil monohydrate, along with their respective anions. In the three lowest-lying structures, **1A**, **1B**, and **1C**, a water molecule is associated with uracil through N-H \cdots O_w and O_w-H_w \cdots O hydrogen bonds, which form a N-H \cdots O_w-H_w \cdots O=C cyclic hydrogen bond (where O_w and H_w designate the oxygen and hydrogen atoms of water). The ZPVE-corrected energies of **1B** and **1C** are higher than that of **1A**, by 1.5 and 2.1 kcal mol⁻¹, respectively. This can be rationalized in terms of the larger dipole moments of **1B** and **1C** (4.00, 4.57, and 5.16 Debye for **1A**, **1B**, and **1C**, respectively). At the B3LYP/DZP++ level of theory, the dipole moment of the unhydrated uracil is predicted to be 4.63 Debye and that of water to be 2.13 Debye.

When these highly polar molecules bind together to form the uracil monohydrate, it might be expected that they would bind in a way that minimizes the polarity of the new system. Thus, the smaller dipole moment of **1A** suggests that hydration in **1A** stabilizes the system more efficiently, although the three lowest-lying structures, **1A**, **1B**, and **1C** have the N-H \cdots O_w-H_w \cdots O=C cyclic hydrogen bond in common. The least stable monohydrate, **1D**, also has a cyclic hydrogen bond. Unlike the other monohydrates, however, the cyclic hydrogen bond in **1D** involves a weaker C₅-H₅ \cdots O_w connection of 2.390 Å, instead of a stronger N-H \cdots O_w hydrogen bond. Structure **1D** lies 3.0 kcal mol⁻¹ above **1A**, while the corresponding value for

the thymine analog³⁶ of **1D** is 3.8 kcal mol⁻¹. For other structures, the differences in relative stabilities of the uracil and thymine monohydrates are predicted to be less than 0.2 kcal mol⁻¹.

Electron attachment to the uracil monohydrates significantly changes the O_w-H_w⋯O=C and N-H⋯O_w hydrogen bond lengths. For example, the O_w-H_w⋯O₂ hydrogen bond of **1A**⁻ is shorter by 0.230 Å than that of its corresponding neutral, **1A**, while the N₁-H₁⋯O_w hydrogen bond is longer by 0.531 Å. As shown in Figure 3.3, upon electron attachment, the “last” electron qualitatively occupies the lowest unoccupied molecular orbital (LUMO) of the neutral uracil, and the excess negative charge develops on the uracil moiety. These negative charges can be delocalized upon formation of the O_w-H_w⋯O=C hydrogen bond, in which the hydrogen atom of the water molecule can withdraw electron density from the uracil moiety.

On the other hand, the N-H⋯O_w hydrogen bond accepts more electron density from the water molecule and delocalization through this hydrogen bond is not favorable. Thus, the delocalization of the excess charge shortens the O_w-H_w⋯O=C hydrogen bonds and elongates the N-H⋯O_w hydrogen bonds. These structural changes upon electron attachment alter the energy ordering of the anionic uracil monohydrates, compared to the corresponding neutrals. While **1D** is the least stable among the neutral monohydrates, its corresponding anion, **1D**⁻, is predicted to be the lowest-energy structure for the anionic monohydrate. Because the hydrogen atom in the C-H⋯O_w arrangement is a weak hydrogen bond donor, the transfer of negative charge density

from the water to the uracil moiety is not significant, compared to the other three anionic monohydrates, which have an N-H \cdots O_w hydrogen bond instead of C-H \cdots O_w.

3.4.2 URACIL DIHYDRATES AND THEIR ANIONS

Because four structures were found for the uracil monohydrate, uracil itself might be considered to have four water-binding sites as shown in Figure 3.4. On the basis of the relative stabilities of the monohydrates, the affinity with a water molecule is expected to decrease in the order: A > B > C > D. For the uracil dihydrate, the most stable structure might be expected to be **2C**, where two water molecules occupy the two most favorable water binding sites, as shown in Figure 3.5. However, **2C** is predicted to be the third lowest-energy structure, indeed higher in energy than **2A** and **2B**, by 2.9 and 0.5 kcal mol⁻¹, respectively.

The noticeable feature of **2A** and **2B** is a cyclic hydrogen bond involving two water molecules. Note that additional hydration from **1A** to **2A** or from **1B** to **2B** makes the N-H \cdots O_w and O_w-H_w \cdots O hydrogen bond angles more nearly linear. For example, the hydration from **1A** to **2A** increases the N₁-H₁ \cdots O_w angle from 144.4 to 176.9° and the O_w-H_w \cdots O₂ angle from 144.3 to 168.0°. This linear arrangement of hydrogen bond donors and acceptors in the dihydrates results in stronger hydrogen bonds. Indeed, the N₁-H₁ \cdots O_w and O_w-H_w \cdots O₂ hydrogen bonds are shorter than in **1A** by 0.144 Å and 0.155 Å, respectively. The hydration from **1A** to **2A** gives

the additional stability of $10.0 \text{ kcal mol}^{-1}$ ($= 18.5 - 8.5 \text{ kcal mol}^{-1}$), which is found from the difference in E_{hyd} between **1A** and **2A**. On the other hand, the stabilization due to hydration from **1A** to **2C** is $7.1 \text{ kcal mol}^{-1}$ ($= 15.6 - 8.5 \text{ kcal mol}^{-1}$), which is almost the same as E_{hyd} of **1B** ($6.9 \text{ kcal mol}^{-1}$). That is, when two water molecules bind to uracil through different binding sites, there is no extra stabilization due to the linear arrangement of the hydrogen-bond donor and acceptor.

The most stable anionic dihydrate, **2H⁻**, corresponds to the combined structure of the two most stable anionic monohydrates, **1D⁻** and **1B⁻**. That is, the two water molecules in **2H⁻** occupy different water-binding sites, contrary to the most stable neutral dihydrate, **2A**. For the anionic dihydrate, the stabilization due to cyclic hydrogen bond formation involving two water molecules is not as large as in the corresponding neutrals. Because electron attachment to the neutral monohydrates causes almost linear arrangement of the $\text{O}_w\text{-H}_w\cdots\text{O}$ hydrogen bond, by shortening the $\text{O}_w\text{-H}_w\cdots\text{O}$ hydrogen bond and elongating the $\text{N-H}\cdots\text{O}_w$ hydrogen bond, the additional hydration at the same water-binding site (e.g. from **1A⁻** to **2A⁻**) does not give as much stabilization as in the neutral dihydrates. For example, while the $\text{O}_w\text{-H}_w\cdots\text{O}_2$ angle increases by 23.7° upon hydration from **1A** to **2A**, it changes only by 7.9° upon hydration from **1A⁻** to **2A⁻**.

The formation of a cyclic hydrogen bond involving two water molecules also forces the unfavorable $\text{N-H}\cdots\text{O}_w$ hydrogen bond, which can destabilize the anionic system by transferring

the negative charge density from water to uracil moiety. Because of this, upon electron attachment to **2B**, a water molecule is shifted by breaking $N_3-H_3\cdots O_w$ and forming the $O_w-H_w\cdots O_2$ hydrogen bond. In the resulting anion, **2B⁻**, both water molecules can act as hydrogen bond donors, which can effectively delocalize the extra negative charge on the uracil moiety. Similarly, electron attachment to **2D** (not shown in Figure 3.5), where the two water molecules are associated with uracil through the $N_3-H_3\cdots O_w$ and $O_w-H_w\cdots O_2$ hydrogen bonds, also causes a similar shift of a water molecule and the geometry optimization of **2D⁻** gives the same structure as **2B⁻**.

3.4.3 URACIL TRI-, TETRA-, PENTAHYDRATES AND THEIR ANIONS

On the basis of the results of the neutral mono- and dihydrates of uracil, we suggest that uracil has four potential water-binding sites (Figure 3.4), which are populated in the order of $A > B > C > D$, and each site can be occupied up to two water molecules. Site D may be an exception because it involves formation of a weak $C-H\cdots O_w$ hydrogen bond. Indeed, as shown in Figure 3.6, the most stable structures for the tri-, tetra-, and pentahydrates of the neutral uracil are consistent with our qualitative prediction. In the most stable neutral pentahydrate, **5A**, all water-binding sites except site D are occupied by water molecules, each of which participates in a cyclic hydrogen bond with at least one water molecules.

Figure 3.7 displays the most stable anions of the uracil tri-, tetra-, and pentahydrates. The most stable anionic tri- and tetrahydrates, $3\mathbf{H}^-$ and $4\mathbf{D}^-$, arise from successive hydration of the most stable anionic dihydrate, $2\mathbf{H}^-$. Note that two of the four water molecules in $4\mathbf{D}^-$ occupy different sites separately (sites B and D in Figure 3.4), while the other two form a cyclic hydrogen bond in one water-binding site (site A). This is because, for the anionic hydrates, the delocalization of an excess negative charge on the uracil moiety is an important stabilizing factor (as explained in the previous section), in addition to the formation of a cyclic hydrogen bond involving two water molecules. It is also noticeable that the additional hydration from $4\mathbf{D}^-$ to $5\mathbf{D}^-$ requires significant reorganization of the hydrating water molecules. While structure $4\mathbf{D}^-$ has two water molecules occupy site A, only one water occupies site A in structure $5\mathbf{D}^-$. Instead, it is more likely that $5\mathbf{D}^-$ arises from direct hydration of $4\mathbf{G}^-$ (Figure 3.8). The ZPVE-corrected energy of $4\mathbf{G}^-$ differs only by $0.1 \text{ kcal mol}^{-1}$ from that of $4\mathbf{D}^-$.

3.4.4 ELECTRON AFFINITIES OF URACIL AND ITS HYDRATES

The VDEs and AEAs for uracil and its hydrates are reported in Table 3.2, and AEA_{abs} are summarized in Table 3.3. For the isolated (unhydrated) uracil, the VDE and ZPVE-corrected AEA are predicted to be 0.76 and 0.24 eV, respectively. The small positive value of the AEA suggests that the valence anion of uracil is only slightly bound. Both the VDE and AEA of

uracil increase with the number of hydrating water molecules in general. Figure 3.9 shows the VDEs for the most stable anions, AEAs for the most stable neutrals and anions, and the absolute AEA (AEA_{abs}) as a function of the number of water molecules. The monotonic increase in the AEA of uracil with the hydration number is consistent with the PD-PE spectroscopy study of Schiedt *et al.*¹⁹ Note that the VDE and AEA for the second lowest-lying anionic tetrahydrate ($4G^-$) were used in Figure 3.9, instead of those of the most stable anion, $4D^-$. Both the VDE and AEA of $4D^-$ are slightly smaller than those of the most stable anionic trihydrate, $3H^-$. However, employing the results for $4G^-$ gives nearly linear plots for the most stable anions. Because the difference in the ZPVE-corrected energy between $4D^-$ and $4G^-$ is only $0.1 \text{ kcal mol}^{-1}$, either or both structures might be responsible for the experimental PD-PE spectra for the anionic tetrahydrate.

Figure 3.10 compares the electron affinities of uracil with those of thymine. In the gas phase, the VDE of uracil (0.75 eV) is predicted to be slightly larger (by 0.07 eV) than that of thymine (0.68 eV).³⁶ The 5-methylation of uracil to thymine also lowers the gas-phase AEA (by 0.04 eV from 0.24 eV and 0.20 eV). While the VDE difference between uracil and thymine tends to slightly increase with the hydration number, the AEA difference between uracil and thymine does not change much upon hydration. The largest gap in electron affinities between the two bases occurs for the monohydrates. This is because the most stable anionic *uracil*

monohydrate is **1D**⁻ while the **1B**⁻ analogue is most stable for the *thymine* anionic monohydrates.

3.5 CONCLUSIONS

The effects of microsolvation on the electron affinities of uracil have been investigated by considering the various structures of uracil hydrates (with up to five water molecules) and their respective anions. On the basis of the four structures for the neutral monohydrate and their relative stabilities, uracil may be considered to have four water-binding sites (Figure 3.4), which might be occupied in the order: A > B > C > D. The results for the neutral dihydrate suggest that each site except site D would be occupied by up to two water molecules. These rules of thumb allow us to predict the most stable structure for a given hydration number. However, the hydration pattern for the anionic hydrates was more complicated than that for the neutrals, because the delocalization of an excess negative charge on the uracil moiety is also an important stabilizing factor, as well as cyclic hydrogen bond formation involving two water molecules.

We note that the relative energies for the multiply hydrated uracil anions are rather small between several isomers. Therefore a number of these isomers may be present in a molecular beam of the sort used in photoelectron spectroscopy. These multiple isomers may effect the resulting photoelectron spectra, adding layers of complexity at very high resolution.

The gas-phase VDE and AEA of uracil were predicted to be 0.76 and 0.24 eV, respectively.

They showed gradual increases with the number of hydrating water molecules. For the pentahydrate, the VDE was predicted to be 1.75 eV and the AEA to be 0.96 eV. The present results indicate that while its valence anion is slightly bound in the gas phase, the uracil anion becomes more strongly bound when it clustered with water molecules, consistent with the results from the PD-PE experiments of Schiedt, Weinkauff, Neumark, and Schlag.¹⁹ Although the uracil anion in aqueous solution is thermodynamically stable relative to its neutral, this does not mandate the kinetic stability of the uracil anion. For example, uracil is thought to be protonated readily at the O₄ or C₆ position and then react with certain reactive radical species.⁴ Thus, the uracil anion can be considered as an intermediate during cascades of reactions leading to radiation-induced DNA damage.

3.6 ACKNOWLEDGEMENTS

This research was performed in part using the computational resources of the Research Computing Center (RCC) at the University of Georgia, which is administered by Enterprise Information Technology Services (EITS) and the Office of Research Services (ORS). This work was supported by the U.S. National Science Foundation, Grant CHE-0451445.

3.7 REFERENCES

- ¹ J. Cadet, S. Bellon, T. Douki, S. Frelon, D. Gasparutto, E. Muller, J.-P. Pouget, J.-L. Ravanat, A. Romieu, and S. Sauvaigo, *J. Environ. Pathol. Toxicol. Oncol.* **23**, 33 (2004).
- ² S. S. Wallace, *Free Radical Biol. Med.* **33**, 1 (2002).
- ³ G. Slupphaug, B. Kavli, and H. E. Krokan, *Mutat. Res.* **531**, 231 (2003).
- ⁴ C. von Sonntag, *The Chemical Basis of Radiation Biology*. (Taylor & Francis, Philadelphia, 1987).
- ⁵ S. Steenken, *Chem. Rev.* **89**, 503 (1989).
- ⁶ S. Steenken, J. P. Telo, H. M. Novais, and L. P. Candeias, *J. Am. Chem. Soc.* **114**, 4701 (1992).
- ⁷ A. O. Colson and M. D. Sevilla, *Int. J. Radiat. Biol.* **67**, 627 (1995).
- ⁸ M. A. Huels, I. Hahndorf, E. Illenberger, and L. Sanche, *J. Chem. Phys.* **108**, 1309 (1998).
- ⁹ E. C. M. Chen, E. S. D. Chen, and W. E. Wentworth, *Biochem. Biophys. Res. Commun.* **171**, 97 (1990).
- ¹⁰ J. R. Wiley, J. M. Robinson, S. Ehdaie, E. C. M. Chen, E. S. D. Chen, and W. E. Wentworth, *Biochem. Biophys. Res. Commun.* **180**, 841 (1991).
- ¹¹ E. S. D. Chen, E. C. M. Chen, N. Sane, and S. Shulze, *Bioelectrochem. Bioenerg.* **48**, 69 (1999).
- ¹² Q. Zhang and E. C. M. Chen, *Biochem. Biophys. Res. Commun.* **217**, 755 (1995).

- ¹³ N. A. Oyler and L. Adamowicz, *J. Phys. Chem.* **97**, 11122 (1993).
- ¹⁴ N. A. Oyler and L. Adamowicz, *Chem. Phys. Lett.* **219**, 223 (1994).
- ¹⁵ G. H. Roehrig, N. A. Oyler, and L. Adamowicz, *J. Phys. Chem.* **99**, 14285 (1995).
- ¹⁶ C. Desfrancois, H. Abdoul-Carime, and J. P. Schermann, *J. Chem. Phys.* **104**, 7792 (1996).
- ¹⁷ J. H. Hendricks, S. A. Lyapustina, H. L. de Clercq, J. T. Snodgrass, and K. H. Bowen, *J. Chem. Phys.* **104**, 7788 (1996).
- ¹⁸ M. D. Sevilla, B. Besler, and A.-O. Colson, *J. Phys. Chem.* **99**, 1060 (1995).
- ¹⁹ J. Schiedt, R. Weinkauff, D. M. Neumark, and E. W. Schlag, *Chem. Phys.* **239**, 511 (1998).
- ²⁰ S. S. Wesolowski, M. L. Leininger, P. N. Pentchev, and H. F. Schaefer, *J. Am. Chem. Soc.* **123**, 4023 (2001).
- ²¹ M. D. Sevilla, B. Besler, and A. O. Colson, *J. Phys. Chem.* **98**, 2215 (1994).
- ²² L. Sanche, in *Excess Electrons in Dielectric Media*, edited by C. Ferradini and J. P. Jay-Gerin (CRC Press, Boca Raton, FL, 1991), pp. 24.
- ²³ J. H. Hendricks, S. A. Lyapustina, H. L. de Clercq, and K. H. Bowen, *J. Chem. Phys.* **108**, 8 (1998).
- ²⁴ V. Periquet, A. Moreau, S. Carles, J. P. Schermann, and C. Desfrancois, *J. Electron Spectrosc. Relat. Phenom.* **106**, 141 (2000).
- ²⁵ O. Dolgounitcheva, V. G. Zakrzewski, and J. V. Ortiz, *J. Phys. Chem. A* **103**, 7912 (1999).

- ²⁶ A. F. Jalbout, C. S. Hall-Black, and L. Adamowicz, *Chem. Phys. Lett.* **354**, 128 (2002).
- ²⁷ J. Smets, W. J. McCarthy, and L. Adamowicz, *J. Phys. Chem.* **100**, 14655 (1996).
- ²⁸ C. A. Morgado, K. Y. Pichugin, and L. Adamowicz, *Phys. Chem. Chem. Phys.* **6**, 2758 (2004).
- ²⁹ J. Smets, D. M. A. Smith, Y. Elkadi, and L. Adamowicz, *J. Phys. Chem. A* **101**, 9152 (1997).
- ³⁰ Z. Cai, X. Li, and M. D. Sevilla, *J. Phys. Chem. B* **106**, 2755 (2002).
- ³¹ R.-B. Zhang, X.-D. Zhang, Z.-W. Qu, X.-C. Ai, X.-K. Zhang, and Q.-Y. Zhang, *Journal of Molecular Structure: Theochem* **624**, 169 (2003).
- ³² S. D. Wetmore, R. J. Boyd, and L. A. Eriksson, *Chem. Phys. Lett.* **322**, 129 (2000).
- ³³ N. Russo, M. Toscano, and A. Grand, *J. Comput. Chem.* **21**, 1243 (2000).
- ³⁴ O. Dolgounitcheva, V. G. Zakrzewski, and J. V. Ortiz, *Int. J. Quantum Chem.* **90**, 1547 (2002).
- ³⁵ S. Harinipriya and M. V. Sangaranarayanan, *J. Mol. Struct.* **644**, 133 (2003).
- ³⁶ S. Kim, S. E. Wheeler, and H. F. Schaefer, *J. Chem. Phys.* **124**, 204310 (2006).
- ³⁷ A. D. Becke, *J. Chem. Phys.* **98**, 5648 (1993).
- ³⁸ C. Lee, W. Yang, and R. G. Parr, *Phys. Rev. B* **37**, 785 (1988).
- ³⁹ S. Huzinaga, *J. Chem. Phys.* **42**, 1293 (1965).
- ⁴⁰ T. H. Dunning, Jr., *J. Chem. Phys.* **53**, 2823 (1970).
- ⁴¹ T. J. Lee and H. F. Schaefer, *J. Chem. Phys.* **83**, 1784 (1985).
- ⁴² J. C. Rienstra-Kiracofe, G. S. Tschumper, H. F. Schaefer, S. Nandi, and G. B. Ellison, *Chem.*

Rev. **102**, 231 (2002).

⁴³ M. J. Frisch, G. W. Trucks, H. B. Schlegel, P. M. W. Gill, B. G. Johnson, M. A. Robb, J. R. Cheeseman, T. Keith, G. A. Petersson, J. A. Montgomery, K. Raghavachari, M. A. Al-Laham, V. G. Zakrzewski, J. V. Ortiz, J. B. Foresman, J. Cioslowski, B. B. Stefanov, A. Nanayakkara, M. Challacombe, C. Y. Peng, P. Y. Ayala, W. Chen, M. W. Wong, J. L. Andres, E. S. Replogle, R. Gomperts, R. L. Martin, D. J. Fox, J. S. Binkley, D. J. Defrees, J. Baker, J. P. Stewart, M. Head-Gordon, C. Gonzalez, and J. A. Pople, Gaussian 94 (Gaussian, Inc., Pittsburgh PA, 1995).

⁴⁴ See EPAPS Document No. E-JCPSA6-125-312638 for optimized geometries of all structures considered. This document can be reached via direct link in the online article's HTML reference section or via the EPAPS homepage (<http://www.aip.org/pubservs/epaps.html>).

Table 3.1. Relative energies (E_{rel}) and hydration energies (E_{hyd}) in kcal mol⁻¹ of uracil hydrates and their anions (ZPVE-corrected values in parentheses). See figures for numbering of the different structures.

Structure	$E_{\text{rel}}^{\text{a}}$	$E_{\text{hyd}}^{\text{b}}$	Structure	$E_{\text{rel}}^{\text{a}}$	$E_{\text{hyd}}^{\text{c}}$
1A	0.0 (0.0)	10.7 (8.5)	1A⁻	1.9 (2.3)	13.1 (10.9)
1B	1.6 (1.5)	9.1 (6.9)	1B⁻	0.2 (0.3)	14.8 (12.9)
1C	2.3 (2.1)	8.4 (6.3)	1C⁻	3.0 (3.1)	12.0 (10.2)
1D	3.4 (3.0)	7.3 (5.4)	1D⁻	0.0 (0.0)	15.0 (13.2)
2A	0.0 (0.0)	23.4 (18.5)	2A⁻	4.2 (4.8)	24.4 (19.9)
2B	2.6 (2.4)	20.8 (16.1)	2B⁻	1.3 (2.1)	27.3 (22.6)
2C	3.4 (2.9)	20.0 (15.6)	2C⁻	0.9 (1.3)	27.6 (23.4)
2D	4.0 (3.5)	19.4 (15.0)	2D⁻	1.3 (2.1)	27.2 (22.6)
2E	4.7 (4.1)	18.6 (14.4)	2E⁻	4.7 (4.9)	23.9 (19.8)
2F	5.4 (4.7)	17.9 (13.8)	2F⁻	1.0 (1.1)	27.6 (23.6)
2G	7.4 (6.5)	15.9 (12.0)	2G⁻	2.3 (2.1)	26.3 (22.6)
2H	7.4 (6.5)	16.0 (12.0)	2H⁻	0.0 (0.0)	28.6 (24.7)
3A	0.0 (0.0)	32.8 (25.8)	3A⁻	1.9 (2.4)	39.1 (32.4)
3B	1.1 (1.0)	31.7 (24.8)	3B⁻	2.6 (2.9)	38.4 (32.0)
3C	1.7 (1.6)	31.1 (24.2)	3C⁻	6.1 (6.4)	34.9 (28.4)
3D	2.2 (1.9)	30.6 (23.9)	3D⁻	2.1 (2.3)	38.9 (32.5)
3E	2.1 (2.1)	30.7 (23.7)	3E⁻	1.0 (2.1)	40.0 (32.7)
3F	3.3 (3.0)	29.4 (22.7)	3F⁻	4.5 (5.4)	36.4 (29.4)
3G	5.4 (4.9)	27.4 (20.8)	3G⁻	1.9 (1.9)	39.0 (33.0)
3H	6.0 (5.1)	26.8 (20.6)	3H⁻	0.0 (0.0)	41.0 (34.8)
3I	6.7 (5.8)	26.1 (20.0)	3I⁻	3.3 (3.1)	37.7 (31.8)
4A	0.0 (0.0)	44.5 (35.0)	4A⁻	2.5 (2.7)	49.9 (41.2)
4B	2.9 (2.6)	41.6 (32.4)	4B⁻	4.8 (5.7)	47.6 (38.2)
4C	3.3 (3.1)	41.2 (31.9)	4C⁻	0.6 (1.6)	51.8 (42.3)
4D	4.8 (4.1)	39.7 (30.8)	4D⁻	0.0 (0.0)	52.4 (43.9)
4E	5.9 (5.2)	38.5 (29.8)	4E⁻	3.6 (3.4)	48.8 (40.5)
4F	6.3 (5.5)	38.2 (29.4)	4F⁻	1.0 (0.9)	51.4 (43.0)
4G	7.1 (6.4)	37.4 (28.6)	4G⁻	-0.7 (0.1)	53.1 (43.8)
4H	7.5 (6.5)	37.0 (28.5)	4H⁻	3.0 (3.4)	49.5 (40.5)
5A	0.0 (0.0)	53.6 (41.7)	5A⁻	1.9 (2.2)	62.7 (50.9)
5B	2.5 (2.1)	51.1 (39.6)	5B⁻	1.6 (1.0)	63.0 (52.2)
5C	4.4 (3.7)	49.2 (38.0)	5C⁻	3.9 (3.8)	60.6 (49.4)
5D	5.8 (5.0)	47.8 (36.7)	5D⁻	0.0 (0.0)	64.6 (53.1)

^a Relative to the most stable structure among anionic or neutral structures with a given hydration number.

^b Enthalpy (0 K) of the reaction: $\text{U} \cdot (\text{H}_2\text{O})_n \rightarrow \text{U} + n\text{H}_2\text{O}$.

^c Enthalpy (0 K) of the reaction: $[\text{U} \cdot (\text{H}_2\text{O})_n]^- \rightarrow \text{U}^- + n\text{H}_2\text{O}$.

Table 3.2. Vertical detachment energies (VDEs) and adiabatic electron affinities (AEAs) in eV for uracil and its hydrates (ZPVE-corrected values in parentheses). See figures for the numbering of the different structures.

	VDE	AEA
Uracil	0.76	0.12 (0.24)
1A/1A⁻	0.97	0.23 (0.35)
1B/1B⁻	1.12	0.37 (0.50)
1C/1C⁻	1.09	0.28 (0.41)
1D/1D⁻	1.19	0.45 (0.58)
2A/2A⁻	0.89	0.17 (0.30)
2B/2B⁻	1.40	0.40 (0.52)
2C/2C⁻	1.29	0.45 (0.58)
2D/2D⁻	1.40	0.47 (0.57)
2E/2E⁻	1.25	0.35 (0.48)
2F/2F⁻	1.36	0.54 (0.67)
2G/2G⁻	1.46	0.57 (0.70)
2H/2H⁻	1.44	0.67 (0.79)
3A/3A⁻	1.20	0.39 (0.53)
3B/3B⁻	1.29	0.41 (0.56)
3C/3C⁻	1.11	0.29 (0.43)
3D/3D⁻	1.28	0.48 (0.62)
3E/3E⁻	1.38	0.52 (0.64)
3F/3F⁻	1.50	0.42 (0.53)
3G/3G⁻	1.54	0.62 (0.77)
3H/3H⁻	1.58	0.73 (0.86)
3I/3I⁻	1.60	0.62 (0.75)
4A/4A⁻	1.21	0.35 (0.51)
4B/4B⁻	1.41	0.38 (0.50)
4C/4C⁻	1.48	0.58 (0.69)
4D/4D⁻	1.48	0.67 (0.81)
4E/4E⁻	1.46	0.56 (0.71)
4F/4F⁻	1.57	0.69 (0.83)
4G/4G⁻	1.67	0.80 (0.91)
4H/4H⁻	1.78	0.66 (0.77)
5A/5A⁻	1.37	0.51 (0.64)
5B/5B⁻	1.48	0.64 (0.79)
5C/5C⁻	1.69	0.62 (0.74)
5D/5D⁻	1.75	0.85 (0.96)

Table 3.3. Absolute adiabatic electron affinities (AEA_{abs}) in eV of uracil and its hydrates (ZPVE-corrected values in parentheses).

Hydration number	Structures	AEA_{abs}
0		0.12 (0.24)
1	1A/1D⁻	0.31 (0.45)
2	2A/2H⁻	0.35 (0.51)
3	3A/3H⁻	0.48 (0.64)
4	4A/4D⁻	0.46 (0.63)
	4A/4G^{-a}	0.49 (0.63)
5	5A/5D⁻	0.60 (0.74)

^a While **4D⁻** has the lowest ZPVE-corrected energy, **4G⁻** is lower lying without ZPVE correction.

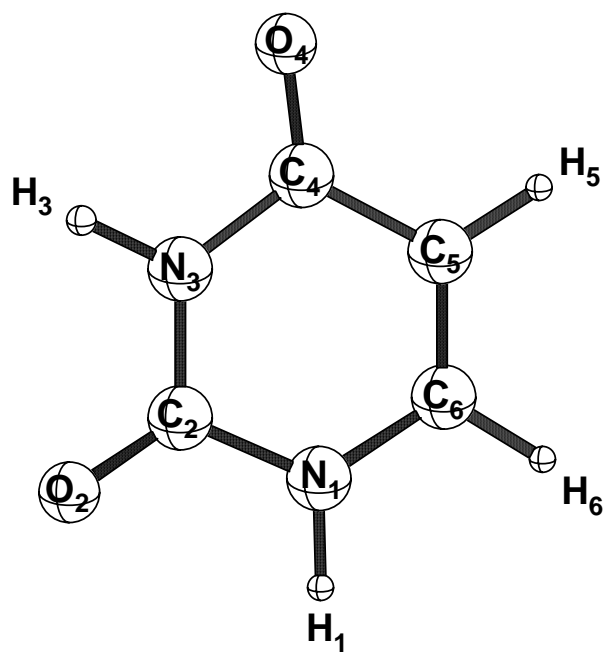


Figure 3.1. Atom numbering scheme for the canonical structure of uracil.

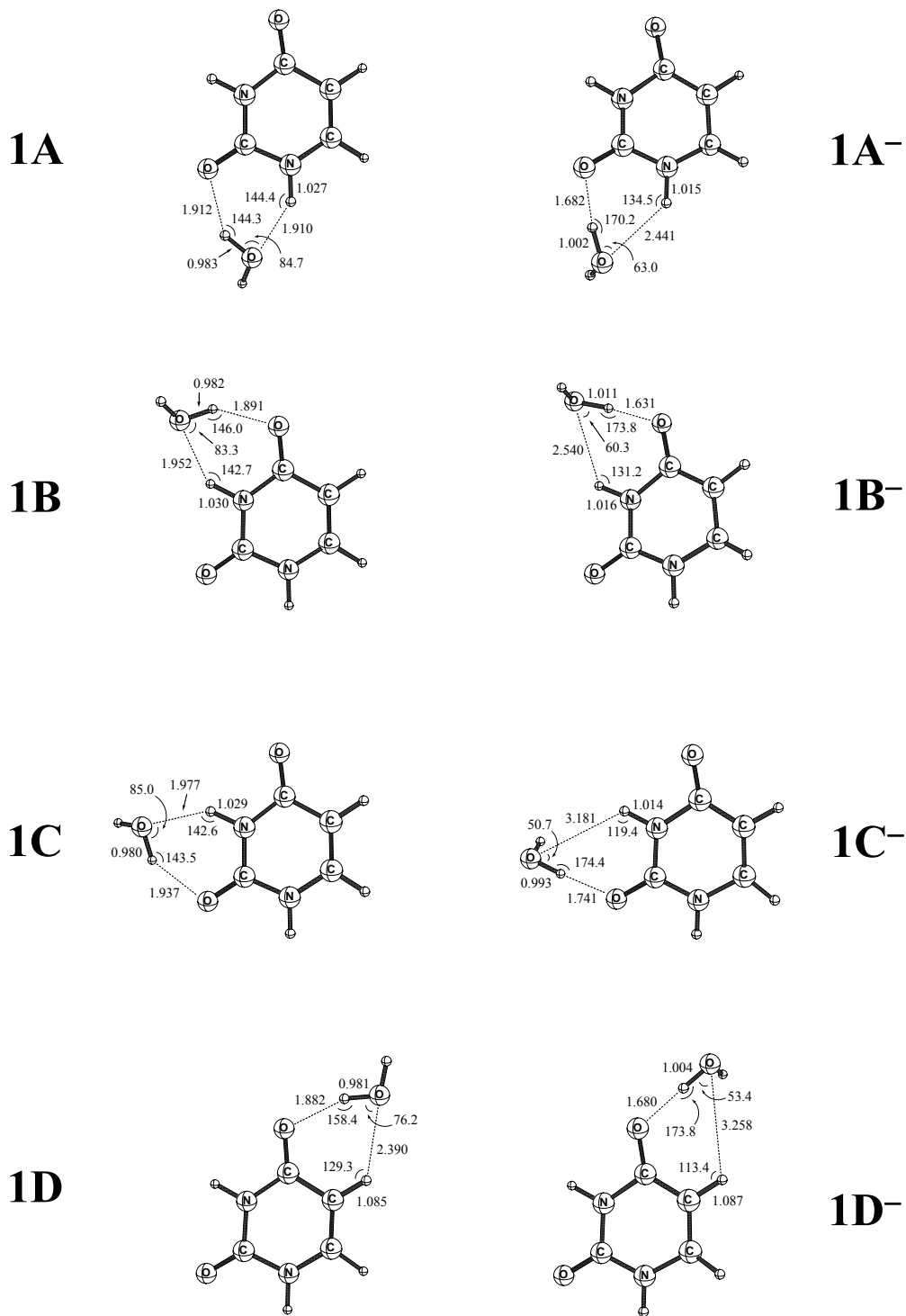


Figure 3.2. Molecular structures for uracil monohydrates (left column) and their respective anions (right column) with selected geometrical parameters, optimized at the B3LYP/DZP++ level of theory.

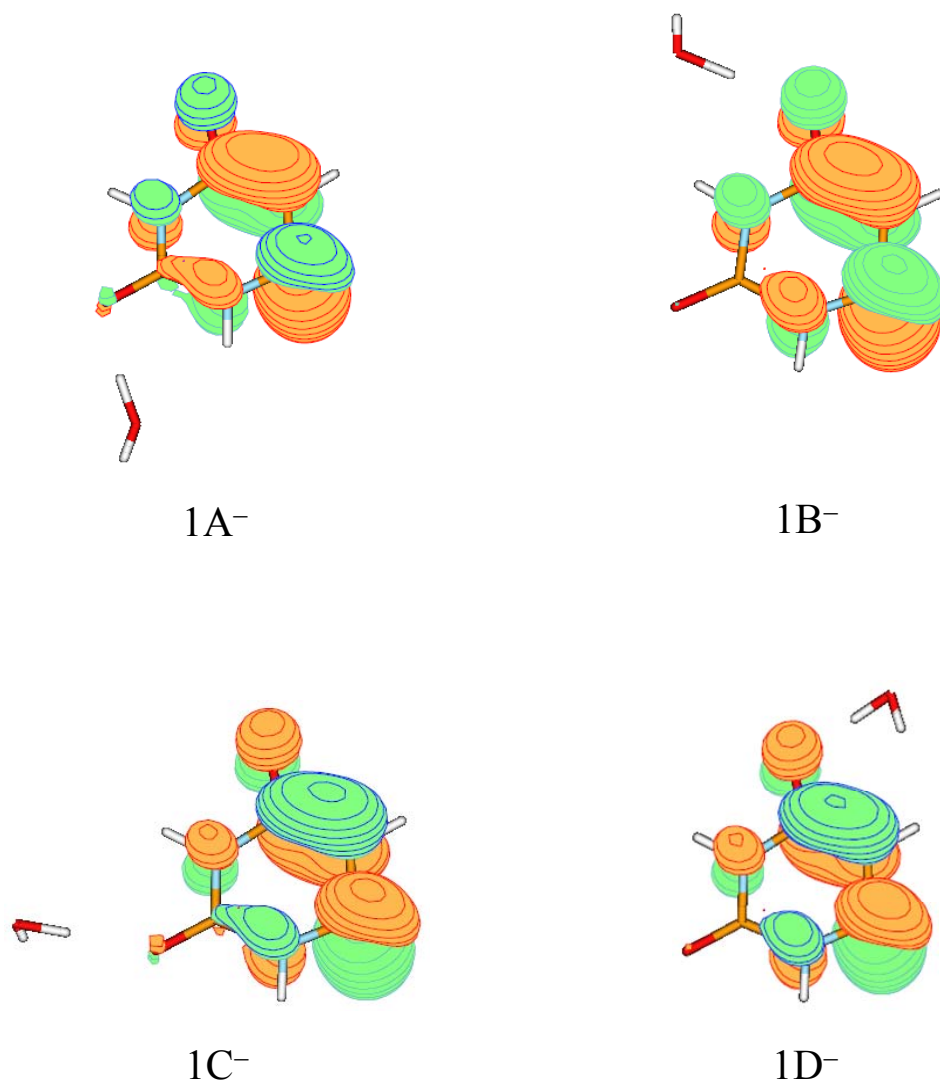


Figure 3.3. The singly occupied molecular orbitals (SOMOs) for the anions of the uracil monohydrates.

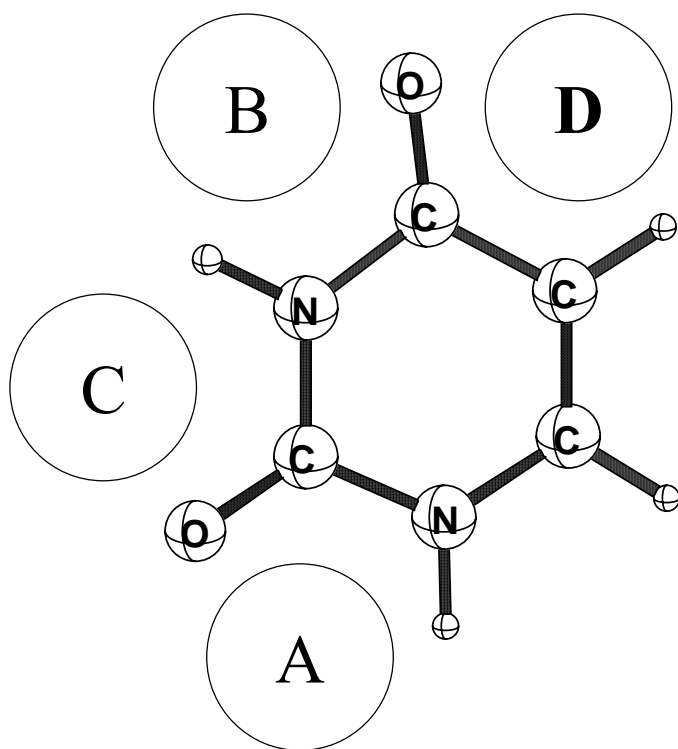


Figure 3.4. Prospective water-binding sites of uracil, populated in the order: $A > B > C > D$ for the neutral monohydrate.

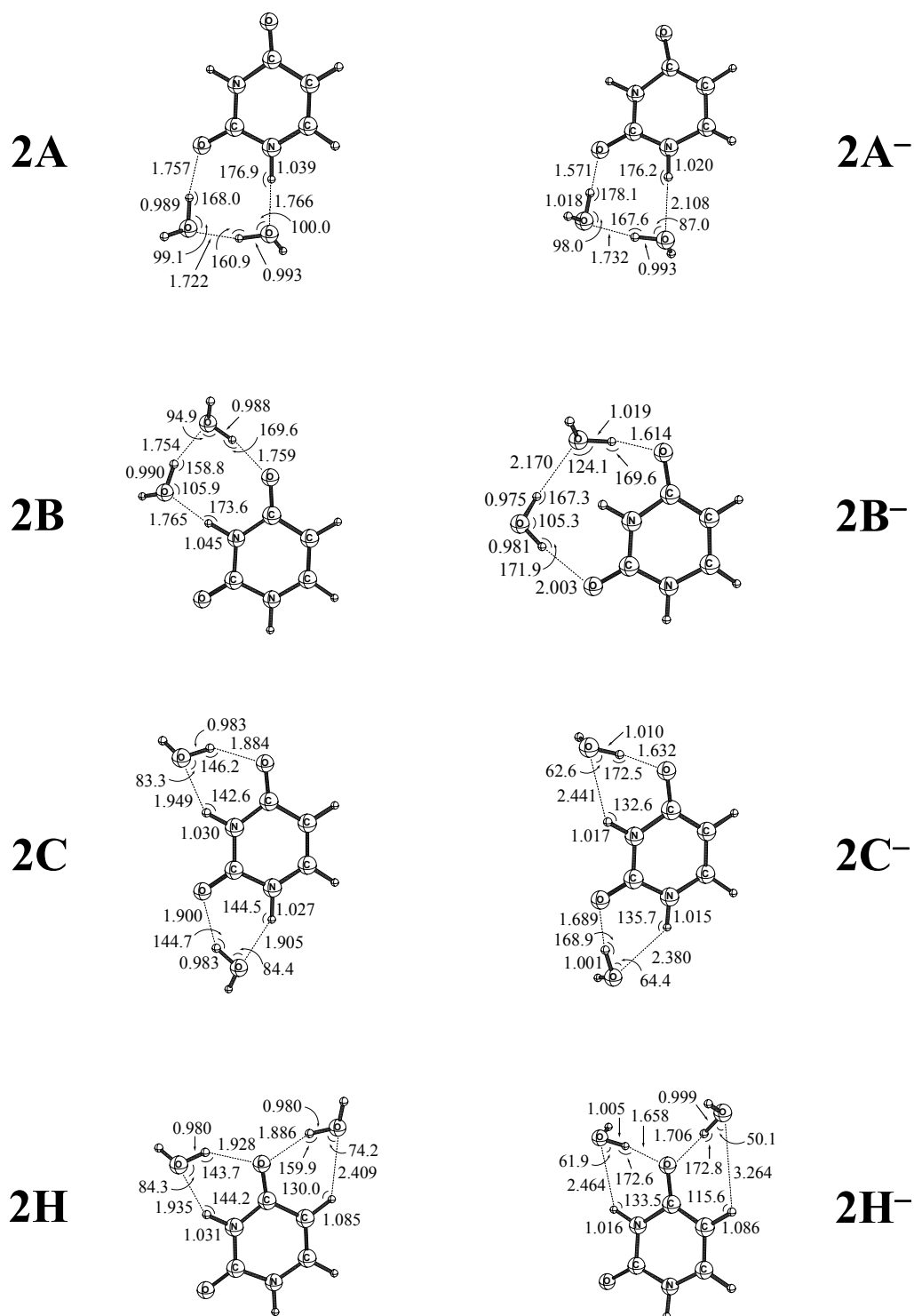
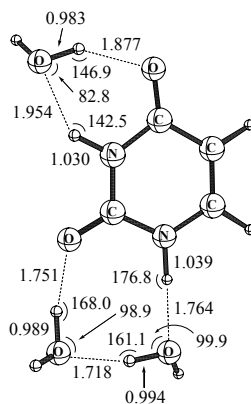
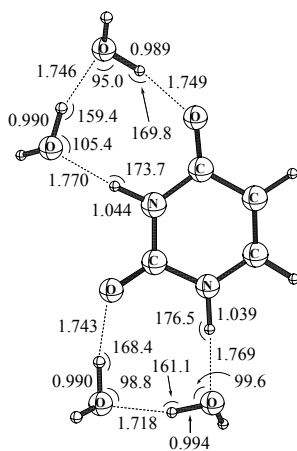


Figure 3.5. Selected structures for neutral uracil dihydrates (left column) and their respective anions (right column), optimized at the B3LYP/DZP++ level of theory.

3A



4A



5A

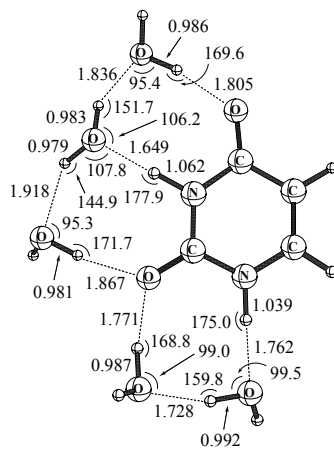
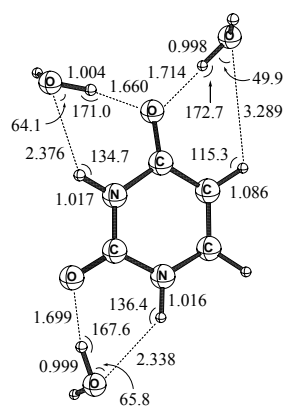
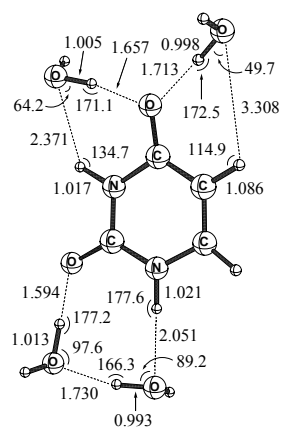


Figure 3.6. The most stable structures for the neutral tri-, tetra-, and pentahydrates of uracil, optimized at the B3LYP/DZP++ level of theory.

3H⁻



4D⁻



5D⁻

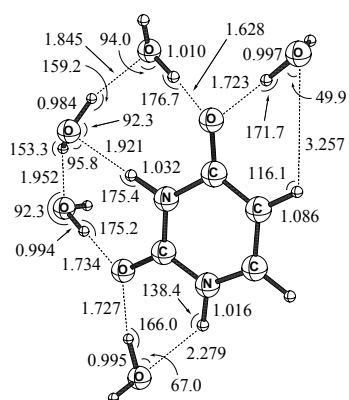


Figure 3.7. The most stable structures for the anionic tri-, tetra-, and pentahydrates of uracil, optimized at the B3LYP/DZP++ level of theory.

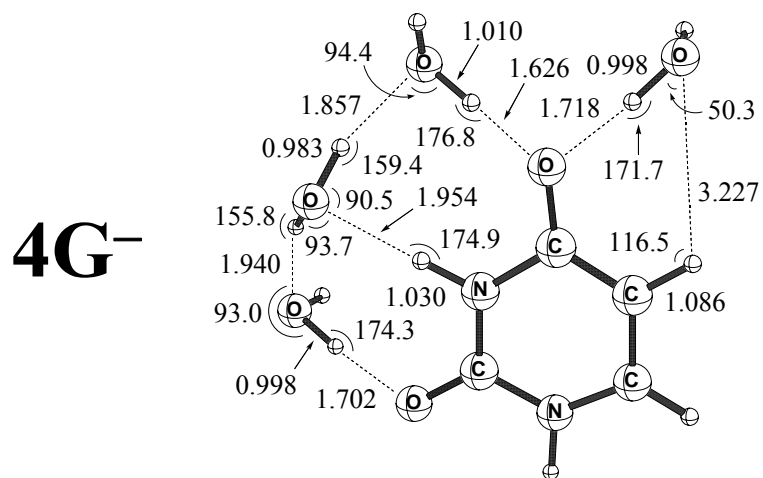


Figure 3.8. The second stable structure for the uracil tetrahydrate anion, optimized at the B3LYP/DZP++ level of theory.

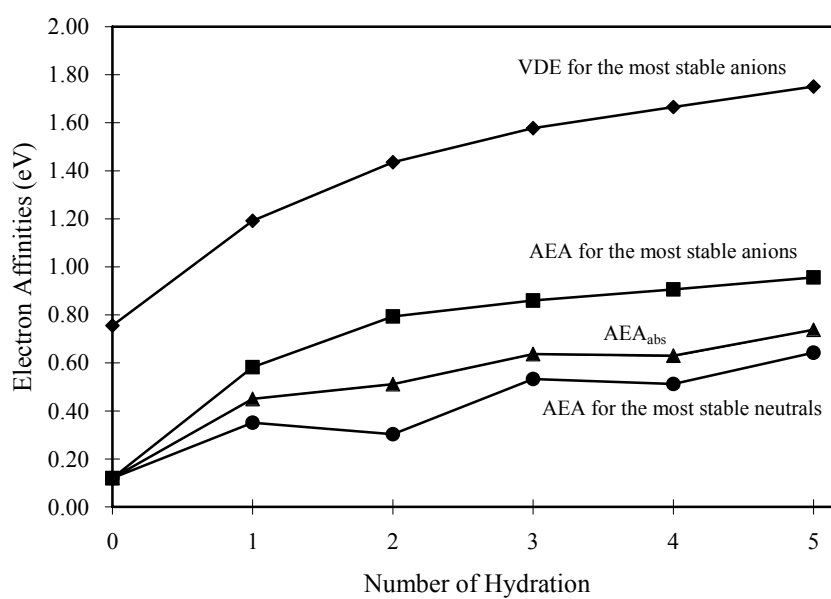


Figure 3.9. Electron affinities in eV for uracil hydrates with up to five water molecules: VDEs for the most stable anionic hydrates(◆); ZPVE-corrected AEAs for the lowest-lying anionic (■) and neutral (●) hydrates; and ZPVE-corrected absolute AEAs (▲).

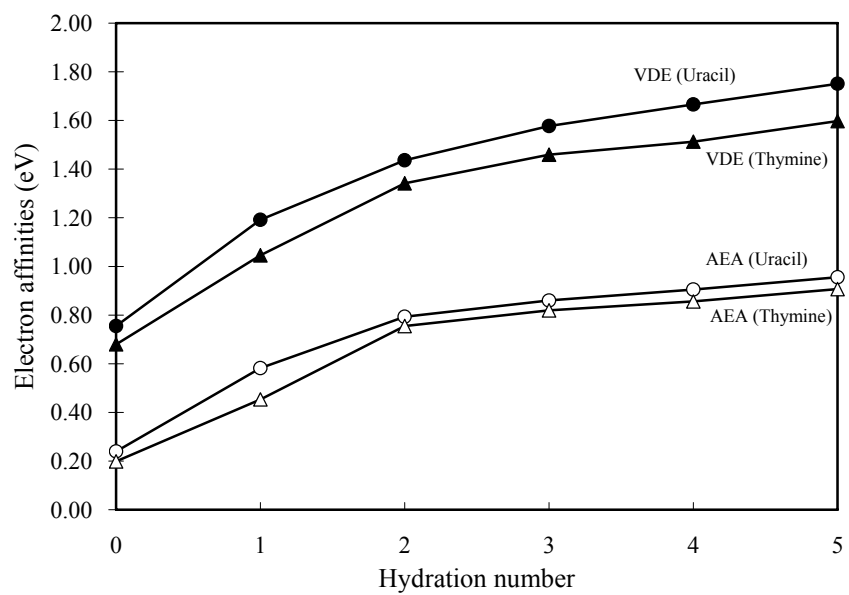


Figure 3.10. Comparison of the VDE and AEA between the uracil hydrates and the thymine hydrates.

CHAPTER 4

MICROHYDRATION OF CYTOSINE AND ITS RADICAL ANION[†]

[†] Reproduced with permission from Sunghwan Kim and Henry F. Schaefer, *J. Chem. Phys.* **126**(6), 064301/1-9 (2007). Copyright 2007, American Institute of Physics.

4.1 ABSTRACT

Microhydration effects on cytosine and its radical anion have been investigated theoretically, by explicitly considering various structures of cytosine complexes with up to five water molecules. Each successive water molecule (through $n=5$) is bound by 7~10 kcal mol⁻¹ to the relevant cytosine complex. The hydration energies are uniformly higher for the analogous anion systems. While the predicted vertical detachment energy (VDE) of the isolated cytosine is only 0.48 eV, it is predicted to increase to 1.27 eV for the lowest-lying pentahydrate of cytosine. The adiabatic electron affinity (AEA) of cytosine was also found to increase from 0.03 eV to 0.61 eV for the pentahydrate, implying that the cytosine anion, while questionable in the gas phase, is bound in aqueous solution. Both the VDE and AEA values for cytosine are smaller than those of uracil and thymine for a given hydration number. These results are in qualitative agreement with available experimental results from photodetachment-photoelectron spectroscopy studies of Schiedt *et al.* [Chem. Phys. **239**, 511 (1998)].

4.2 INTRODUCTION

Exposure to ionizing radiation can cause lethal damage to DNA, the carrier of the genetic information in living organisms.¹⁻²⁶ In an early stage of radiation-induced DNA damage, high-energy radiation may ionize nucleic acid bases (NABs), generating positive holes in the DNA

strands.^{12-15,17} Through charge transfer along the DNA strands, these positive holes migrate to guanine sites,¹³⁻¹⁷ which are the most easily oxidized among the NABs due to guanine having the lowest ionization potential.²⁷⁻³³ These cationic guanine bases participate in further reactions which may lead to oxidative DNA damage.¹³ On the other hand, radiation-induced DNA damage results not only from the primary impact of high-energy quanta, but also from secondary particles generated during the ionization process.^{2,3,17-26} In particular, low-energy electrons can cause lethal DNA lesions such as single- and double-strand breaks (SSBs and DSBs) even if their energies are below the ionization threshold of DNA.^{2,3} In his 2003 density functional theory (DFT) study, Walch³³ concluded that attachment of an additional electron to the NABs is favorable, because of their low-lying π^* orbitals. Thus, the NAB electron affinities, which govern their electron capturing abilities, are key thermodynamical parameters to understand the mechanism of radiation-induced DNA damage.

Wiley *et al.*³⁴ estimated the gas-phase adiabatic electron affinities (AEAs) of the five DNA and RNA bases (uracil, thymine, cytosine, adenine, and guanine) from the scaled reversible reduction potentials in aprotic solvent. The estimated AEAs, which were larger than 0.56 eV for all five bases, implied that the anions of the bases were stable with respect to electron detachment. The results using the Austin model 1 (AM1) semiempirical method gave the same conclusion.³⁵ In contrast, other studies have suggested near-zero or negative AEAs for the

NABs. In an important anion photoelectron spectroscopy study, Bowen and coworkers³⁶ determined the AEAs of uracil and thymine to be 0.093 ± 0.007 and 0.069 ± 0.007 eV, respectively. In Rydberg electron transfer (RET) experiments by Desfrancois *et al.*,³⁷ the AEAs of uracil, thymine, and adenine were found to be 0.054 ± 0.035 eV, 0.068 ± 0.020 eV, and 0.012 ± 0.005 eV, respectively. These near-zero AEAs, which are much smaller than those of Wiley *et al.*, are thought to arise from dipole-bound anions of NABs.³⁸⁻⁴⁰ In a dipole-bound anion, an extra electron is trapped in a dipole field of the neutral molecule, due to its large dipole moment. On the other hand, the AEAs arising from the conventional (valence-bound) anions are also thought to be very small or negative. In a photodetachment-photoelectron (PD-PE) study, Schiedt, Weinkauff, Neumark, and Schlag⁴¹ estimated the AEAs of the conventional anions to be 0.15 ± 0.12 , 0.12 ± 0.12 , and 0.13 ± 0.12 eV for uracil, thymine and cytosine, respectively, by extrapolating the AEAs of the complexes of NABs with up to five water molecules. In their RET spectroscopy study, Desfrancois *et al.*³⁷ claimed that the conventional valence anions were detected for uracil and thymine, although they could not determine the absolute values of their AEAs. Most theoretical studies using *ab initio* or DFT methods also suggested near-zero or negative electron affinities.^{30-32,42-46} In the 2001 DFT study of Wesolowski *et al.*⁴² the AEAs were predicted to be 0.19, 0.16, 0.07, -0.02 and -0.17 eV for uracil, thymine, adenine, cytosine, guanine, respectively. They concluded that the isolated gas-phase NABs are not bound or

weakly bound at most.

In aqueous solution, the interaction between solute and solvent molecules may cause significant changes in the molecular structures and properties of the solute molecules, compared to those in the gas phase.⁴⁷⁻⁵¹ Indeed, another important observation in the PD-PE study of Neumark and Schlag⁴¹ was that the electron affinities of the three pyrimidine nucleobases, cytosine, uracil, and thymine increased linearly with hydration number, consistent with results from recent theoretical studies on uracil-water clusters^{52,53} and thymine-water clusters.⁵⁴ This implies that the electron capturing abilities of NABs in aqueous solution and living organisms are fundamentally different from those in the gas-phase. To better understand the mechanism of radiation-induced DNA damage, it is essential to investigate the effects of solvation on the electron affinities of the NABs. In the present paper, we investigate microsolvation effects upon the electron affinities of cytosine. Earlier researchers^{29,43,46} investigated solvation effects on the electron affinity of cytosine using polarized continuum models (PCM), but these do not account for detailed microsolvation effects such as hydrogen bonding interactions between solute and solvent molecules. In the present study, we investigate microsolvation effects upon the electron affinities by explicitly considering the cytosine complexes with up to five water molecules. In addition, the present research is compared with the earlier results for uracil⁵³ and thymine.⁵⁴

4.3 COMPUTATIONAL METHODS

All geometry optimizations and harmonic vibrational frequency analyses have been performed using the Gaussian 94 package of programs.⁵⁵ The equilibrium structures of cytosine and its complexes with up to five water molecules have been optimized using the B3LYP density functional, which is Becke's three-parameter functional (B3),⁵⁶ in conjunction with the correlation functional of Lee, Yang, and Parr (LYP).⁵⁷ We used the canonical structure of cytosine (Figure 4.1), among its various possible tautomeric structures, to construct the initial structures of the cytosine hydrates. We assumed that water molecules in the microsolvation shell bind directly with cytosine through at least one hydrogen bond. Because the hydrogen bond donors (the H_{4a} and H_{4b} atoms in Figure 4.1) and acceptors (the O₂ and N₂ atoms) of cytosine are located in the molecular plane of cytosine, the water molecules are also roughly located in the molecular plane. We did not consider the cases where water molecules were above the molecular plane of cytosine.

We used double- ζ quality basis sets with polarization and diffuse functions (DZP++). These were constructed by adding one set of *p*-type polarization functions for each H atom and one set of five *d*-type polarization functions for each C, N, and O atom (where $\alpha_p(\text{H})=0.75$, $\alpha_d(\text{C})=0.75$, $\alpha_d(\text{N})=0.80$, $\alpha_d(\text{O})=0.85$) to the Huzinaga-Dunning (9s5p) contractions.^{58,59} Further augmentation with one even tempered *s* diffuse function for each H atom and even

tempered s and p diffuse functions for each heavy atom completes the DZP++ basis set. The even tempered orbital exponents were determined according to the prescription,⁶⁰

$$\alpha_{diffuse} = \frac{1}{2} \left[\frac{\alpha_1}{\alpha_2} + \frac{\alpha_2}{\alpha_3} \right] \alpha_1$$

where α_1 , α_2 , and α_3 are the three smallest Gaussian orbital exponents of the s - or p -type primitive functions for a given atom ($\alpha_1 < \alpha_2 < \alpha_3$). The final DZP++ basis set contains six functions per H atom and 19 functions per C, N, or O atom.

The corresponding anions of the cytosine hydrates have also been fully optimized using the B3LYP functional with the DZP++ basis set. In the present study, we considered the vertical detachment energy (VDE), adiabatic electron affinity (AEA), and absolute AEA (AEA_{abs}), which are given by the following definitions:

$$\text{VDE} = E(\text{neutral at optimized anion geometry}) - E(\text{optimized anion})$$

$$\text{AEA} = E(\text{optimized neutral}) - E(\text{optimized anion})$$

$$\text{AEA}_{\text{abs}} = E(\text{global minimum optimized neutral}) - E(\text{global minimum optimized anion}).$$

4.4 RESULTS

All structures optimized at the B3LYP/DZP++ level of theory have been included as supplementary material,⁶¹ and their relative stabilities and hydration energies are listed in Table

4.1. For convenience, we denote the neutral cytosine hydrate with a number followed by an uppercase letter. The number indicates the number of the hydrating water molecules for a given structure, and the uppercase letter represents its relative stability among the structures with the same hydration number, based on their zero-point vibrational energy (ZPVE)-corrected energies. For example, **2C** means the third energetically most favorable structure of the neutral cytosine dihydrate. The corresponding anion for a given neutral hydrate is indicated with a negative-sign superscript (*e.g.*, **2C**⁻). Note that the letter in the notation for the anionic species still indicates the relative stability of the corresponding neutral species, *not* of the anionic species. That is, anion **2C**⁻ is not the third lowest-energy anionic structure for the cytosine dihydrate, but the anion of the third most favorable neutral dihydrate. In addition, for some cases, there have been found two anionic structures for one neutral hydrate (to be discussed later). These two alternate structures are represented with a lowercase letter subscript (*e.g.*, **2D_a**⁻ vs. **2D_b**⁻).

4.4.1 CYTOSINE MONOHYDRATES AND THEIR ANIONS

Three structures have been found for the neutral cytosine monohydrate and they are displayed in Figure 4.2, along with their respective anions. The optimized geometries and relative energies for the neutral monohydrates are consistent with recent theoretical studies by Hunter, Rutledge, and Wetmore⁶² and by Chandra *et al.*⁶³ In the lowest-energy structure, **1A**,

the water molecule is associated with cytosine via the H₁ and O₂ atoms of cytosine. Its ZPVE-corrected hydration energy due to this N₁-H₁⋯O_w-H_w⋯O₂=C₂ cyclic hydrogen bond formation is predicted to be 9.7 kcal mol⁻¹. The second most favorable structure, **1B**, in which the water molecule forms an N₃⋯H_w-O_w⋯H_{4a} cyclic hydrogen bond with cytosine, lies only 0.5 kcal mol⁻¹ above **1A**. The energetic favoredness of **1A** over **1B** is due to the stronger hydrogen bonds in **1A**, compared to those in **1B**. Because the N₁-H₁ hydrogen is more acidic than the N₄-H_{4a} hydrogen,⁶³ the former acts as a stronger hydrogen bond donor, as implied in the N₁-H₁⋯O_w hydrogen bond length (1.921 Å) in **1A**, which is shorter than the N₄-H_{4a}⋯O_w bond length (1.981 Å) in **1B**. In addition, due to the higher electronegativity of oxygen than nitrogen, the carbonyl oxygen O₂ is more basic than the N₃ atom and is a better hydrogen bond acceptor. The O_w-H_w⋯O₂ bond length in **1A** is predicted to be 1.783 Å and the O_w-H_w⋯N₃ bond length in **1B** to be 1.894 Å. Thus, the N₁-H₁⋯O_w-H_w⋯O₂=C₂ cyclic hydrogen bond in **1A** is stronger than the N₄-H_{4a}⋯O_w-H_w⋯N₃ cyclic hydrogen bond in **1B**. The highest-energy structure, **1C**, where the water molecule binds to cytosine through the N₄-H_{4b}⋯O_w hydrogen bond, does not involve a cyclic hydrogen bond. For this reason, it is higher in energy than **1A** and **1B**, by 5.1 and 4.6 kcal mol⁻¹, respectively.

Figure 4.3 shows the singly occupied molecular orbitals (SOMOs) for the anions of cytosine and its monohydrates. As one can see, for the anions **1A**⁻ and **1B**⁻, the excess electron occupies

the antibonding π^* orbital of the neutral cytosine molecule. This implies that excess negative charge density is localized on the cytosine moiety. If a hydrogen atom of the water molecule acts as a hydrogen bond donor to form a hydrogen bond with cytosine, this can stabilize the system by withdrawing the localized charge density on the cytosine moiety toward the water molecule, and the resulting hydrogen bond in a cytosine monohydrate anion would be strengthened, compared to the corresponding neutral. On the other hand, a hydrogen bond where the oxygen atom of the water molecule acts as a hydrogen bond acceptor would be weakened because the transfer of negative charge density from water to cytosine is unfavorable. Indeed, upon electron attachment to **1A** to form **1A⁻**, the $O_w-H_w\cdots O_2$ hydrogen bond length (1.616 Å) is shortened by 0.167 Å, while the $N_1-H_1\cdots O_w$ hydrogen bond length (2.410 Å) becomes longer by 0.489 Å. The $O_w-H_w\cdots O_2$ hydrogen bond angle (172.8°) in **1A⁻**, which is close to linearity, also reflects the strengthening of the $O_w-H_w\cdots O_2$ hydrogen bond and the weakening of the $N_1-H_1\cdots O_w$ hydrogen bond.

The structural changes upon electron attachment to **1B** are even more significant. That is, the water molecule migrates by breaking the $N_4-H_{4a}\cdots O_w$ hydrogen bond and forming the $O_w-H_w\cdots O_2$ hydrogen bond. Thus, in the resulting structure, **1B⁻**, both hydrogen atoms of the water molecule act as hydrogen bonding donors, and they can stabilize the system more efficiently by withdrawing negative charge density from the cytosine moiety. Because of this, while neutral

1B is higher in energy than **1A**, the corresponding anion, **1B⁻**, lies 1.6 kcal mol⁻¹ below **1A⁻**, and it has the lowest energy among the anionic monohydrates.

As shown in Figure 4.3, an excess electron in **1C⁻** is localized on the water moiety, unlike the other two anions. This is surprising because a water molecule is unlikely to accept an extra electron to form a stable anion, because its ZPVE-corrected AEA is predicted to be very negative (-0.73 eV at the B3LYP/DZP++ level of theory). In addition, the AEA of cytosine (0.03 eV) suggests that the electron attachment is more favorable on the cytosine moiety than on the water molecule. However, it should also be noted that the oxygen atom of the water molecule in **1C** participates in the non-cyclic hydrogen bond as a hydrogen bond acceptor, resulting in electron density transfer from water to cytosine. Because of this, a partial negative charge is developed on the cytosine moiety of **1C**, while a partial positive charge resides on the water, in a very qualitative view of the electron density. Thus, electron attachment to the cytosine moiety would cause significant charge separation between the cytosine and water molecules. Instead, an additional electron is more favorable to capture on the water moiety of **1C⁻**. The electron attachment on the water moiety results in a shortening of the N₄-H_{4b}···O_w hydrogen bond (by 0.145 Å), indicating the increase in the hydrogen bond strength. Anion **1C⁻** is higher in energy than **1A⁻** and **1B⁻**, by 7.1 and 8.7 kcal mol⁻¹, respectively, because it requires only one (non-cyclic) hydrogen bond to stabilize the system, as in the case of the corresponding neutral **1C**.

4.4.2 CYTOSINE DIHYDRATES AND THEIR ANIONS

Among six structures found for the neutral cytosine dihydrate, the three lowest-energy structures and the corresponding anions are displayed in Figure 4.4. Because **1A** and **1B** are the two lowest-energy structures for the neutral monohydrate, structure **2C**, in which one water molecule forms a cyclic hydrogen bond via the H₁ and O₂ atoms and the other via the N₃ and H_{4a} atoms, might be expected to have the lowest energy among the neutral dihydrates. However, **2C** is found to be higher in energy than the most favorable neutral dihydrate, **2A**, by 1.2 kcal mol⁻¹. As shown in Figure 4.4, **2A** has an N₁-H₁⋯O_w-H_w⋯O_w-H_w⋯O₂=C₂ cyclic hydrogen bond involving the cytosine and two water molecules. The stabilization energy due to hydration of a second water molecule in **2A**, estimated from the difference in hydration energy between **1A** and **2A**, is 10.2 kcal mol⁻¹ (= 19.9 - 9.7 kcal mol⁻¹). Note that **2A** has an intermolecular hydrogen bond between the two water molecules. Considering the predicted dimerization energy (*D_e*) of water of 5.6 kcal mol⁻¹ at the B3LYP/DZP++ level of theory, the formation of the cyclic hydrogen bond in **2A** might be regarded to give an energy lowering of 4.6 kcal mol⁻¹ (= 10.2 - 5.6 kcal mol⁻¹). This extra stability is mainly due to the linear arrangement of the hydrogen bond donors and acceptors in **2A**. In **1A**, the deviation of the N₁-H₁⋯O_w (143.6°) and O_w-H_w⋯O₂ angles (152.3°) from linearity is inevitable in forming the cyclic hydrogen bonds, and the resulting bent hydrogen bonds are weak. However, additional

hydration from **1A** to **2A** makes the $N_1-H_1\cdots O_w$ and $O_w-H_w\cdots O_2$ angles become almost linear (176.6° and 171.3° , respectively) and the water molecules can form hydrogen bonds with cytosine more strongly. Indeed, the $N_1-H\cdots O_w$ hydrogen bond distance in **2A** is predicted to be 1.799 \AA and shorter by 0.122 \AA than in **1A**. The $O_w-H_w\cdots O_2$ hydrogen bond distance of 1.683 \AA for **2A** is also shorter by 1.000 \AA , compared with **1A**. Similar effects were found for **2B**. On the other hand, in structure **2C**, the two water molecules form cyclic hydrogen bonds individually, and there is no additional stabilization effect comparable to that found in **2A** or **2B**. Thus, the hydration energy of **2C** ($18.6 \text{ kcal mol}^{-1}$) is almost the same as the sum of the hydration energies of **1A** and **1B**. In addition, the hydrogen bond distances and angles for **2C** do not differ significantly from those for **1A** and **1B**.

Figure 4.5 depicts the structures of **2D** and its related anions. Note that there are two anions, $2D_a^-$ and $2D_b^-$. If the optimized geometry of **2D** is used as an initial geometry, upon optimization for the corresponding anions, the resulting structure is $2D_a^-$. That is, upon electron attachment to **2D**, the shift of a water molecule occurs by breaking the $N_4-H_{4a}\cdots O_w$ hydrogen bond and forming the $O_w-H_w\cdots N_3$ hydrogen bond. Due to this shift, both water molecules act as hydrogen bond donors with respect to cytosine and stabilize the system by pulling the localized electron density from the cytosine moiety. Structure $2D_b^-$ also has the same geometrical characteristics as $2D_a^-$. These two structures differ only in the orientation of

the intermolecular hydrogen bond between the water molecules. Anion $\mathbf{2D}_b^-$ is lower in energy than $\mathbf{2D}_a^-$, by $0.8 \text{ kcal mol}^{-1}$. While electron attachment to $\mathbf{2D}$ leads directly to $\mathbf{2D}_a^-$, electron detachment both from $\mathbf{2D}_a^-$ and $\mathbf{2D}_b^-$ give rise to $\mathbf{2D}$ (*i.e.*, optimizations for the corresponding neutrals using geometries of $\mathbf{2D}_a^-$ and $\mathbf{2D}_b^-$ as initial geometries give the same neutral structure, $\mathbf{2D}$).

These two anions ($\mathbf{2D}_a^-$ and $\mathbf{2D}_b^-$) are the two lowest-energy structures for the anionic dihydrate, while the corresponding neutral, $\mathbf{2D}$, is the fourth lowest-energy structure for the neutral dihydrate. The origin of the stability of $\mathbf{2D}_a^-$ and $\mathbf{2D}_b^-$ arises from the fact that the water molecules in both structures can effectively pull excess electron density from cytosine by acting as hydrogen bond donors. In this respect, anions $\mathbf{2B}^-$ and $\mathbf{2C}^-$ are also of special interest. For both structures, electron attachment results in the shift of water molecules as found in $\mathbf{1B}/\mathbf{1B}^-$. Indeed, the shift of a water molecule upon electron attachment to $\mathbf{2B}$ even causes loss of direct contact between cytosine and the other water molecule.

In the high-energy structures $\mathbf{2E}$ and $\mathbf{2F}$ and their respective anions (not shown in Figures 4.4 and 4.5), one of the two water molecules binds to the cytosine molecule through a non-cyclic $\text{N}_4\text{-H}_{4b}\cdots\text{O}_w$ as found in $\mathbf{1C}$. This is understandable because the non-cyclic hydrogen bonding through the H_{4b} atom is least favorable for the monohydrate. $\mathbf{2E}$ and $\mathbf{2F}$ are higher in energy

than **2A** by 5.7 and 6.3 kcal mol⁻¹, respectively. **2E⁻** and **2F⁻** are higher in energy than **2D_b⁻** by 10.3 and 10.8 kcal mol⁻¹, respectively.

4.4.3 CYTOSINE TRI-, TETRA-, AND PENTAHYDRATES AND THEIR ANIONS

Figure 4.6 shows the lowest-energy structures for the tri-, tetra-, and pentahydrates of the neutral cytosine. The most stable tri- and tetrahydrates, **3A** and **4A**, correspond to the association of one or two water molecules with the most stable dihydrate, **2A**. This is accomplished by forming a cyclic hydrogen bond through the H_{4a} and N₃ atoms of cytosine. In the lowest-lying neutral pentahydrate, **5A**, the fifth water molecule is associated with **4A**, through the O₂ atom of cytosine and the H_w atom of one of the water molecules. All five water molecules in **5A** form hydrogen bonds with cytosine and at least one other water molecule, generating a compact hydrogen-bond network around the cytosine moiety.

Figure 4.7 displays the two lowest-lying structures for the anionic tri-, tetra-, and pentahydrates. While structures **3D_a⁻**, **4C_a⁻**, and **5A_a⁻** arise from successive hydration to the anionic dihydrate **2D_a⁻**, the other three structures, **3D_b⁻**, **4C_b⁻**, and **5A_b⁻** come from **2D_b⁻**. Similar to the case of neutral dihydrate **2D** and its anions, **2D_a⁻** and **2D_b⁻**, electron attachment to **3D**, **4C**, and **5A** results only in **3D_a⁻**, **4C_a⁻**, and **5A_a⁻**, respectively, while electron detachment from all six anions in Figure 4.7 gives the corresponding neutrals. For example, the anion

optimization using the geometry of neutral **3D** as an initial geometry gives only **3D_a⁻**, while the optimizations for neutral hydrates using the geometries of **3D_a⁻** and **3D_b⁻** result in the same neutral geometry, **3D**. As shown in Figure 4.7, anions **4C_b⁻** and **5A_b⁻** have a particularly interesting structural feature. In these anions, the lone pair of the N₄ atom participates in a hydrogen bond as a hydrogen bond acceptor. On the contrary, in **4C_a⁻** and **5A_a⁻**, the H_{4a} atom forms a hydrogen bond with a water molecule. It should also be noted that the energy differences between **4C_a⁻** and **4C_b⁻** and between **5A_a⁻** and **5A_b⁻** are 0.2 and 0.1 kcal mol⁻¹, respectively, while those between **2D_a⁻** and **2D_b⁻** and between **3D_a⁻** and **3D_b⁻** are 0.8 and 0.9 kcal mol⁻¹, respectively. Because in **4C_b⁻** and **5A_b⁻** the water molecules which form the hydrogen bonds with the N₄ atom of cytosine behave as hydrogen bond donors, they can stabilize the system by withdrawing excess negative charge from cytosine.

4.4.4 ELECTRON AFFINITIES OF CYTOSINE AND ITS HYDRATES

Table 4.2 lists the VDEs and AEAs of cytosine and its hydrates with up to five water molecules and Table 4.3 shows their AEA_{abs}. In the PD-PE spectroscopy of Neumark and coworkers⁴¹ the AEA of cytosine was found to increase linearly with the number of hydrating water molecules. Because their experiments dealt with electron detachment processes in which anions change into neutrals by losing an electron, the measured electron affinities may

correspond to those of the most stable anions, rather than the most stable neutrals. The computed VDE and AEA values of the most stable anionic hydrates of cytosine are displayed in Figure 4.8, along with the AEA of the most stable neutrals and the AEA_{abs} . For the isolated cytosine molecule, the VDE and AEA are predicted to be 0.48 eV and 0.03 eV, respectively. As shown in Figure 4.8, the VDE and AEA of the most stable anions of cytosine monotonically increase with hydration number (up to four), but there is a small decrease in both VDE and AEA for pentahydrates, while in the PD-PE spectroscopy study of Neumark, the AEA was found to gradually increase with up to five water molecules. It should be noted that the PD-PE spectra in their study may arise not only from the most stable anions, but also from all energetically accessible structures according to the Boltzmann distribution. For example, the second stable anionic pentahydrate, $5A_b^-$, which is higher in energy by only $0.1 \text{ kcal mol}^{-1}$, has a much larger VDE (1.65 eV) than the most stable anionic and pentahydrate, $5A_a^-$ (1.27 eV). Figure 4.9 compares the electron affinities of cytosine hydrates with those of uracil hydrates⁵³ and thymine hydrates.⁵⁴ In the gas phase, both the VDE and AEA of cytosine are smaller than those of uracil and thymine. Hydration increases the VDE and AEA for all pyrimidine bases, but the electron affinities of cytosine are lower than those of uracil and thymine for a given hydration number.

4.5 CONCLUSIONS

Microsolvation effects on cytosine and its anion have been investigated theoretically. The existence of three favorable structures for the neutral cytosine monohydrate indicates that there are three important water-binding sites, as shown in Figure 4.10. The shift of the water molecule upon electron attachment to **1B** to form **1B⁻** implies that site B' can also be a potential binding site. Considering the relative energies of the three neutral monohydrates, water molecules will occupy these sites in the order of $A > B > C$. The results for the neutral dihydrates suggest that sites A and B would accommodate up to two water molecules, while site C would be occupied one water molecule. These rules of thumb make it possible to predict the lowest-energy structures for the neutral mono- through tetrahydrates. For the neutral pentahydrate, the fifth water molecule occupies site B', rather than site C, forming a cyclic hydrogen bond with the cytosine and the adjacent water molecule. As a result, for the neutral cytosine hydrates, the manner in which the maximum number of cyclic hydrogen bonds can be achieved is the most important factor in predicting the lowest-energy structures for a given hydration number.

For the anionic hydrates, the prediction of the lowest-energy structure for a given hydration number is more difficult. The issue of how efficiently excess negative charge density localized on cytosine can be transferred to water molecules should be considered. This factor requires

that water molecules act as hydrogen bond donors when they bind to cytosine. In turn, this causes the shift of water molecules upon electron attachment (*e.g.*, **1B⁻** and **2C⁻**) and loss of a water molecule from the first solvation shell (*e.g.*, **2B⁻**). In addition, for the tetra- and pentahydrate, the cytosine N₄ atom can participate in a hydrogen-bond network, resulting in very low-lying complexes (*e.g.*, **4C_b⁻** and **5A_b⁻**) which show almost the same stability as the most energetically favorable anionic hydrates.

In the gas phase, the VDE and AEA for the isolated cytosine are predicted to be 0.48 and 0.03 eV, respectively. Upon hydration, both measures of electron capture are predicted to increase up to 1.27 and 0.61 eV, respectively, for the lowest-energy pentahydrate, qualitatively consistent with the PD-PE spectroscopy study of Neumark and coworkers. This implies that a cytosine molecule in aqueous solution can form a stable anion upon electron attachment. On the other hand, the AEA of cytosine, which is predicted to be smaller than those of uracil and thymine, suggests that cytosine sites in DNA and RNA strands are less favorable for electron trapping, compared to uracil or thymine sites.

4.6 ACKNOWLEDGEMENTS

This work was supported by the U.S. National Science Foundation under Grant No. CHE-0451445. This research was performed in part using the computational resources of the

Research Computing Center (RCC) at the University of Georgia, which is administered by Enterprise Information Technology Services (EITS) and the Office of Research Services (ORS).

4.7 REFERENCES

- ¹ O. Kovalchuk, Y. E. Dubrova, A. Arkhipov, B. Hohn, and I. Kovalchuk, *Nature* **407**, 583 (2000).
- ² B. Boudaiffa, P. Cloutier, D. Hunting, M. A. Huels, and L. Sanche, *Science* **287**, 1658 (2000).
- ³ B. D. Michael and P. O'Neill, *Science* **287**, 1603 (2000).
- ⁴ A. J. Grosovsky, *Proc. Natl. Acad. Sci. U. S. A.* **96**, 5346 (1999).
- ⁵ B. M. Sutherland, P. V. Bennett, O. Sidorkina, and J. Laval, *Proc. Natl. Acad. Sci. U. S. A.* **97**, 103 (2000).
- ⁶ V. G. Tusher, R. Tibshirani, and G. Chu, *Proc. Natl. Acad. Sci. U. S. A.* **98**, 5116 (2001).
- ⁷ K. Datta, R. D. Neumann, and T. A. Winters, *Proc. Natl. Acad. Sci. U. S. A.* **102**, 10569 (2005).
- ⁸ W. F. Morgan and M. B. Sowa, *Proc. Natl. Acad. Sci. U. S. A.* **102**, 14127 (2005).
- ⁹ M. R. Barvian and M. M. Greenberg, *J. Am. Chem. Soc.* **117**, 8291 (1995).
- ¹⁰ M. M. Greenberg, M. R. Barvian, G. P. Cook, B. K. Goodman, T. J. Matray, C. Tronche, and H. Venkatesan, *J. Am. Chem. Soc.* **119**, 1828 (1997).
- ¹¹ R. Cathcart, E. Schwiers, R. L. Saul, and B. N. Ames, *Proc. Natl. Acad. Sci. U. S. A.* **81**, 5633 (1984).

- ¹² K.-W. Choi, J.-H. Lee, and S. K. Kim, *J. Am. Chem. Soc.* **127**, 15674 (2005).
- ¹³ G. Pratviel and B. Meunier, *Chem. Eur. J.* **12**, 6018 (2006).
- ¹⁴ S. Kanvah and G. B. Schuster, *J. Am. Chem. Soc.* **124**, 11286 (2002).
- ¹⁵ I. Saito, T. Nakamura, K. Nakatani, Y. Yoshioka, K. Yamaguchi, and H. Sugiyama, *J. Am. Chem. Soc.* **120**, 12686 (1998).
- ¹⁶ H.-A. Wagenknecht, *Charge Transfer in DNA*. (Wiley-VCH, Weinheim, 2005).
- ¹⁷ P. Swiderek, *Angew. Chem., Int. Ed.* **45**, 4056 (2006).
- ¹⁸ X. Bao, J. Wang, J. Gu, and J. Leszczynski, *Proc. Natl. Acad. Sci. U. S. A.* **103**, 5658 (2006).
- ¹⁹ I. Bald, J. Kopyra, and E. Illenberger, *Angew. Chem., Int. Ed.* **45**, 4851 (2006).
- ²⁰ J. Gu, J. Wang, and J. Leszczynski, *J. Am. Chem. Soc.* **128**, 9322 (2006).
- ²¹ J. Simons, *Acc. Chem. Res.* **39**, 772 (2006).
- ²² S. G. Ray, S. S. Daube, and R. Naaman, *Proc. Natl. Acad. Sci. U. S. A.* **102**, 15 (2005).
- ²³ Y. Zheng, P. Cloutier, D. J. Hunting, L. Sanche, and J. R. Wagner, *J. Am. Chem. Soc.* **127**, 16592 (2005).
- ²⁴ L. Sanche, *Eur. Phys. J. D* **35**, 367 (2005).
- ²⁵ X. Li, M. D. Sevilla, and L. Sanche, *J. Am. Chem. Soc.* **125**, 13668 (2003).
- ²⁶ L. Sanche, *Phys. Scr.* **68**, C108 (2003).
- ²⁷ N. S. Hush and A. S. Cheung, *Chem. Phys. Lett.* **34**, 11 (1975).

- ²⁸ V. M. Orlov, A. N. Smirnov, and Y. M. Varshavsky, *Tetrahedron Lett.* **48**, 4377 (1976).
- ²⁹ A. O. Colson, B. Besler, and M. D. Sevilla, *J. Phys. Chem.* **97**, 13852 (1993).
- ³⁰ M. D. Sevilla, B. Besler, and A.-O. Colson, *J. Phys. Chem.* **99**, 1060 (1995).
- ³¹ N. Russo, M. Toscano, and A. Grand, *J. Comput. Chem.* **21**, 1243 (2000).
- ³² S. D. Wetmore, R. J. Boyd, and L. A. Eriksson, *Chem. Phys. Lett.* **322**, 129 (2000).
- ³³ S. P. Walch, *Chem. Phys. Lett.* **374**, 496 (2003).
- ³⁴ J. R. Wiley, J. M. Robinson, S. Ehdaie, E. C. M. Chen, E. S. D. Chen, and W. E. Wentworth, *Biochem. Biophys. Res. Commun.* **180**, 841 (1991).
- ³⁵ Q. Zhang and E. C. M. Chen, *Biochem. Biophys. Res. Commun.* **217**, 755 (1995).
- ³⁶ J. H. Hendricks, S. A. Lyapustina, H. L. de Clercq, J. T. Snodgrass, and K. H. Bowen, *J. Chem. Phys.* **104**, 7788 (1996).
- ³⁷ C. Desfrancois, H. Abdoul-Carime, and J. P. Schermann, *J. Chem. Phys.* **104**, 7792 (1996).
- ³⁸ N. A. Oyler and L. Adamowicz, *J. Phys. Chem.* **97**, 11122 (1993).
- ³⁹ N. A. Oyler and L. Adamowicz, *Chem. Phys. Lett.* **219**, 223 (1994).
- ⁴⁰ G. H. Roehrig, N. A. Oyler, and L. Adamowicz, *J. Phys. Chem.* **99**, 14285 (1995).
- ⁴¹ J. Schiedt, R. Weinkauff, D. M. Neumark, and E. W. Schlag, *Chemical Physics* **239**, 511 (1998).
- ⁴² S. S. Wesolowski, M. L. Leininger, P. N. Pentchev, and H. F. Schaefer, *J. Am. Chem. Soc.* **123**, 4023 (2001).

- ⁴³ X. Li, Z. Cai, and M. D. Sevilla, *J. Phys. Chem. A* **106**, 1596 (2002).
- ⁴⁴ D. M. A. Smith, A. F. Jalbout, J. Smets, and L. Adamowicz, *Chem. Phys.* **260**, 45 (2000).
- ⁴⁵ O. Dolgounitcheva, V. G. Zakrzewski, and J. V. Ortiz, *J. Phys. Chem. A* **105**, 8782 (2001).
- ⁴⁶ A. Alparone, A. Millefiori, and S. Millefiori, *Chem. Phys.* **312**, 261 (2005).
- ⁴⁷ P. Kebarle, *Annu. Rev. Phys. Chem.* **28**, 445 (1977).
- ⁴⁸ G. W. Caldwell, T. F. Magnera, and P. Kebarle, *J. Am. Chem. Soc.* **106**, 959 (1984).
- ⁴⁹ G. Markovich, S. Pollack, R. Giniger, and O. Cheshnovsky, *J. Chem. Phys.* **101**, 9344 (1994).
- ⁵⁰ R. Ayala, J. M. Martinez, R. R. Pappalardo, and E. S. Marcos, *Theor. Chem. Acc.* **116**, 691 (2006).
- ⁵¹ A. K. Pathak, T. Mukherjee, and D. K. Maity, *J. Chem. Phys.* **124**, 024322 (2006).
- ⁵² X. Bao, H. Sun, N.-B. Wong, and J. Gu, *J. Phys. Chem. B* **110**, 5865 (2006).
- ⁵³ S. Kim and H. F. Schaefer, *J. Chem. Phys.* **125**, 144305 (2006).
- ⁵⁴ S. Kim, S. E. Wheeler, and H. F. Schaefer, *J. Chem. Phys.* **124**, 204310 (2006).
- ⁵⁵ M. J. Frisch, G. W. Trucks, H. B. Schlegel, P. M. W. Gill, B. G. Johnson, M. A. Robb, J. R. Cheeseman, T. Keith, G. A. Petersson, J. A. Montgomery, K. Raghavachari, M. A. Al-Laham, V. G. Zakrzewski, J. V. Ortiz, J. B. Foresman, J. Cioslowski, B. B. Stefanov, A. Nanayakkara, M. Challacombe, C. Y. Peng, P. Y. Ayala, W. Chen, M. W. Wong, J. L. Andres, E. S. Replogle, R. Gomperts, R. L. Martin, D. J. Fox, J. S. Binkley, D. J. Defrees, J. Baker, J. P. Stewart, M. Head-

Gordon, C. Gonzalez, and J. A. Pople, Gaussian 94 (Gaussian, Inc., Pittsburgh PA, 1995).

⁵⁶ A. D. Becke, J. Chem. Phys. **98**, 5648 (1993).

⁵⁷ C. Lee, W. Yang, and R. G. Parr, Phys. Rev. B **37**, 785 (1988).

⁵⁸ S. Huzinaga, J. Chem. Phys. **42**, 1293 (1965).

⁵⁹ T. H. Dunning, J. Chem. Phys. **53**, 2823 (1970).

⁶⁰ T. J. Lee and H. F. Schaefer, J. Chem. Phys. **83**, 1784 (1985).

⁶¹ See EPAPS Document No. E-JCPSA6-126-006705 for optimized geometries of all structures considered. This document can be reached via a direct link in the online article's HTML reference section or via the EPAPS homepage (<http://www.aip.org/pubservs/epaps.html>).

⁶² K. C. Hunter, L. R. Rutledge, and S. D. Wetmore, J. Phys. Chem. A **109**, 9554 (2005).

⁶³ A. K. Chandra, D. Michalska, R. Wysokinsky, and T. Zeegers-Huyskens, J. Phys. Chem. A **108**, 9593 (2004).

Table 4.1. Relative energies (E_{rel}) and microhydration energies (E_{hyd}) in kcal mol⁻¹ for the cytosine hydrates and their anions (ZPVE-corrected values in parentheses).

Structure	$E_{\text{rel}}^{\text{a}}$	$E_{\text{hyd}}^{\text{b}}$	Structure	$E_{\text{rel}}^{\text{a}}$	$E_{\text{hyd}}^{\text{c}}$
1A	0.0 (0.0)	12.1 (9.7)	1A⁻	2.0 (1.6)	15.7 (13.7)
1B	0.6 (0.5)	11.5 (9.1)	1B⁻	0.0 (0.0)	17.7 (15.3)
1C	6.1 (5.1)	6.0 (4.5)	1C⁻	8.0 (8.7)	9.7 (6.6)
2A	0.0 (0.0)	24.8 (19.9)	2A⁻	6.0 (5.0)	27.6 (23.7)
2B	1.4 (1.2)	23.5 (18.6)	2B⁻	2.2 (2.0)	31.4 (26.8)
2C	1.5 (1.2)	23.3 (18.6)	2C⁻	1.3 (0.8)	32.3 (27.9)
2D	2.8 (2.4)	22.0 (17.5)	2D_a⁻	0.8 (0.8)	32.9 (28.0)
			2D_b⁻	0.0 (0.0)	33.6 (28.7)
2E	6.6 (5.7)	18.2 (14.2)	2E⁻	10.9 (10.3)	22.7 (18.4)
2F	7.3 (6.3)	17.5 (13.6)	2F⁻	11.4 (10.8)	22.2 (18.0)
3A	0.0 (0.0)	36.1 (28.9)	3A⁻	3.5 (2.9)	43.6 (37.5)
3B	1.0 (0.9)	35.2 (28.0)	3B⁻	1.9 (1.9)	45.2 (38.5)
3C	1.1 (1.7)	35.1 (27.2)	3C_a⁻	0.4 (1.2)	46.6 (39.2)
			3C_b⁻	0.6 (1.3)	46.5 (39.1)
3D	2.4 (2.1)	33.8 (26.8)	3D_a⁻	0.7 (0.9)	46.4 (39.5)
			3D_b⁻	0.0 (0.0)	47.1 (40.4)
3E	5.3 (4.5)	30.8 (24.4)	3E⁻	12.3 (12.3)	34.8 (28.1)
3F	6.6 (5.8)	29.5 (23.1)	3F⁻	11.5 (10.9)	35.6 (29.4)
3G	6.7 (6.0)	29.4 (22.9)	3G⁻	13.1 (12.7)	34.0 (27.7)
3H	9.2 (7.9)	26.9 (20.9)	3H_a⁻	11.2 (10.8)	35.9 (29.6)
			3H_b⁻	10.7 (10.3)	36.4 (30.0)
4A	0.0 (0.0)	48.3 (38.5)	4A⁻	4.0 (2.7)	55.9 (47.6)
4B	2.1 (1.6)	46.2 (36.8)	4B_a⁻	2.7 (2.1)	57.1 (48.2)
			4B_b⁻	0.9 (0.7)	59.0 (49.6)
4C	2.2 (2.5)	46.2 (36.0)	4C_a⁻	0.0 (0.0)	59.9 (50.3)
			4C_b⁻	0.0 (0.2)	59.8 (50.1)
4D	6.1 (5.2)	42.2 (33.3)	4D⁻	12.3 (11.4)	47.6 (38.9)
4E	7.1 (6.7)	41.3 (31.8)	4E⁻	11.5 (10.8)	48.4 (39.5)
4F	7.2 (6.2)	41.2 (32.3)	4F⁻	12.6 (11.3)	47.2 (39.0)
4G	9.9 (8.4)	38.4 (30.1)	4G⁻	11.2 (10.0)	48.7 (40.3)
5A	0.0 (0.0)	58.4 (45.7)	5A_a⁻	0.0 (0.0)	70.7 (59.0)
			5A_b⁻	-0.3 (0.1)	71.0 (59.0)
5B	4.2 (3.0)	54.2 (42.7)	5B⁻	11.6 (10.6)	59.1 (48.4)
5C	6.0 (5.2)	52.4 (40.5)	5C⁻	9.7 (9.0)	61.0 (50.0)
5D	7.6 (5.9)	50.8 (39.9)	5D⁻	11.2 (10.3)	59.6 (48.7)

^aRelative to the most stable structure among anionic or neutral structures with a given hydration number.

^bEnthalpy (0 K) of the reaction $\text{C}\cdot(\text{H}_2\text{O})_n \rightarrow \text{C} + n\text{H}_2\text{O}$.

^cEnthalpy (0 K) of the reaction $[\text{C}\cdot(\text{H}_2\text{O})_n]^- \rightarrow \text{C}^- + n\text{H}_2\text{O}$.

Table 4.2. Vertical detachment energies (VDEs) and adiabatic electron affinities (AEAs) in eV for cytosine and its hydrates (ZPVE-corrected values in parentheses).

Structure	VDE	AEA
cytosine	0.48	-0.09 (0.03)
1A/1A⁻	0.73	0.07 (0.21)
1B/1B⁻	0.93	0.18 (0.30)
1C/1C⁻	0.15	0.07 (0.12)
2A/2A⁻	0.72	0.03 (0.20)
2B/2B⁻	1.20	0.25 (0.39)
2C/2C⁻	1.09	0.30 (0.44)
2D/2D_a⁻	1.17	0.38 (0.49)
2D/2D_b⁻	1.21	0.41 (0.52)
2E/2E⁻	0.22	0.11 (0.22)
2F/2F⁻	0.26	0.11 (0.22)
3A/3A⁻	0.96	0.23 (0.41)
3B/3B⁻	1.24	0.35 (0.49)
3C/3C_a⁻	1.23	0.41 (0.55)
3C/3C_b⁻	1.54	0.40 (0.55)
3D/3D_a⁻	1.28	0.46 (0.58)
3D/3D_b⁻	1.30	0.49 (0.62)
3E/3E⁻	0.19	0.08 (0.19)
3F/3F⁻	0.43	0.17 (0.31)
3G/3G⁻	0.37	0.11 (0.24)
3H/3H⁻	0.60	0.30 (0.41)
3H/3H_b⁻	0.66	0.32 (0.43)
4A/4A⁻	1.07	0.24 (0.43)
4B/4B_a⁻	1.22	0.38 (0.53)
4B/4B_b⁻	1.27	0.46 (0.59)
4C/4C_a⁻	1.34	0.50 (0.66)
4C/4C_b⁻	1.68	0.50 (0.65)
4D/4D⁻	0.39	0.14 (0.28)
4E/4E⁻	0.45	0.22 (0.37)
4F/4F⁻	0.52	0.17 (0.32)
4G/4G⁻	0.78	0.36 (0.48)
5A/5A_a⁻	1.27	0.44 (0.61)
5A/5A_b⁻	1.65	0.46 (0.61)
5B/5B⁻	0.41	0.12 (0.28)
5C/5C⁻	0.69	0.28 (0.45)
5D/5D⁻	0.71	0.29 (0.42)

Table 4.3. Absolute adiabatic electron affinities (AEA_{abs}) in eV of cytosine and its hydrates (ZPVE-corrected values in parentheses).

Hydration number	Structures	AEA_{abs}
0		-0.09 (0.03)
1	1A/1B ⁻	0.16 (0.28)
2	2A/2D _b ⁻	0.29 (0.42)
3	3A/3D _b ⁻	0.39 (0.53)
4	4A/4C _a ⁻	0.41 (0.55)
5	5A/5A _a ⁻	0.44 (0.61)

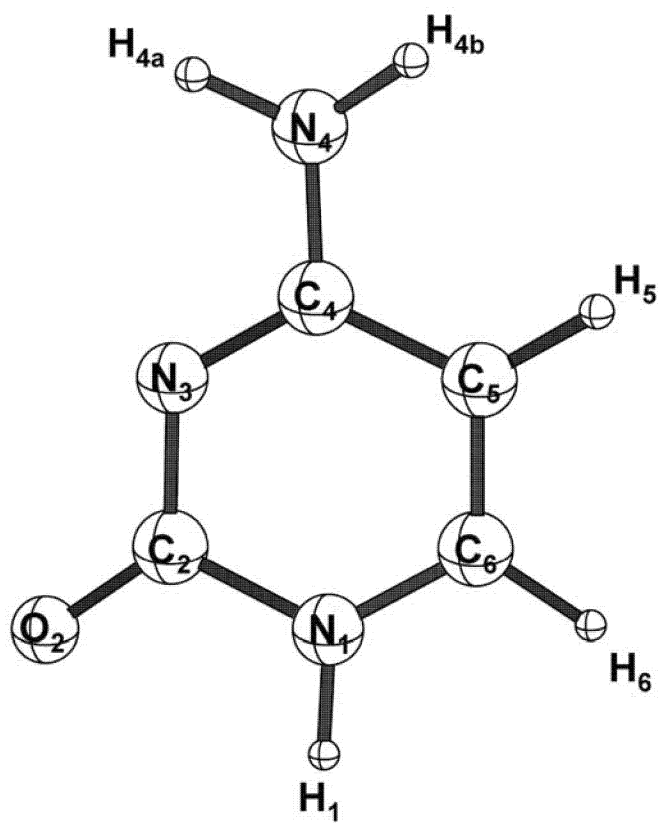


Figure 4.1. The canonical structure of cytosine with atom numbering scheme.

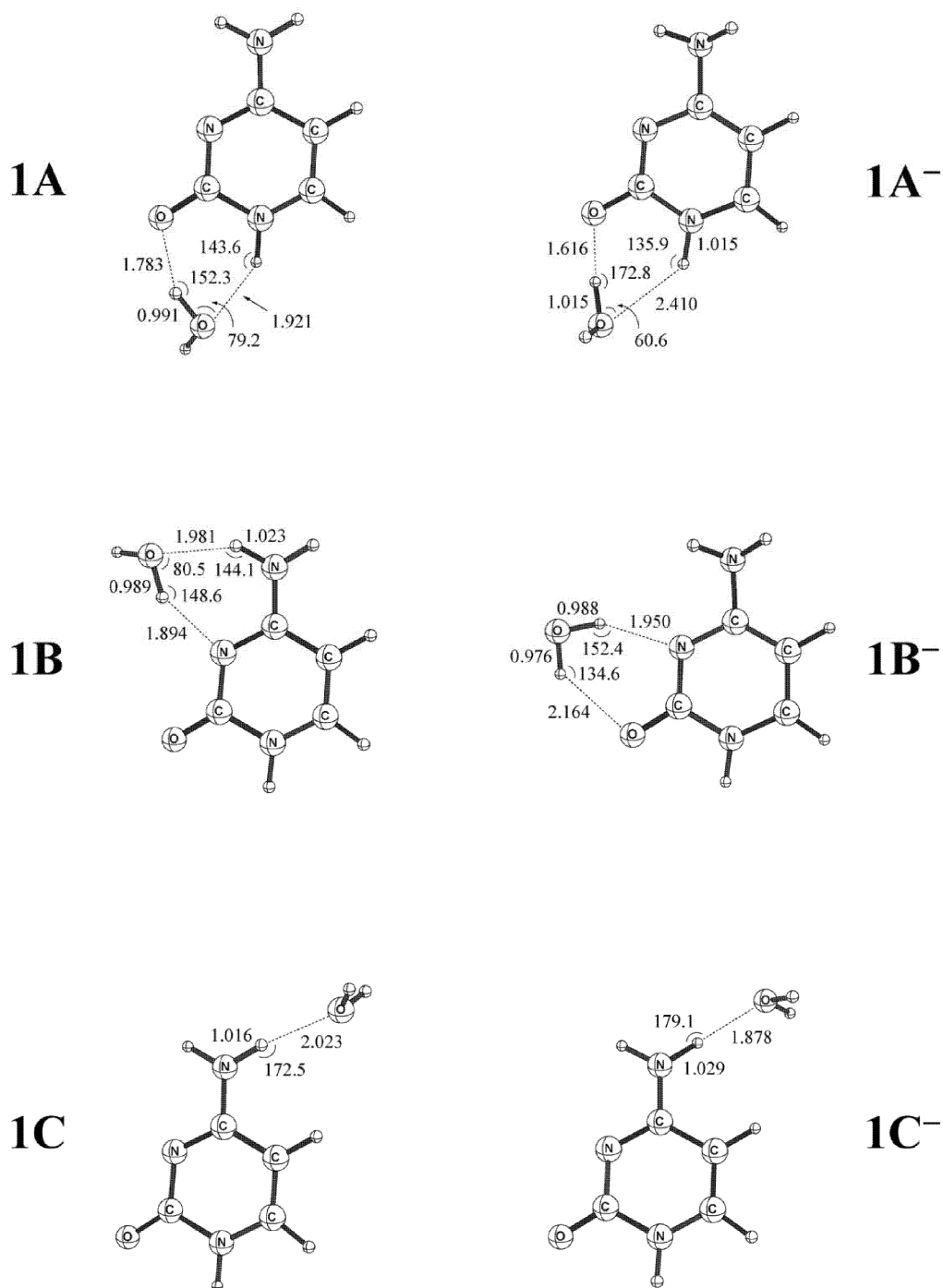
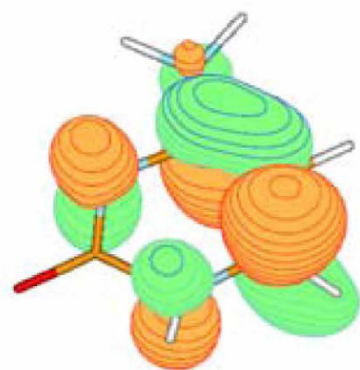
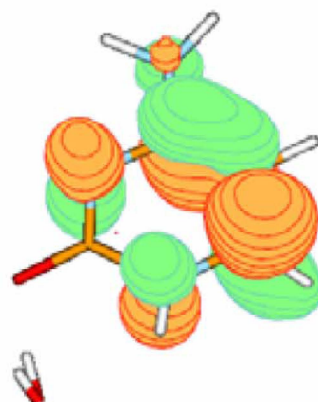


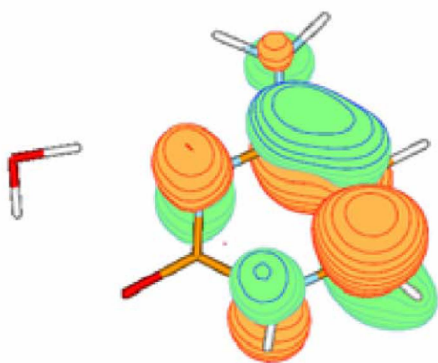
Figure 4.2. Molecular structures for cytosine monohydrates (left column) and their respective anions (right column), optimized at the B3LYP/DZP++ level of theory.



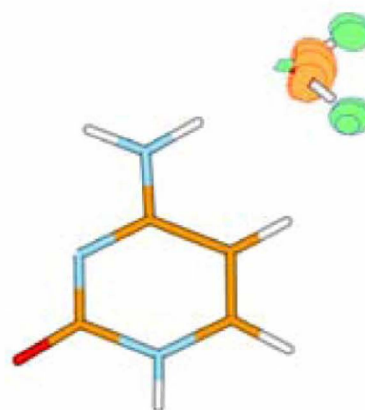
(a) Cytosine anion



(b) 1A⁻



(c) 1B⁻



(d) 1C⁻

Figure 4.3. Singly occupied molecular orbitals (SOMOs) for the anions of cytosine and its monohydrates: (a) the cytosine anion, (b) 1A⁻, (c) 1B⁻, and (d) 1C⁻.

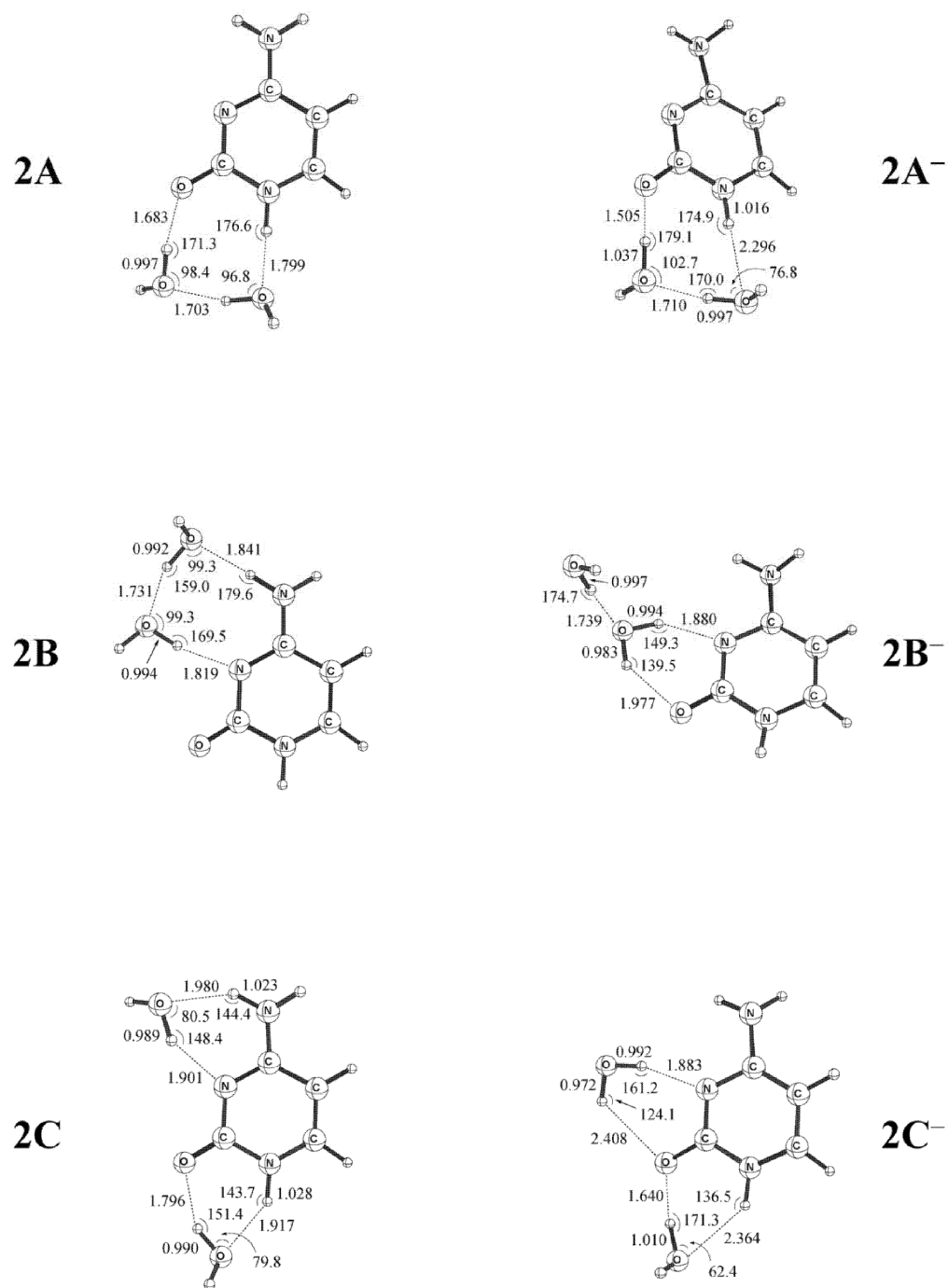
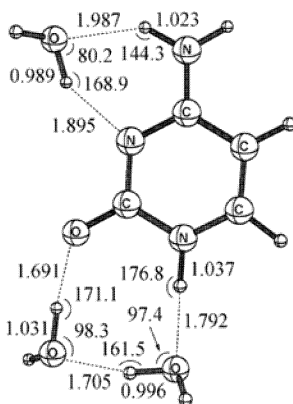
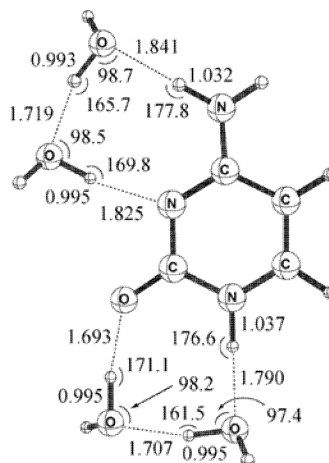


Figure 4.4. The three lowest-energy structures for the cytosine dihydrate and their respective anions.

3A



4A



5A

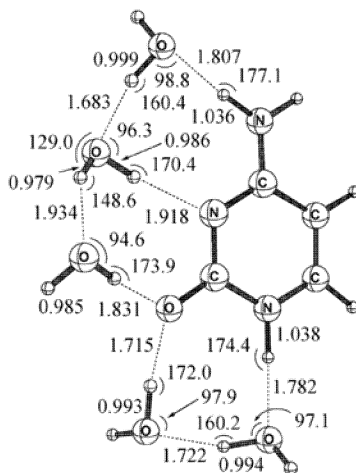


Figure 4.6. The most stable structures for the neutral tri-, tetra-, and pentahydrates of cytosine.

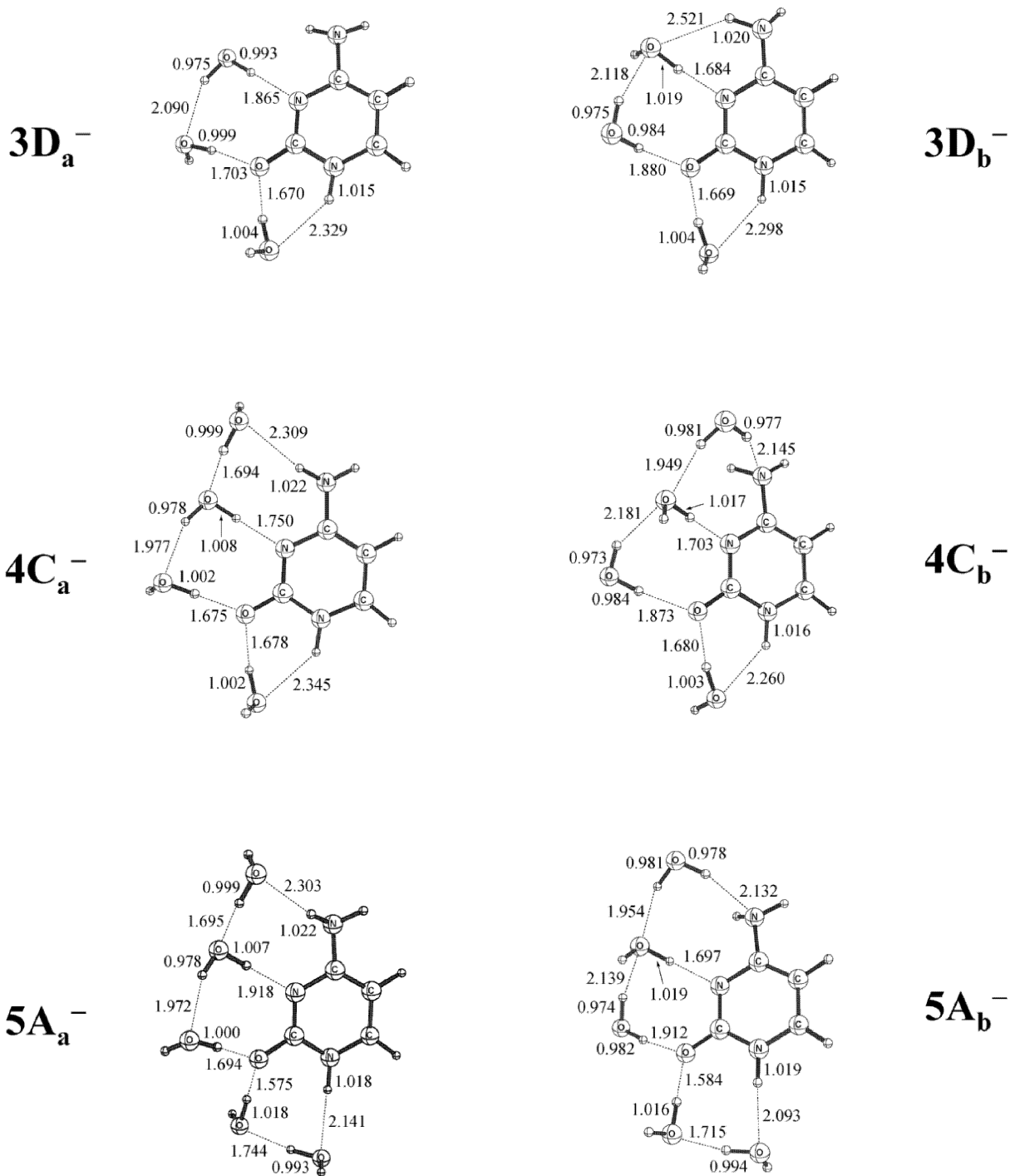


Figure 4.7. Selected theoretical structures for the anionic tri-, tetra-, pentahydrates of cytosine.

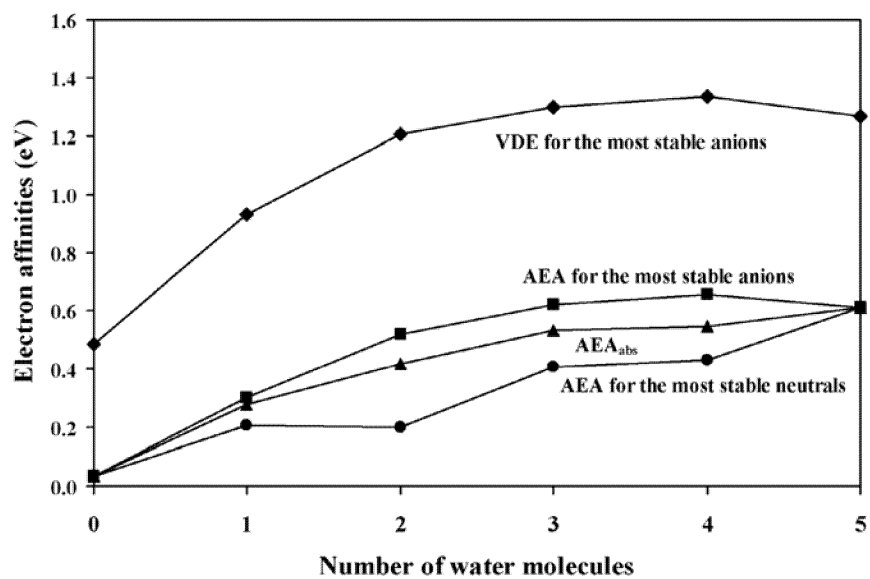


Figure 4.8. Electron affinities in eV for cytosine hydrates with up to five water molecules: VDEs for the most stable anionic hydrates (◆), ZPVE-corrected AEAs for the most stable anionic (■) and neutral (●) hydrates, and ZPVE-corrected absolute AEAs (▲).

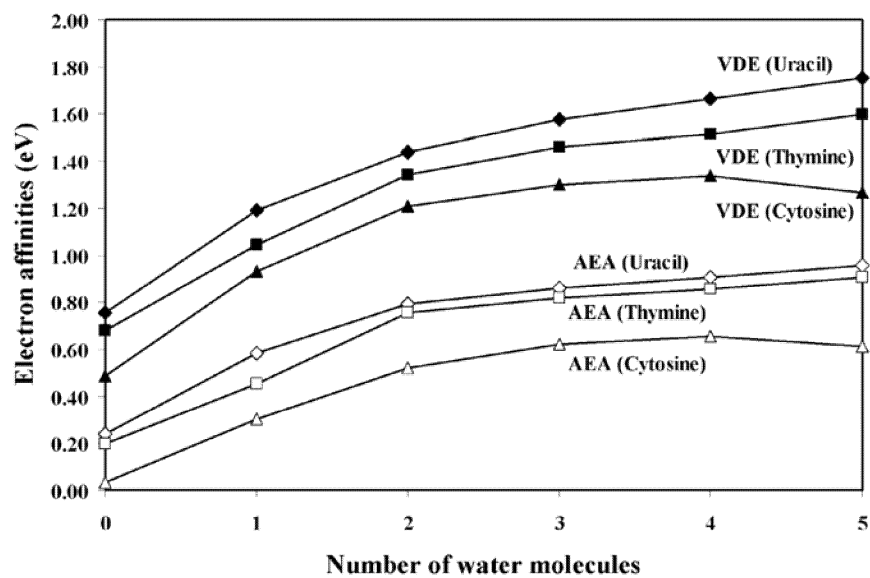


Figure 4.9. Comparison of the VDE and AEA among the uracil, thymine, and cytosine hydrates.

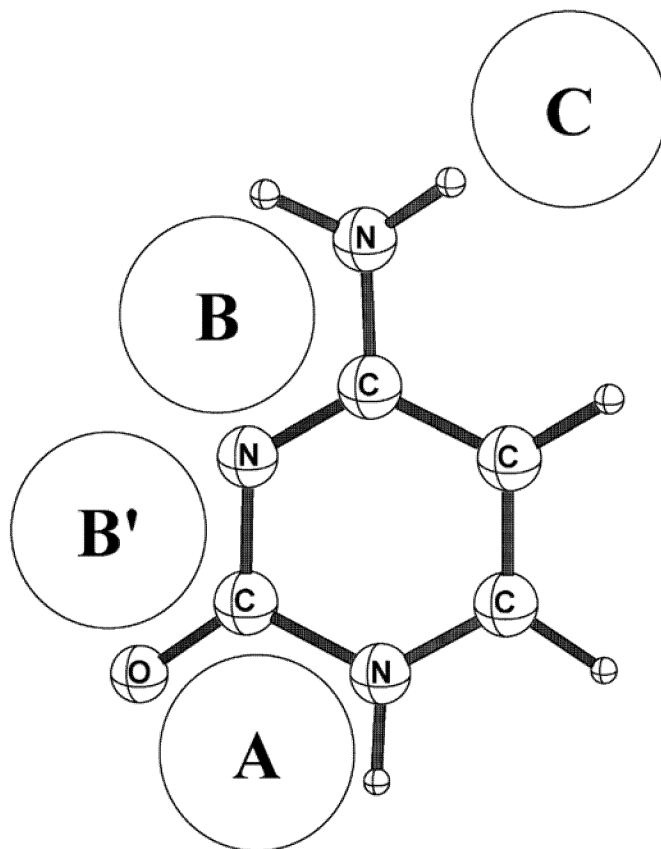


Figure 4.10. Prospective water-binding sites of cytosine. While site B is preferred by the neutral cytosine, site B' is preferred by the cytosine anion.

CHAPTER 5

HYDROGEN ATOM ABSTRACTION FROM THE ADENINE-URACIL BASE PAIR[†]

[†] Reproduced with permission from Sunghwan Kim, Tyler Meehan, and Henry F. Schaefer, *J. Phys. Chem. A*, Published on web (03/15/2007, DOI: 10.1021/jp070225x). Copyright 2007, American Chemical Society.

5.1 ABSTRACT

The hydrogen abstracted radicals from the adenine-uracil (AU) base pair have been studied at the B3LYP/DZP++ level of theory. The **A(N9)-U** and **A-U(N1)** radicals, which correspond to hydrogen atom abstraction at the adenine N9 and the uracil N1 atoms, were predicted to be the two lowest-lying among the nine AU-H radicals studied in this study. The removal of an amino hydrogen of the adenine moiety which forms a hydrogen bond with the uracil O4 atom in the AU pair resulted in radical **A(N6a)-U**, which has the smallest base pair dissociation energy, 5.9 kcal mol⁻¹. This radical is more likely to dissociate into the two isolated bases than to recover the hydrogen bond with the O4 atom through the N6-H bond rotation along the C6-N6 bond. In general, the radicals generated by C-H bond breaking were higher in energy than those arising from the N-H bond cleavage, because the unpaired electrons in the carbon-centered radicals were mainly localized on the carbon atom from which the hydrogen atom was removed. However, the highest-lying radical was found to arise from removal of the N3 hydrogen of uracil. The most remarkable structural feature of this radical is a very short C-H...O distance of 2.094 Å, consistent with a substantial hydrogen bond. Although this radical lost the N1...H-N3 hydrogen bond between the two bases, its dissociation energy was predicted to be 12.9 kcal mol⁻¹, similar to that of the intact AU base pair. This is due to the electron density transfer from the adenine N1 atom to the uracil N3 atom.

5.2 INTRODUCTION

High-energy radiation produces potentially lethal DNA lesions such as modified bases, abasic sites, and single-, and double-strand breaks (SSBs and DSBs). The direct impact on DNA by ionizing radiation generates positive holes within the DNA strands through one-electron oxidation of the nucleic acid bases (NABs).¹⁻⁴ Due to guanine having the lowest ionization potential among the NABs,⁵⁻¹⁰ these positive holes migrate to guanine sites through the DNA strands.¹¹⁻¹⁴ Many experimental and theoretical studies have shown that the 5'-terminus of poly-guanine (G_n) sequences in DNA act as a very efficient trap for the positive holes.¹⁵⁻²⁹ The cationic guanine radical subsequently reacts with reactive oxygen species generated by radiolysis of water to form 8-oxo-7,8-dihydroguanine and other oxidation products.³⁰⁻³³

A substantial amount of DNA damage is also attributed to the formation and transport of negative charges within the DNA strands, which arise from attachment of low-energy electrons to NABs.³⁴⁻⁴⁹ Such electrons, which have energies below 30 eV, are generated by the radiolysis of water.⁵⁰ In 2000, Sanche and coworkers demonstrated that such electrons can cause SSBs and DSBs even if their energies are lower than the ionization threshold (7.5 eV) of DNA.³⁴ Recent theoretical and experimental studies have suggested that electrons with energies even at or near 0 eV can result in DNA strand breaks.³⁵⁻³⁸ In addition, as shown in the experimental studies of Bowen and coworkers using anion photoelectron spectroscopy,³⁹⁻⁴³ electron attachment to the NABs can produce non-canonical tautomers through barrier-free proton transfer.

Along with positively and negatively charged species, various neutral radicals can also play

an important role during the radiation-induced DNA damage process.⁵¹⁻⁶⁶ An example of this is the radicals arising from the homolytic C-H or N-H bond cleavage of the NABs.⁵¹⁻⁶¹ Such radicals are generated either by direct abstraction of one hydrogen atom from the neutral NABs or by deprotonation of the oxidized (cationic) NABs.^{57,59,60} For example, the radical generated by removal of a hydrogen atom from the methyl group of thymine is known to be readily oxidized to give modified nucleobases such as 5-(hydroxymethyl)uracil or 5-formyluracil. In addition, the recent studies of Greenberg and coworkers showed that this radical can also generate an interstrand cross-link in double-stranded DNA.⁶⁷⁻⁷⁰

Because hydrogen bonding between two NABs is a key ingredient to storing genetic information in living organisms, hydrogen abstraction from the nucleobases may cause a significant change in the hydrogen bonding pattern of a base pair in the double stranded DNA, leading to crucial modifications in DNA. In the present research, we investigate the effect of hydrogen atom abstraction from the adenine-uracil (AU) base pair (Figure 5.1). Although uracil is predominantly found in RNA, the AU base pair is also of great importance because of its structural similarity to the adenine-thymine base pair in DNA duplexes.

5.3 COMPUTATIONAL METHODS

All geometry optimizations and harmonic vibrational frequency analyses have been performed using the Q-Chem 3.0 package of programs.⁷¹ The equilibrium structures of the radicals generated by removal of one hydrogen atom from the Watson-Crick AU base pair (AU-

H) have been optimized with density functional theory. In particular, we used the B3LYP density functional, which is Becke's three-parameter exchange functional (B3),⁷² in conjunction with the correlation functional of Lee, Yang, and Parr (LYP).⁷³ For numerical integrations, an Euler-Maclaurin-Lebedev-(75,302) grid, having 75 radial shells and 302 angular points per shell, was employed.⁷⁴ We used double- ζ quality basis sets with polarization and diffuse functions (DZP++). These were constructed by adding one set of p -type polarization functions for each H atom and one set of five d -type polarization functions for each C, N, and O atom (where $\alpha_p(\text{H})=0.75$, $\alpha_d(\text{C})=0.75$, $\alpha_d(\text{N})=0.80$, $\alpha_d(\text{O})=0.85$) to the Huzinaga-Dunning (9s5p/4s2p) contractions.^{75,76} Further augmentation with one even tempered s diffuse function for each H atom and even tempered s and p diffuse functions for each heavy atom completes the DZP++ basis set. The even tempered orbital exponents were determined according to the following formula,⁷⁷

$$\alpha_{diffuse} = \frac{1}{2} \left[\frac{\alpha_1}{\alpha_2} + \frac{\alpha_2}{\alpha_3} \right] \alpha_1$$

where α_1 , α_2 , and α_3 are the three smallest Gaussian orbital exponents of the s - or p -type primitive functions for a given atom ($\alpha_1 < \alpha_2 < \alpha_3$). The final DZP++ basis set contains six functions per H atom and 19 functions per C, N, or O atom. For the closed-shell AU base pair, this amounts to 396 contracted gaussian basis functions.

The dissociation energy (DE), relaxation energy (RE), and X-H bond dissociation energy (BDE) for a given AU-H radical were evaluated according to the following definitions:

Dissociation energy

$$DE = E[A-(U-H)] - E(A) - E(U-H)$$

or

$$DE = E[(A-H)-U] - E(A-H) - E(U)$$

Relaxation energy

$$RE = E(\text{radical at optimized A-U geometry}) - E(\text{optimized radical})$$

X-H bond dissociation energy

$$BDE = E[(A-H)-U] + E(H) - E(A-U)$$

or

$$BDE = E[A-(U-H)] + E(H) - E(A-U)$$

5.4 RESULTS

The structures of the AU-H radicals optimized at the B3LYP/DZP++ level of theory are shown in Figures 5.2 and 5.3, and their relative energies, dissociation energies, and relaxation energies are listed in Table 5.1. The selected interatomic distances for the AU base pair and the AU-H radicals are compared in Table 5.2.

5.4.1 A(N9)-U AND A-U(N1) RADICALS

Radical A(N9)-U, which corresponds to removal of the hydrogen atom at the N9 position of the adenine unit in the AU base pair, was found to be the lowest-lying among the nine AU-H

radicals studied in the present study. The second lowest-energy structure was radical **A-U(N1)**, generated by hydrogen abstraction from the N1 atom of the uracil base. The latter structure was predicted to lie 2.5 kcal mol⁻¹ above **A(N9)-U**. Note that in nucleosides, nucleotides, and DNA duplexes, the N9 atom of adenine and the N1 atom of uracil are covalently connected to the pentose sugar unit through an N-glycosidic linkage.

Although the N1···H-N3 hydrogen bond lengthens by 0.045 Å (from 1.792 to 1.837 Å) upon formation of **A(N9)-U** from the AU pair, the N6-H6a···O4 hydrogen bond shortens by 0.106 Å (from 1.891 to 1.785 Å). The increased interaction between the two base units in **A(N9)-U** is reflected in the dissociation energy of 13.7 kcal mol⁻¹ for **A(N9)-U**, which is greater by 1.0 kcal mol⁻¹ than that predicted for the intact AU base pair (12.7 kcal mol⁻¹). On the other hand, hydrogen abstraction from atom N1 of the uracil moiety of the AU pair to generate **A-U(N1)** decreases its dissociation energy by 0.4 kcal mol⁻¹ (from 12.7 to 12.3 kcal mol⁻¹). The elongation of the N6-H6a···O4 hydrogen bond by 0.061 Å (from 1.891 to 1.952 Å) is more pronounced than the shortening of the N1···H-N3 hydrogen bond by 0.014 Å (from 1.792 to 1.778 Å).

Because the N9-H bond of adenine and the N1-H bond of uracil are σ -type bonds, the homolytic cleavage of these bonds may be expected to give σ -type radicals, where the unpaired electron is mainly localized in the molecular plane. However, the spin density plots for the **A(N9)-U** and **A-U(N1)** radicals shown in Figure 5.4 suggest that the unpaired electrons are

delocalized on the π -conjugated ring system. This delocalization of the unpaired electrons is a contributor to the energetic favoredness of **A(N9)-U** and **A-U(N1)**.

5.4.2 **A(N6a)-U** AND **A(N6b)-U** RADICALS

The next lowest-lying radicals were predicted to be **A(N6b)-U** and **A(N6a)-U**, generated by removing one of the hydrogen atoms of the adenine amino group. As shown in Figure 5.4, like **A(N9)-U** and **A-U(N1)**, these two radicals are also π -type radicals, in which the unpaired electrons are largely delocalized on the aromatic ring system. They are higher in energy than **A(N9)-U** by 7.5 and 11.5 kcal mol⁻¹ for **A(N6b)-U** and **A(N6a)-U**, respectively. Although the H6b atom is not involved in the intermolecular hydrogen bonds between the two base units, abstraction of the H6b atom results in lengthening of the N1...H-N3 hydrogen bond by 0.052 Å, compared to the AU pair. The change is even more significant for the N6-H6a...O4 hydrogen bond, which is elongated by 0.244 Å. These geometrical changes in **A(N6b)-U** imply a weakening of the interaction between the two bases. Indeed, the dissociation energy for **A(N6b)-U** was predicted to be 8.9 kcal mol⁻¹, smaller by 3.8 kcal mol⁻¹ than that for the AU pair.

Formation of the **A(N6a)-U** radical results in loss of the N6-H6a...O4 hydrogen bond, which is reflected in the decreased dissociation energy of 5.9 kcal mol⁻¹. Interestingly, while the N1...H-N3 hydrogen bond length increases by 0.260 Å, the C2-H...O2 contact becomes shorter by 0.573 Å. For the intact AU pair, the interatomic distance between the C2-H hydrogen atom of adenine and the O2 atom of uracil is predicted to be 2.840 Å, which is in the range of the sum of

the van der Waals radii for oxygen and hydrogen atoms (2.70 ~ 2.95 Å).^{78,79} Although the existence of C-H...O hydrogen bonding is disputable, it seems to be clear that such an interaction is much weaker than N-H...O or O-H...O hydrogen bonding. Thus, it would be difficult to induce a significant shortening of the C-H...O interatomic distance, as found in **A(N6a)-U**. Instead, we conclude that the significant change in the C2-H...O2 distance arises from the lone pair repulsion between the N6 atom of adenine and O4 atom of uracil. In the AU pair, the N6...O4 interatomic distance of 2.913 Å is slightly shorter than the sum of the van der Waals radii for oxygen and nitrogen atoms (3.05 Å).⁷⁸ Removal of the H6a atom of adenine causes repulsion between the lone pairs of the N6 and O4 atoms, and the N6...O4 distance for **A(N6a)-U** is predicted to increase to 3.961 Å.

Note that radicals **A(N6b)-U** and **A(N6a)-U** can be interconverted. That is, the loss of the N6-H6a...O4 hydrogen bond in **A(N6a)-U** radical can be recovered through rotation of the N6-H bond along the C6-N6 bond. Figure 5.5 compares the dissociation energy for the two radical conformers and the rotation barrier between them. The transition state between the two radicals (Figure 5.6) lies 11.0 kcal mol⁻¹ above **A(N6b)-U**, and the rotational barrier from **A(N6a)-U** to **A(N6b)-U** is 7.0 kcal mol⁻¹. This is higher by 1.1 kcal mol⁻¹ than the dissociation energy of **A(N6a)-U**, implying that if the **A(N6a)-U** radical is generated by losing the H6a hydrogen atom, the dissociation process into the two isolated bases will be slightly favored compared to conformational isomerism to **A(N6b)-U**.

5.4.3 **A(C2)-U**, **A(C8)-U**, **A-U(C5)**, AND **A-U(C6)** RADICALS

The radicals which arise from homolytic C-H bond breaks were predicted to be higher in energy than those from N-H homolytic bond cleavage (except for **A-U(N3)**). This is because the C-H bond break results in σ -type radicals (as implied in Figures 5.4), in which the unpaired electrons are localized in the molecular plane. Hydrogen abstraction from the C2 atom of adenine gives radical **A(C2)-U**, which lies $12.6 \text{ kcal mol}^{-1}$ above the global minimum. Because the C2-H \cdots O2 interaction is expected to be weak, the loss of the C2-H \cdots O2 contact will not cause a significant decrease in the dissociation energy, compared to **A(N6a)-U**. Indeed, the predicted dissociation energy for **A(C2)-U** is smaller by only $1.7 \text{ kcal mol}^{-1}$ than that for the AU pair. Whereas the N6-H6a \cdots O4 hydrogen bond distance for **A(C2)-U** decreases by 0.058 \AA (from 1.891 to 1.833 \AA) compared to that for the AU pair, the N1 \cdots H-N3 distance increases by 0.121 \AA (from 1.792 to 1.913 \AA).

The hydrogen atoms at the C8 position of adenine and at the C5 and C6 positions of uracil are not involved in the hydrogen bond network between the two bases. Thus, radicals generated by abstraction of these hydrogens are expected to have the similar dissociation energies to that of the AU pair. Indeed, the predicted dissociation energies were 12.6 , 13.0 , and $13.1 \text{ kcal mol}^{-1}$ for **A(C8)-U**, **A-U(C5)**, and **A-U(C6)**, respectively. For the same reason, the N6-H6a \cdots O4 and N1 \cdots H-N3 hydrogen bond lengths predicted for the three radicals do not differ very much from those of the intact AU pair. The largest difference was predicted for **A-U(C5)**, where the N6-

H6a \cdots O4 hydrogen bond is longer by 0.014 Å and the N1 \cdots H-N3 hydrogen bond is shorter by 0.029 Å, compared to those of the AU pair.

5.4.4 A-U(N3) RADICAL

The removal of the N3-H hydrogen atom from the uracil part of the AU base pair might be expected to weaken the binding of the base pair due to the loss of the N1 \cdots H-N3 hydrogen bond. Surprisingly, however, the dissociation energy of 12.9 kcal mol⁻¹ for the resulting radical, **A-U(N3)**, is very similar to that of the AU base pair. The N6-H6a \cdots O hydrogen bond length becomes shorter by 0.244 Å upon the removal of the H3 atom. In addition, the C2-H \cdots O2 contact becomes even shorter, by 0.746 Å (from 2.840 Å to 2.094 Å). Because of this significant decrease in the C2-H \cdots O2 interatomic distance, one might think that the enhanced interaction between C2-H and O2 atoms would be the main stabilizing factor responsible for the large DE value for **A-U(N3)**. However, note that if we assume that the lost N3 \cdots H1-N1 hydrogen bond destabilizes the system by ~ 5 kcal mol⁻¹, there must be a stabilizing factor that can lower the energy of **A-U(N3)** by ~ 5 kcal mol⁻¹. The increase in the C2-H \cdots O2 interaction does not seem to be able to provide this amount of energy because the C-H \cdots O hydrogen bonding is normally thought to be much weaker than other strong hydrogen bonding such as O-H \cdots O or N-H \cdots O hydrogen bonding. For example, in the recent study of Quinn, Zimmerman, Del Bene, and Shavitt,⁸⁰ the stability due to the C-H \cdots O contact in the adenine-thymine base pair was estimated

to be 2-2.5 kcal mol⁻¹. This amount of stabilization does not appear large enough to compensate for the loss of the N3...H-N1 hydrogen bond in the AU pair.

The key to understanding the unexpectedly large dissociation energy of the **A-U(N3)** radical is hinted at by its spin density plot (Figure 5.4). The unpaired electron of the **A-U(N3)** radical is located between the N1 atom of adenine and the N3 atom of uracil in the molecular plane. Figure 5.4 indicates that the system is stabilized by transfer of electron density from the lone pair orbital associated with the adenine N1 atom to the (half-filled) singly-occupied molecular orbital (SOMO) of the N3 atom of uracil. This effect is depicted schematically in Figure 5.7, along with the contrasting situation, where the SOMO is perpendicular to the molecular plane. If the **A-U(N3)** radical is a π radical, where the unpaired electron is perpendicular to the molecular plane and delocalized through the uracil ring system, the system would be destabilized by lone pair repulsion between the N1 atom of adenine and the N3 atom of uracil, and the dissociation energy would decrease. An example of this opposite case is radical **A(N6a)-U**. For this radical, the unpaired π -electron is delocalized on the purine ring and the repulsive potential occurs between the σ -type lone pairs of the adenine N6 and uracil O4 atoms. This is the reason why **A-U(N3)** has a similar dissociation energy than the AU pair, while the removal of adenine H6a atom decreases the dissociation energy significantly.

5.5 DISCUSSION

The hydrogen abstracted radicals of the AU base pair have been investigated at the B3LYP/DZP++ level of theory. The two lowest-energy structures are radicals **A(N9)-U** and **A-U(N1)**, which correspond to hydrogen abstraction at the N9 atom of adenine and the N1 atom of uracil, respectively. However, because these nitrogen atoms are covalently bonded to the ribose moiety in nucleosides and nucleotides, the next lowest energy structures, **A(N6b)-U** and **A(N6a)-U**, generated by removing one of the amino hydrogen atoms of the adenine moiety, should be more important in biological systems. The abstraction of the H6a atom from adenine causes a loss of the N6-H6a \cdots O4 hydrogen bond and the resulting **A(N6a)-U** radical has the smallest dissociation energy, 5.9 kcal mol⁻¹, suggesting that it could be a potential lesion in the DNA/RNA strand. The N1 \cdots H-N3 hydrogen bond in **A(N6a)-U** can be recovered through rotation of the N6-H6b group along the C6-N6 bond. However, the rotational barrier of 7.0 kcal mol⁻¹ for this process is higher than the dissociation energy of the **A(N6a)-U** radical, implying that the latter is more likely to dissociate than to convert to **A(N6b)-U**.

Except for the highest-energy radical, **A-U(N3)**, the unpaired electrons of the radicals generated through homolytic N-H bond cleavage are found to be delocalized on the π system of the ring structure. On the contrary, for the radicals generated by C-H homolytic bond breaking, the unpaired electrons are localized at the corresponding carbon atom and primarily have σ character. Because of this, the carbon-centered radicals are predicted to lie above the nitrogen-centered radicals in general. The only exception for this is radical **A-U(N3)**. Although removal

of the N3-H hydrogen atom of uracil causes a loss of the N1...H-N3 hydrogen bond, the resulting radical, **A-U(N3)**, can be stabilized by electron density transfer to the half-filled orbital on N3 atom of uracil because the radical center is located on the molecular plane. Due to this effect, the **A-U(N3)** radical has a dissociation energy similar to the intact AU pair, although it is the highest-lying radical.

The relaxation energy of a given radical is a measure of the effect of hydrogen abstraction upon the geometrical change. For example, the radicals where the unpaired electrons are delocalized (e.g., the four lowest-lying AU-H radicals) showed large relaxation energies (4 to 13 kcal mol⁻¹, as listed in Table 5.1), implying that their geometries are quite different compared to the geometry of the AU base pair. On the contrary, if the unpaired electrons are localized at the atom from which the hydrogen atom is removed (e.g., all carbon-centered radicals), such radicals have small relaxation energies only about 1-2 kcal mol⁻¹. The **A-U(N3)** radical shows a relatively large relaxation energy because of the electron density transfer from the uracil N3 to the adenine N1 atoms.

The relative energies for the hydrogen abstracted radicals of the isolated adenine and uracil (A-H and U-H) are summarized in Table 5.3. Previous studies⁸¹ on hydrogen abstracted radicals of adenine (A-H) predicted the energetic ordering of **A(N9)** < **A(N6b)** < **A(N6a)** < **A(C2)** < **A(C8)**. The energetic ordering for the hydrogen abstracted radicals of uracil (U-H) predicted in the present study is **U(N1)** < **U(C6)** < **U(C5)** < **U(N3)**. These two sets of the energetic orderings are maintained in the energetic orderings for the base pair AU-H radicals.

Figure 5.8 depicts two possible pathways to formation of AU-H radicals from adenine and uracil bases. From Figure 5.8, an important relation between BDE and DE may be derived.

$$\text{BDE}_{\text{A-H}} + \text{DE}_{[(\text{A-H})\text{U}]} = \text{BDE}_{[(\text{A-H})\text{U}]} + \text{DE}_{\text{AU}}$$

$$\text{BDE}_{[(\text{A-H})\text{U}]} - \text{BDE}_{\text{A-H}} = \text{DE}_{[(\text{A-H})\text{U}]} - \text{DE}_{\text{AU}}$$

Similarly,

$$\text{BDE}_{[\text{A}(\text{U-H})]} - \text{BDE}_{\text{U-H}} = \text{DE}_{[\text{A}(\text{U-H})]} - \text{DE}_{\text{AU}}$$

The above equations imply that the BDE for a specific AU-H radical can be deduced from the difference in DE between the radical and AU base pair. For example, the decrease in DE by 1.0 kcal mol⁻¹ for **A(N9)-U** (compared to the AU pair) results in the increase in BDE by 1.0 kcal mol⁻¹, (0.043 eV). As listed in Table 5.4, the BDE of A-H or U-H radicals are typically greater than 4.12 eV at least (equivalent to 95 kcal mol⁻¹) while the biggest change in DE upon hydrogen abstraction from the AU base pair is predicted to be 6.8 kcal mol⁻¹ (~ 0.3 eV). That is, due to the nature of the hydrogen bonding which is responsible for base pairing, the changes in DE values for the AU-H radicals are very small compared to their BDE values. This implies that the energetics of the radicals can be predicted from those for the A-H or U-H radicals.

5.6 ACKNOWLEDGEMENTS

This work was supported by National Science Foundation Grant CHE-0451445.

5.7 REFERENCES

- ¹ S. K. Kim, W. Lee, and D. R. Herschbach, *J. Phys. Chem.* **100**, 7933 (1996).
- ² H.-W. Jochims, M. Schwell, H. Baumgaertel, and S. Leach, *Chem. Phys.* **314**, 263 (2005).
- ³ S. Steenken, *Chem. Rev.* **89**, 503 (1989).
- ⁴ M. Ratner, *Nature* **397**, 480 (1999).
- ⁵ X. Li, Z. Cai, and M. D. Sevilla, *J. Phys. Chem. A* **106**, 9345 (2002).
- ⁶ C. E. Crespo-Hernandez, R. Arce, Y. Ishikawa, L. Gorb, J. Leszczynski, and D. M. Close, *J. Phys. Chem. A* **108**, 6373 (2004).
- ⁷ A. O. Colson, B. Besler, D. M. Close, and M. D. Sevilla, *J. Phys. Chem.* **96**, 661 (1992).
- ⁸ M. Hutter and T. Clark, *J. Am. Chem. Soc.* **118**, 7574 (1996).
- ⁹ J. Sponer, J. Leszczynski, and P. Hobza, *J. Phys. Chem.* **100**, 5590 (1996).
- ¹⁰ F. Prat, K. N. Houk, and C. S. Foote, *J. Am. Chem. Soc.* **120**, 845 (1998).
- ¹¹ U. Diederichsen, *Angew. Chem., Int. Ed. Engl.* **36**, 2317 (1997).
- ¹² E. Nir, K. Kleinermanns, and M. S. de Vries, *Nature* **408**, 949 (2000).
- ¹³ J. Bertran, A. Oliva, L. Rodriguez-Santiago, and M. Sodupe, *J. Am. Chem. Soc.* **120**, 8159 (1998).
- ¹⁴ V. Guallar, A. Douhal, M. Moreno, and J. M. Lluch, *J. Phys. Chem. A* **103**, 6251 (1999).
- ¹⁵ D. B. Hall, R. E. Holmlin, and J. K. Barton, *Nature* **382**, 731 (1996).
- ¹⁶ D. B. Hall and J. K. Barton, *J. Am. Chem. Soc.* **119**, 5045 (1997).
- ¹⁷ S. M. Gasper and G. B. Schuster, *J. Am. Chem. Soc.* **119**, 12762 (1997).

- ¹⁸ B. Armitage, D. Ly, T. Koch, H. Frydenlund, H. Orum, H. G. Batz, and G. B. Schuster, Proc. Natl. Acad. Sci. U. S. A. **94**, 12320 (1997).
- ¹⁹ E. Meggers, D. Kusch, M. Spichy, U. Wille, and B. Giese, Angew. Chem., Int. Ed. **37**, 460 (1998).
- ²⁰ I. Saito, M. Takayama, H. Sugiyama, K. Nakatani, A. Tsuchida, and M. Yamamoto, J. Am. Chem. Soc. **117**, 6406 (1995).
- ²¹ H. Sugiyama and I. Saito, J. Am. Chem. Soc. **118**, 7063 (1996).
- ²² D. T. Breslin and G. B. Schuster, J. Am. Chem. Soc. **118**, 2311 (1996).
- ²³ D. Ly, Y. Kan, B. Armitage, and G. B. Schuster, J. Am. Chem. Soc. **118**, 8747 (1996).
- ²⁴ K. Kino, I. Saito, and H. Sugiyama, J. Am. Chem. Soc. **120**, 7373 (1998).
- ²⁵ K. Ito and S. Kawanishi, Biochemistry **36**, 1774 (1997).
- ²⁶ E. D. A. Stemp, M. R. Arkin, and J. K. Barton, J. Am. Chem. Soc. **119**, 2921 (1997).
- ²⁷ J. G. Muller, R. P. Hickerson, R. J. Perez, and C. J. Burrows, J. Am. Chem. Soc. **119**, 1501 (1997).
- ²⁸ H.-C. Shih, N. Tang, C. J. Burrows, and S. E. Rokita, J. Am. Chem. Soc. **120**, 3284 (1998).
- ²⁹ A. Spassky and D. Angelov, Biochemistry **36**, 6571 (1997).
- ³⁰ I. Saito, T. Nakamura, K. Nakatani, Y. Yoshioka, K. Yamaguchi, and H. Sugiyama, J. Am. Chem. Soc. **120**, 12686 (1998).
- ³¹ G. B. Schuster, Acc. Chem. Res. **33**, 253 (2000).
- ³² F. D. Lewis, R. L. Letsinger, and M. R. Wasielewski, Acc. Chem. Res. **34**, 159 (2001).

- ³³ C. J. Burrows and J. G. Muller, *Chem. Rev.* **98**, 1109 (1998).
- ³⁴ B. Boudaiffa, P. Cloutier, D. Hunting, M. A. Huels, and L. Sanche, *Science* (Washington, D. C.) **287**, 1658 (2000).
- ³⁵ X. Li, M. D. Sevilla, and L. Sanche, *J. Am. Chem. Soc.* **125**, 13668 (2003).
- ³⁶ X. Bao, J. Wang, J. Gu, and J. Leszczynski, *Proc. Natl. Acad. Sci. U. S. A.* **103**, 5658 (2006).
- ³⁷ J. Simons, *Acc. Chem. Res.* **39**, 772 (2006).
- ³⁸ I. Bald, J. Kopyra, and E. Illenberger, *Angew. Chem., Int. Ed.* **45**, 4851 (2006).
- ³⁹ I. Dabkowska, J. Rak, M. Gutowski, J. M. Nilles, S. T. Stokes, and K. H. Bowen, *J. Chem. Phys.* **120**, 6064 (2004).
- ⁴⁰ M. Haranczyk, I. Dabkowska, J. Rak, M. Gutowski, J. M. Nilles, S. Stokes, D. Radisic, and K. H. Bowen, *J. Phys. Chem. B* **108**, 6919 (2004).
- ⁴¹ M. Haranczyk, J. Rak, M. Gutowski, D. Radisic, S. T. Stokes, and K. H. Bowen, Jr., *Isr. J. Chem.* **44**, 157 (2004).
- ⁴² M. Haranczyk, J. Rak, M. Gutowski, D. Radisic, S. T. Stokes, and K. H. Bowen, Jr., *J. Phys. Chem. B* **109**, 13383 (2005).
- ⁴³ D. Radisic, K. H. Bowen, Jr., I. Dabkowska, P. Storonik, J. Rak, and M. Gutowski, *J. Am. Chem. Soc.* **127**, 6443 (2005).
- ⁴⁴ P. Swiderek, *Angew. Chem., Int. Ed.* **45**, 4056 (2006).
- ⁴⁵ J. Gu, J. Wang, and J. Leszczynski, *J. Am. Chem. Soc.* **128**, 9322 (2006).
- ⁴⁶ S. G. Ray, S. S. Daube, and R. Naaman, *Proc. Natl. Acad. Sci. U. S. A.* **102**, 15 (2005).

- ⁴⁷ Y. Zheng, P. Cloutier, D. J. Hunting, L. Sanche, and J. R. Wagner, *J. Am. Chem. Soc.* **127**, 16592 (2005).
- ⁴⁸ L. Sanche, *Eur. Phys. J. D* **35**, 367 (2005).
- ⁴⁹ L. Sanche, *Phys. Scr.* **68**, C108 (2003).
- ⁵⁰ International Commission on Radiation Units and Measurements, ICRU Report 31 (ICRU, Washington, DC), 1979.
- ⁵¹ Y. Chen and D. Close, *J. Mol. Struct.* **549**, 55 (2001).
- ⁵² D. M. Close, L. A. Eriksson, E. O. Hole, E. Sagstuen, and W. H. Nelson, *J. Phys. Chem. B* **104**, 9343 (2000).
- ⁵³ S. D. Wetmore, R. J. Boyd, and L. A. Eriksson, *J. Phys. Chem. B* **102**, 5369 (1998).
- ⁵⁴ E. O. Hole, E. Sagstuen, W. H. Nelson, and D. M. Close, *J. Phys. Chem.* **95**, 1494 (1991).
- ⁵⁵ S. D. Wetmore, R. J. Boyd, and L. A. Eriksson, *J. Phys. Chem. B* **102**, 10602 (1998).
- ⁵⁶ E. Sagstuen, E. O. Hole, W. H. Nelson, and D. M. Close, *J. Phys. Chem.* **96**, 1121 (1992).
- ⁵⁷ E. Malinen and E. Sagstuen, *Radiat. Res.* **160**, 186 (2003).
- ⁵⁸ D. M. Close, *Radiat. Res.* **135**, 1 (1993).
- ⁵⁹ W. A. Bernhard, *Adv. Radiat. Biol.* **9**, 199 (1981).
- ⁶⁰ D. Becker and M. D. Sevilla, *Adv. Radiat. Biol.* **17**, 121 (1993).
- ⁶¹ W. A. Bernhard, J. Barnes, K. R. Mercer, and N. Mroczka, *Radiat. Res.* **140**, 199 (1994).
- ⁶² Y. Chen and D. Close, *Struct. Chem.* **13**, 203 (2002).
- ⁶³ S. D. Wetmore, R. J. Boyd, and L. A. Eriksson, *J. Phys. Chem. B* **102**, 7674 (1998).

- ⁶⁴ S. D. Wetmore, R. J. Boyd, and L. A. Eriksson, *J. Phys. Chem. B* **102**, 9332 (1998).
- ⁶⁵ M. G. Debije, D. M. Close, and W. A. Bernhard, *Radiat. Res.* **157**, 235 (2002).
- ⁶⁶ E. Westhof, W. Flossmann, H. Zehner, and A. Mueller, *Faraday Disc. Chem. Soc.* **63**, 248 (1977).
- ⁶⁷ I. S. Hong and M. M. Greenberg, *J. Am. Chem. Soc.* **127**, 3692 (2005).
- ⁶⁸ I. S. Hong and M. M. Greenberg, *J. Am. Chem. Soc.* **127**, 10510 (2005).
- ⁶⁹ I. S. Hong, H. Ding, and M. M. Greenberg, *J. Am. Chem. Soc.* **128**, 485 (2006).
- ⁷⁰ I. S. Hong, H. Ding, and M. M. Greenberg, *J. Am. Chem. Soc.* **128**, 2230 (2006).
- ⁷¹ Y. Shao, L. F. Molnar, Y. Jung, J. Kussmann, C. Ochsenfeld, S. T. Brown, A. T. B. Gilbert, L. V. Slipchenko, S. V. Levchenko, D. P. O'Neill, R. A. DiStasio, R. C. Lochan, T. Wang, G. J. O. Beran, N. A. Besley, J. M. Herbert, C. Y. Lin, T. Van Voorhis, S. H. Chien, A. Sodt, R. P. Steele, V. A. Rassolov, P. E. Maslen, P. P. Korambath, R. D. Adamson, B. Austin, J. Baker, E. F. C. Byrd, H. Dachsel, R. J. Doerksen, A. Dreuw, B. D. Dunietz, A. D. Dutoi, T. R. Furlani, S. R. Gwaltney, A. Heyden, S. Hirata, C.-P. Hsu, G. Kedziora, R. Z. Khalliulin, P. Klunzinger, A. M. Lee, M. S. Lee, W. Liang, I. Lotan, N. Nair, B. Peters, E. I. Proynov, P. A. Pieniazek, Y. M. Rhee, J. Ritchie, E. Rosta, C. D. Sherrill, A. C. Simmonett, J. E. Subotnik, H. L. Woodcock, W. Zhang, A. T. Bell, A. K. Chakraborty, D. M. Chipman, F. J. Keil, A. Warshel, W. J. Hehre, H. F. Schaefer, J. Kong, A. I. Krylov, P. M. W. Gill, and M. Head-Gordon, *Phys. Chem. Chem. Phys.* **8**, 3172 (2006).
- ⁷² A. D. Becke, *J. Chem. Phys.* **98**, 5648 (1993).

- ⁷³ C. Lee, W. Yang, and R. G. Parr, Phys. Rev. B **37**, 785 (1988).
- ⁷⁴ B. N. Papas and H. F. Schaefer, J. Mol. Struct. **768**, 175 (2006).
- ⁷⁵ S. Huzinaga, J. Chem. Phys. **42**, 1293 (1965).
- ⁷⁶ T. H. Dunning, J. Chem. Phys. **53**, 2823 (1970).
- ⁷⁷ T. J. Lee and H. F. Schaefer, J. Chem. Phys. **83**, 1784 (1985).
- ⁷⁸ A. Bondi, J. Phys. Chem. **68**, 441 (1964).
- ⁷⁹ N. L. Allinger, J. A. Hirsch, M. A. Miller, I. J. Tyminski, and F. A. Van Catledge, J. Am. Chem. Soc. **90**, 1199 (1968).
- ⁸⁰ J. R. Quinn, S. C. Zimmerman, J. E. DelBene, and I. Shavitt, J. Am. Chem. Soc. **129**, 934 (2007).
- ⁸¹ F. A. Evangelista, A. Paul, and H. F. Schaefer, J. Phys. Chem. A **108**, 3565 (2004).

Table 5.1. Relative energies (E_{rel}), dissociation energies (DE), and relaxation energies (RE) (kcal mol^{-1}) of the AU-H radicals generated by hydrogen atom abstraction from the adenine-uracil pair (ZPVE-corrected values in parentheses). Dissociation energies are for fragmentation to either $(\text{A-H})^\bullet + \text{U}$ or $\text{A} + (\text{U-H})^\bullet$, depending on the radical site. Each relaxation energy is the radical energy lowering found in going from the optimized closed-shell AU structure to the equilibrium geometry of the specified radical.

	E_{rel}	DE	RE
AU		13.8 (12.7)	
A(N9)-U	0.0 (0.0)	15.0 (13.7)	12.8
A-U(N1)	3.2 (2.5)	13.4 (12.3)	4.8
A(N6b)-U	7.9 (7.5)	9.8 (8.9)	4.4
A(N6a)-U	12.2 (11.5)	6.5 (5.9)	8.3
A(C2)-U	12.3 (12.6)	12.3 (11.0)	2.3
A-U(C6)	15.0 (14.8)	14.2 (13.1)	1.6
A(C8)-U	18.3 (18.6)	13.8 (12.6)	1.3
A-U(C5)	21.4 (21.6)	14.1 (13.0)	1.3
A-U(N3)	22.4 (22.3)	15.4 (12.9)	8.3

Table 5.2. Selected interatomic distances (Å) for the A-U base pair and its hydrogen abstracted radicals.

	A(N6-H6a)⋯U(O4)	A(N1)⋯U(H-N3)	A(C2-H)⋯U(O2)
A-U	1.891	1.792	2.840
A(N9)-U	1.785	1.837	3.028
A-U(N1)	1.952	1.778	2.808
A(N6b)-U	2.135	1.844	2.710
A(N6a)-U	NA	2.052	2.267
A(C2)-U	1.833	1.913	NA
A-U(C6)	1.901	1.771	2.799
A(C8)-U	1.884	1.803	2.852
A-U(C5)	1.905	1.763	2.761
A-U(N3)	1.647	NA	2.094

Table 5.3. Relative energies (E_{rel}) in kcal mol⁻¹ of the isolated A-H and U-H radicals.

Radical	E_{rel}	Radical	E_{rel}
A(N9)	0.0 (0.0)	U(N1)	0.0 (0.0)
A(N6b)	2.7 (2.7)	U(C6)	12.6 (13.0)
A(N6a)	3.7 (3.7)	U(C5)	18.9 (19.7)
A(C2)	9.6 (9.9)	U(N3)	21.2 (20.3)
A(C8)	17.1 (17.5)		

Table 5.4. X-H bond dissociation energies (BDE) in eV for adenine, uracil, and A-U base pair. Each entry is labeled by the name of the particular radical resulting from hydrogen atom removal.

Base Radical	BDE	Base Pair Radical	BDE
A(N9)	4.50 (4.12)	A(N9)-U	4.44 (4.08)
U(N1)	4.57 (4.17)	A-U(N1)	4.58 (4.19)
A(N6b)	4.61 (4.24)	A(N6b)-U	4.79 (4.40)
A(N6a)	4.66 (4.28)	A(N6a)-U	4.97 (4.58)
A(C2)	4.91 (4.55)	A(C2)-U	4.98 (4.62)
U(C6)	5.11 (4.74)	A-U(C6)	5.09 (4.72)
A(C8)	5.24 (4.88)	A(C8)-U	5.24 (4.88)
U(C5)	5.39 (5.03)	A-U(C5)	5.37 (5.01)
U(N3)	5.49 (5.05)	A-U(N3)	5.42 (5.04)

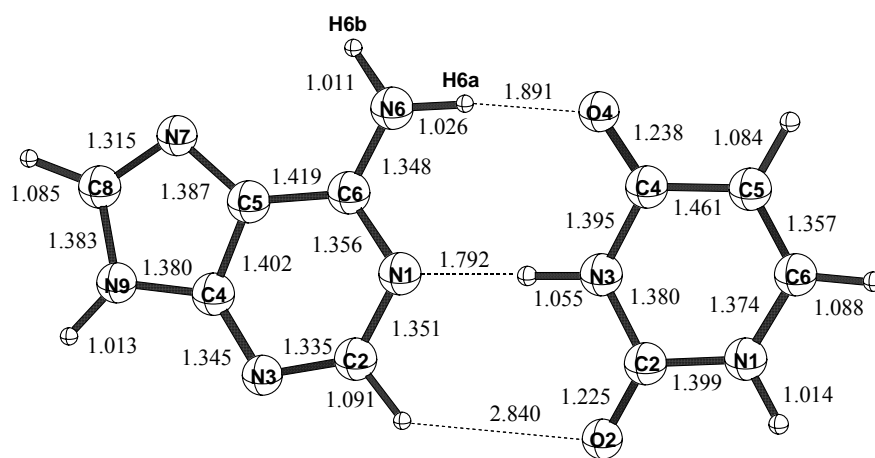


Figure 5.1. Optimized molecular geometry of the adenine-uracil (AU) base pair with atom numbering scheme.

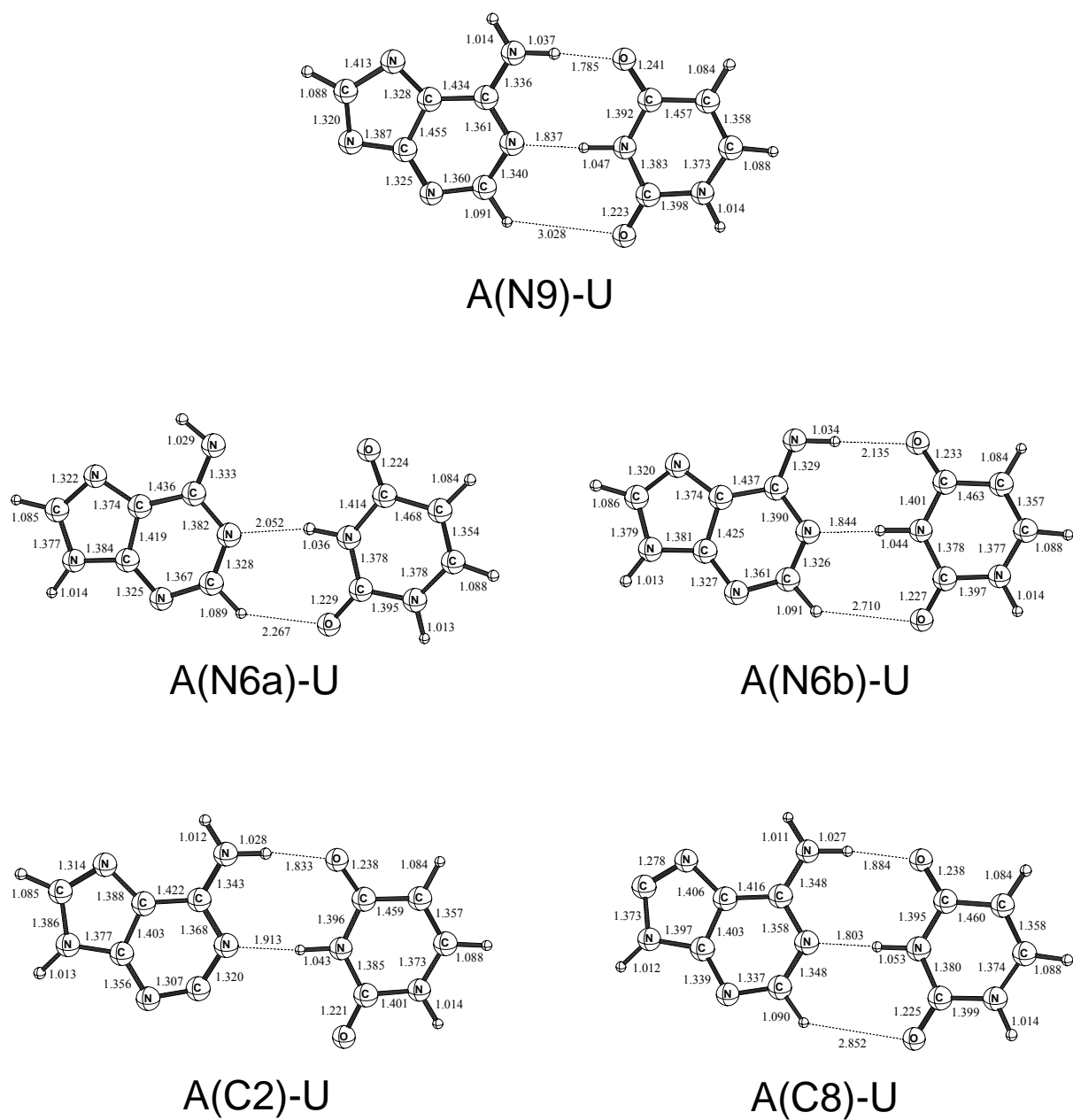
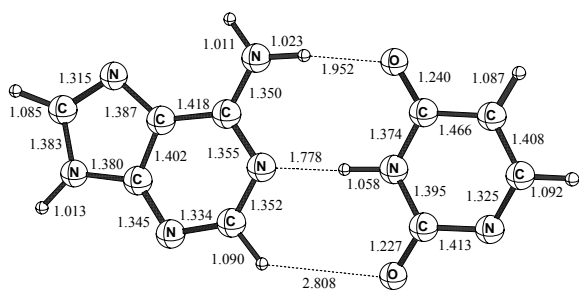
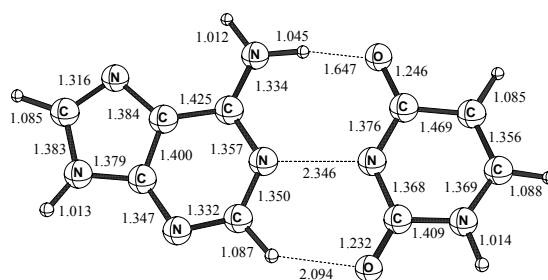


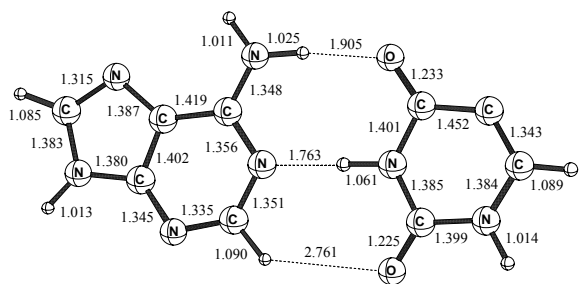
Figure 5.2. Optimized molecular structures of the radicals generated by hydrogen atom abstraction from the adenine unit of the AU base pair.



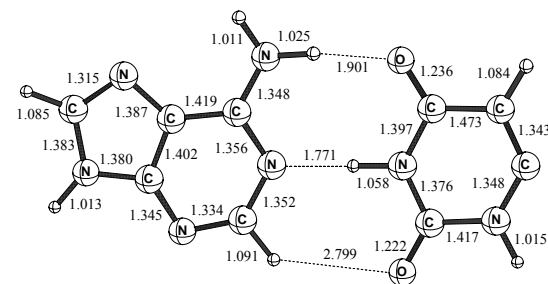
A-U(N1)



A-U(N3)



A-U(C5)



A-U(C6)

Figure 5.3. Optimized molecular structures of the radicals generated by hydrogen atom abstraction from the uracil unit of the AU base pair.

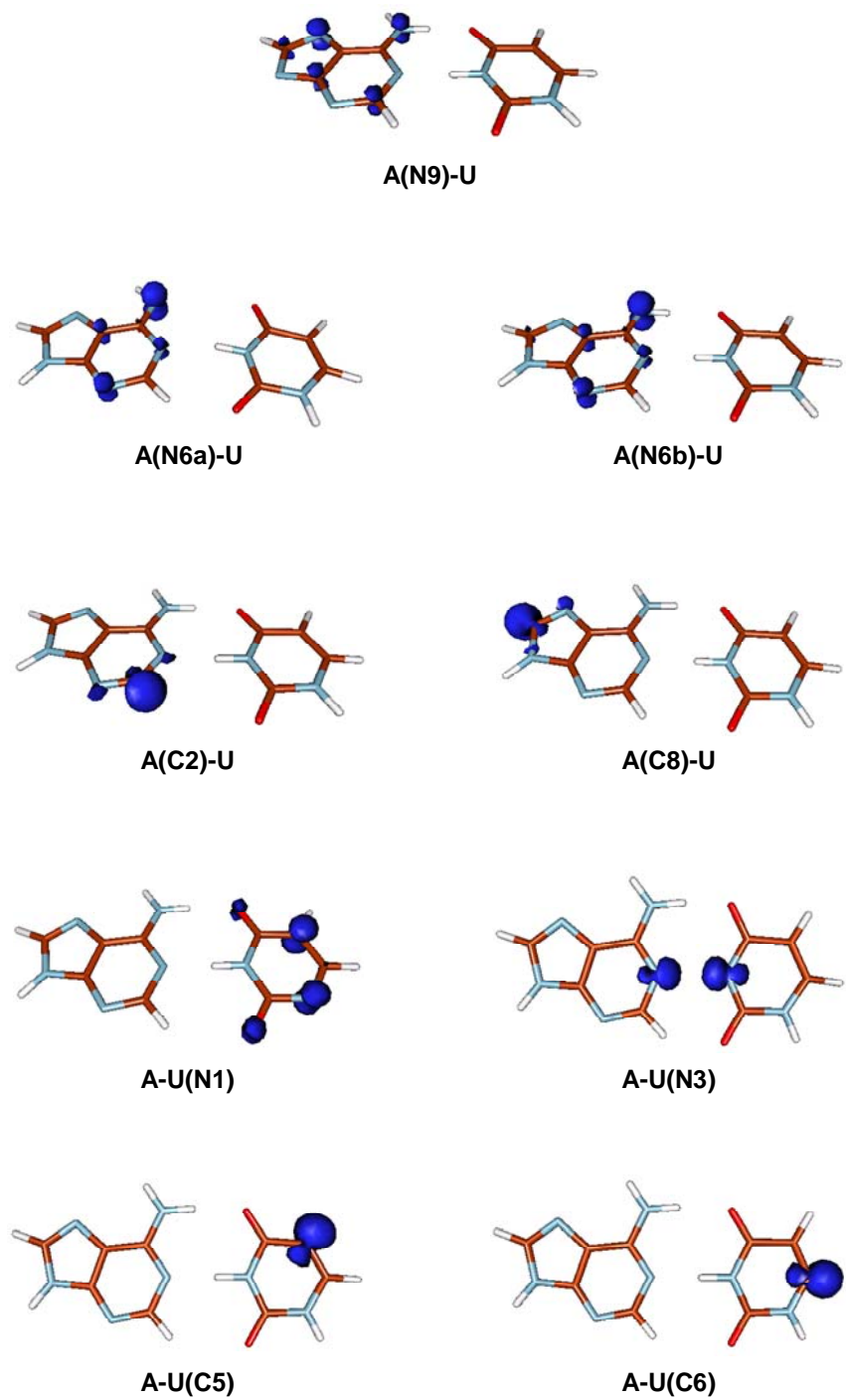


Figure 5.4. Spin density plots for the radicals generated by hydrogen abstraction from the AU base pair.

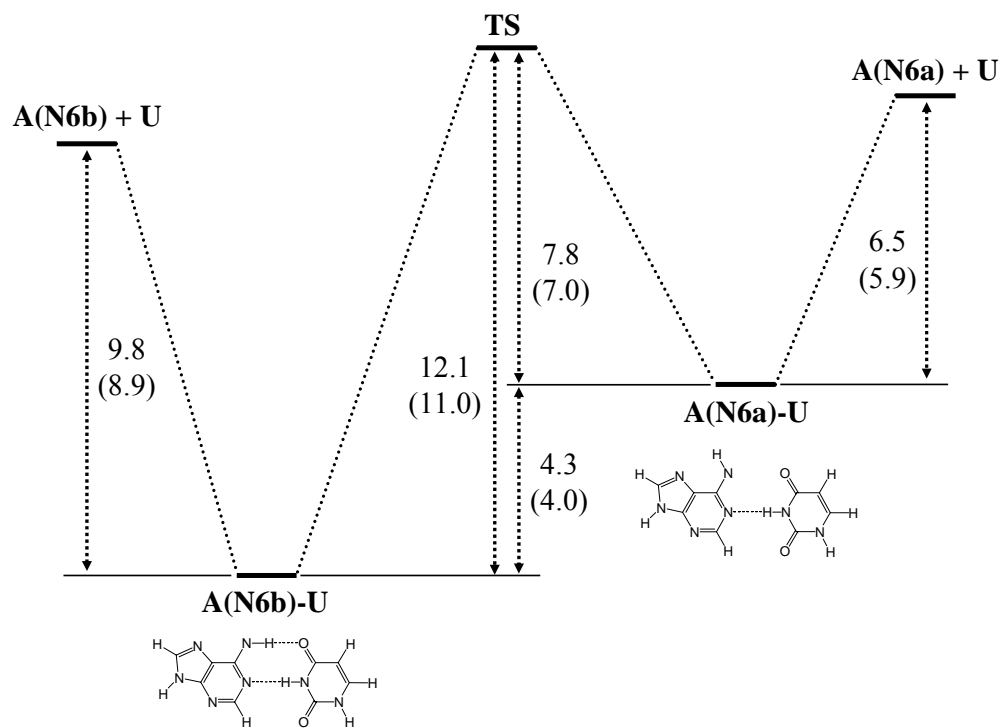


Figure 5.5. The schematic energy diagram for the dissociation of base pair radicals **A(N6a)-U** and **A(N6b)-U** and the rotational barrier connecting them (ZPVE-corrected values in parentheses).

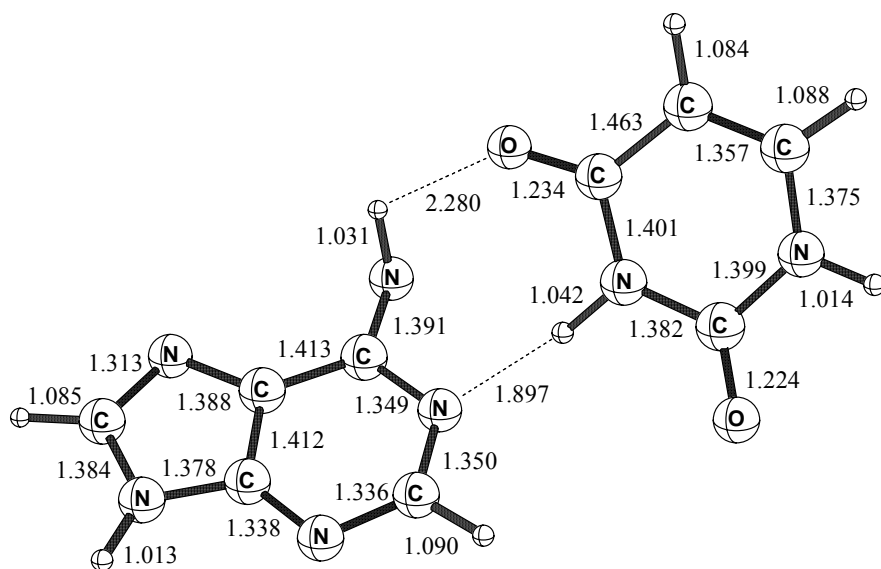


Figure 5.6. Transition structure between radicals **A(N6a)-U** and **A(N6b)-U**.

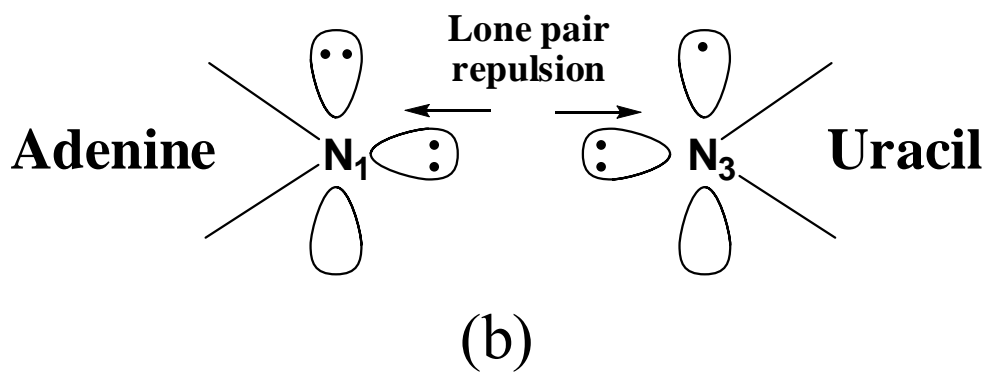
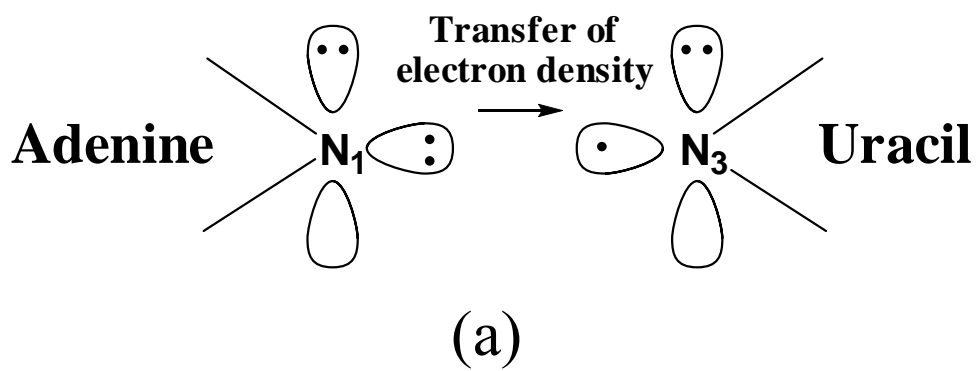


Figure 5.7. Two possible orientation of the unpaired electron in the A-U(N3) radical.

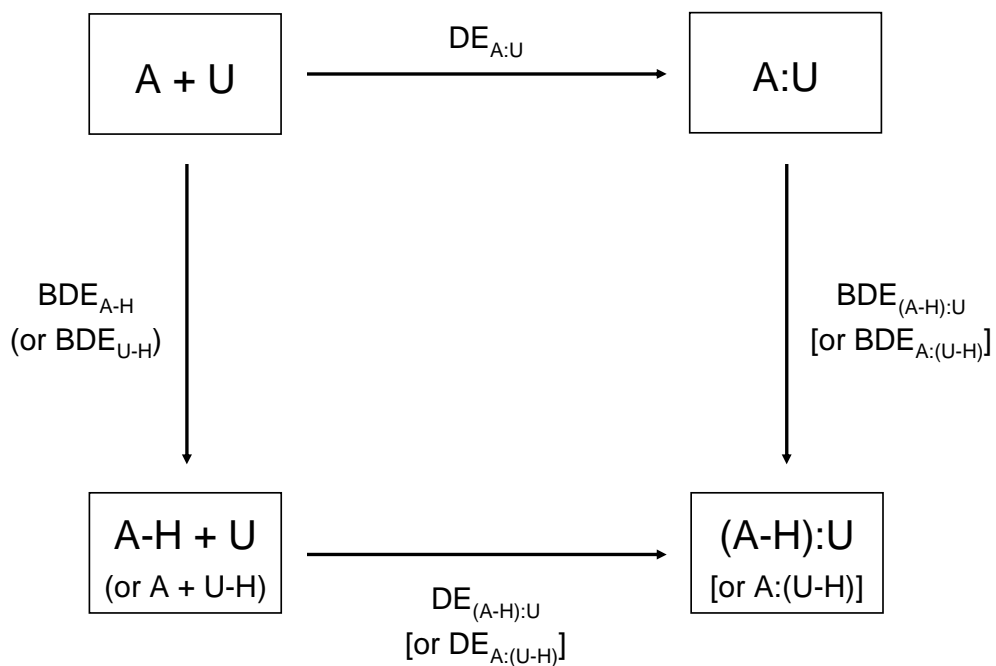


Figure 5.8. Two possible pathways to generating the hydrogen abstracted radicals from the isolated adenine and uracil bases.

CHAPTER 6

CONCLUDING REMARKS

In Chapters 2 through 4, microhydration effects on three pyrimidine nucleic acid bases (NABs), thymine, uracil, and cytosine, and their negative ions have been investigated by explicitly considering various structures of complexes of the NABs with up to five water molecules and their respective anions at the B3LYP/DZP++ level of theory. The vertical detachment energies (VDEs) of the three nucleobases were predicted to increase gradually with the number of hydrating water molecules. For all three bases, the adiabatic electron affinities (AEAs) were also found to increase with the hydration number, implying that the NABs may form stable anions in aqueous solution while the conventional valence anions of the NABs in the gas phase are only marginally bound. For a given hydration number, uracil has the largest VDE and AEA while cytosine has the smallest. These results were consistent with the experimental observations from a photodetachment-photoelectron spectroscopy study [Schiedt, Weinkauff, Neumark, and Schlag, *Chem. Phys.* **239**, 511 (1998)].

In Chapter 5, the hydrogen-abstracted radicals from the adenine-uracil (AU) base pair have been studied at the B3LYP/DZP++ level of theory. Removal of an amino hydrogen of the adenine moiety which forms a hydrogen bond with the uracil O4 atom in the AU pair resulted in radical **A(N6a)-U**, which has the smallest base pair dissociation energy (5.9 kcal mol⁻¹). This radical is more likely to dissociate into the two isolated bases than to recover the hydrogen bond with the O4 atom through the N6-H bond rotation along the C6-N6 bond. On the other hand, removal of the N3 hydrogen atom of uracil does not result in the dissociation of the AU base pair because the resulting radical, **A-U(N3)**, was predicted to have a base pair dissociation energy similar to that of the intact AU base pair (12.7 kcal mol⁻¹). This is due to the electron density transfer from the adenine N1 atom to the uracil N3 atom.

In general, conventional high-level *ab initio* methods are considered to be more accurate than the DFT approach. However, they are limited only to a small system because they require more computational resources. On the other hand, as shown in this dissertation, with proper choice of functionals and basis sets, the DFT approach can provide a reliable tool to investigate biological problems.